Abstract

Uncovering the Molecular Mechanisms of Ligand Binding to Parathyroid Hormone 1 Receptor

Kelly Culhane

2019

Family B G protein-coupled receptors (GPCRs) are important drug targets for many metabolic diseases, including diabetes, osteoporosis, and cardiovascular disease. Despite this importance, the structure and function of family B GPCRs is poorly understood. Our lab uses parathyroid hormone 1 receptor (PTH1R) as a model to examine the molecular mechanisms of family B GPCRs. PTH1R is expressed in the bone and kidney cells and binds two endogenous hormones: parathyroid hormone (PTH) and parathyroid hormone related peptide (PTHrP). PTH is an endocrine hormone released from the parathyroid gland to regulate serum Ca^{2+} levels through the bone remodeling process, during which Ca^{2+} can reach concentrations up to 40 mM. Thus, PTH1R is an important drug target for osteoporosis. The second hormone, PTHrP, is a paracrine/autocrine hormone that is important for tissue development. Truncated versions of both hormones, PTH(1-34) and PTHrP(1-36), are full agonists of PTH1R and are FDA-approved treatments for severe osteoporosis. A more complete understanding of PTH1R ligand binding and activation may uncover new treatment strategies for osteoporosis and other bone diseases.

The Yan laboratory developed a novel nanodisc purification protocol to incorporate PTH1R in artificial lipid bilayers, to overcome the significant technical challenges associated with purifying active transmembrane receptors through traditional

methods. I used fluorescence anisotropy to study PTH(1-34) binding to PTH1R purified in nanodiscs and found PTH(1-34) binds to PTH1R 5-fold tighter in the presence of 15 mM Ca^{2+} than in its absence. However, the binding of PTHrP(1-36) was not affected by the presence of Ca^{2+}. The observed Ca^{2+} dependent binding of PTH(1-34) requires full-length PTH1R, and is specific to Ca^{2+}. I performed sequence alignments to identify possible Ca^{2+}-binding residues in both PTH(1-34) and PTH1R, developing the hypothesis that non-conserved, negatively charged residues of both PTH(1-34) and PTH1R are necessary for Ca^{2+}-dependent binding. I mutated the identified glutamic and aspartic acid residues of interest in both PTH(1-34) and PTH1R to alanine in order to remove the negative charges and tested these mutants for changes in ligand binding.

Fluorescence anisotropy assays showed mutating two glutamic residues, Glu19 and Glu22, in PTH(1-34) strongly decreased the Ca^{2+}-effect on PTH(1-34) binding. In addition, mutations of PTH1R change the Ca^{2+}-effect on PTH(1-34) binding. Mutating eight negatively charged residues of the PTH1R extracellular domain does not significantly affect the Ca^{2+} dependence, while mutating six negatively charged residues in the PTH1R extracellular loop 1 (ECL1) significantly decreased the Ca^{2+}-effect on PTH(1-34) binding. However, because neither of these mutations of PTH(1-34) or PTH1R abolished the Ca^{2+}-effect, I tested the binding of PTH(1-34)E19AE22A to the PTH1R ECL1 mutants, which removed the Ca^{2+}-effect on PTH(1-34) binding. Thus, I proposed that residues of PTH(1-34) and PTH1R form a weak Ca^{2+}-binding site that affects PTH(1-34) binding to PTH1R.

In order to better understand how the presence of Ca^{2+} modulates the interaction of PTH(1-34) with PTH1R, I collaborated with Dr. Pat Loria to perform preliminary

protein Nuclear Magnetic Resonance (NMR) studies to investigate changes in the peptide backbone dynamics of PTH(1-34) as it interacts with PTH1R in the presence and absence of Ca^{2+}. We measured changes in the transverse relaxation rates of ^{15}N-PTH(1-34) in the presence and absence of PTH1R and/or 15 mM Ca^{2+}. The preliminary data showed that residues that interact with PTH1R have increased relaxation rates when PTH1R is present. When mapped onto the crystal structure of a PTH(1-34) analogue bound to PTH1R, the changes in relaxation rates supported previously identified binding interactions of PTH(1-34) and highlighted additional dynamic residues. The preliminary data shows the protein NMR method developed here is effective in identifying changing in PTH(1-34) dynamics in the presence of PTH1R.

In addition, I developed a surface plasmon resonance (SPR) platform in order to investigate allosteric interactions of PTH1R across the transmembrane domain. Future studies of ligand and G protein binding to PTH1R using this SPR platform in combination with protein NMR experiments to measure changes in peptide dynamics may begin to show how complicated allosteric interactions affect PTH1R.

In this work I investigate the molecular mechanisms of ligand binding interactions of family B GPCRs using PTH1R as a model. The ligand binding studies by fluorescence anisotropy uncovered a novel modulation of PTH(1-34) binding by millimolar concentrations of Ca^{2+}. Preliminary data from protein NMR experiments identified changes in the dynamics of PTH(1-34) in the presence PTH1R. The preliminary data demonstrates the ability to measure changes in the dynamics of PTH(1-34) under many different conditions, such as with 15 mM Ca^{2+} or different PTH1R mutants. By combining my data on the Ca^{2+}-modulation of PTH1R function with previous structural

information, we are beginning to piece together a full picture of ligand binding to PTH1R, which will help in understanding the molecular details of the bone remodeling process, leading to new treatments for osteoporosis. In addition, this work provides novel insights into allosteric modulation of family B GPCRs, building on the strong foundation of structural and biochemical studies investigating the role of peptide hormone binding and activation of these important receptors.

Uncovering the Molecular Mechanisms of Ligand Binding to Parathyroid Hormone 1 Receptor

A Dissertation
Presented to the Faculty of the Graduate School
of
Yale University
in Candidacy for the Degree of
Doctor of Philosophy

By

Kelly Culhane

Dissertation Director: Elsa C. Y. Yan

May 2019

Table of Contents

Chapter 1: Introduction 1

1.1 Overview of G protein-coupled receptors 1

1.2 Peptide ligand binding and activation of family B GPCRs 5

1.3 The role of parathyroid hormone in bone remodeling and osteoporosis 16

1.4 Overview and scope of dissertation 19

Chapter 2: PTH(1-34) binding to PTH1R shows calcium dependence 22

2.1 Introduction 23

2.2 Experimental Materials and Methods 27

2.3 Results 35

2.3.1 Calcium increases PTH(1-34), but not PTHrP(1-36), binding to purified PTH1R .. 35

2.3.2 Calcium does not affect ligand binding to all family B GPCRs 38

2.3.3 Mg^{2+} and Ca^{2+} modulate PTH(1-34) binding to PTH1R differently 40

2.3.4 Full length PTH1R is required for calcium dependent binding 42

2.3.5 PTH(1-34) binds to PTH1R on the cell surface with calcium dependence 45

2.3.6 Extracellular Ca^{2+} affects PTH(1-34) activation of PTH1R 47

2.4 Discussion and conclusions 49

Chapter 3: PTH(1-34) senses extracellular calcium to regulate binding and activation of PTH1R 53

3.1 Introduction 54

3.2 Experimental Materials and Methods 57

3.3 Results 58

3.3.1. Design and characterization of mutants ligands to investigate the PTH(1-34) Ca^{2+} dependence 58

3.3.2. Mutant ligands bind to PTH1R in the presence and absence of calcium 60

3.3.3. Mutant ligands activate PTH1R in cAMP assays 63

3.4 Discussion and conclusions 65

Chapter 4: Residues of PTH1R modulate the calcium-sensing ability of PTH(1-34) 69

4.1 Introduction 70

4.2 Experimental Materials and Methods 72

4.3 Results 74

4.3.1 Stable cell lines express PTH1R mutants 74

4.3.2 Calcium affects PTH(1-34) binding to PTH1R mutants 75

4.3.3 Calcium shows differential effects on PTH(1-34)E19AE22A binding to PTH1R mutants 78

4.3.4 Residues of PTH1R extracellular loop 1 regulate Ca^{2+} dependence 81

4.3.5 PTH(1-34) activates PTH1R mutants in cAMP assays 88

4.4 Discussion and conclusions 90

Chapter 5: Solution NMR studies show ligand binding dynamics to PTH1R 96

5.1 Introduction 98

5.2 Experimental Materials and Methods 102

5.3 Results 104

5.3.1 PTH(1-34) expression and purification from *E. coli* 104

5.3.2 2D ^{1}H ^{15}N HSQC of ^{15}N-PTH(1-34) 108

5.3.3 R_2 values of each residue of PTH(1-34) indicate rigidity 109

5.3.4 PTH(1-34) R_2 values change in the presence of PTH1R 111
5.3.5 15 mM Ca^{2+} does not greatly change the R_2 values of PTH(1-34) 113
5.4 Discussion and future directions 116
Chapter 6: Novel method development to investigate allosteric mechanisms of PTH1R 123
6.1 Introduction 125
6.2 Experimental Materials and Methods 128
6.3 Results 131
6.3.1 Triblock molecules activate PTH1R 131
6.3.2 Surface plasmon resonance assays show ligand binding to PTH1R 133
6.4 Discussion and future directions 134
Chapter 7: Conclusions and future directions 136
Chapter 8: References 140

List of Figures

Figure 1.1. Simplified GPCR activation model…… 2
Figure 1.2: A comparison of GPCR families. ……... 3
Figure 1.3: Two domain binding model of family B GPCRs. …….. 7
Figure 1.4: Dual binding site trigger for family B GPCRs. …… 10
Figure 1.5: Structural comparison of an inactive and an active family B GCPR…… 12
Figure 1.6: Interactions of various isoforms of G proteins with family B GPCRs…….. 14
Figure 1.7: PTH regulation of the bone remodeling processing…….. 18
Figure 2.1: PTH(1-34) bound to PTH1R shown in a nanodisc …… 24
Figure 2.2: Fluorescent peptide design …….. 29
Figure 2.3: Binding of peptide ligands to PTH1R in nanodiscs (PTH1R-ND)…… 36
Figure 2.4: Ligand binding to GLP1R …… 39
Figure 2.5: Specific Ca^{2+} effect on PTH(1-34) binding to PTH1R-ND …… 41
Figure 2.6: Binding of PTH(1-34) to the extracellular domain (ECD) of PTH1R……. 43
Figure 2.7: PTH(1-34) binding to PTH1R stabilized in detergent micelles…… 44
Figure 2.8: Flow Cytometry titrations of HEK293S cells …… 46
Figure 2.9: PTH(1-34) activates PTH1R in the presence and absence of 15 mM Ca^{2+}... 48
Figure 3.1. Structural alignment of PTH(15-34) and PTHrP(15-36) binding ……..... 56
Figure 3.2: Sequence alignment of the PTH and PTHrP ligands under study …… 58
Figure 3.3: Chimeric and mutant peptides maintain their secondary structures …… 59
Figure 3.4: Binding of mutant peptide ligands to PTH1R …….. 62
Figure 3.5: Chimeric and mutant peptides activate PTH1R to produce cAMP……... 64
Figure 3.6: Extracellular domain of PTH1R has a high density of negatively charged residues …… 67
Figure 4.1: Sequence alignment of family B GPCRs …… 71
Figure 4.2: Expression levels of established stable cell lines. …… 75
Figure 4.3: Mutant PTH1R binds PTH(1-34) …… 77
Figure 4.4: PTH(1-34)E19AE22A binds to PTH1R mutants …… 80
Figure 4.5: Homology model of PTH(1-34) bound to PTH1R …….. 82
Figure 4.6: Single mutants of PTH1R ECL1 bind PTH(1-34) ……... 84
Figure 4.7: PTH(1-34)E19AE22A binding to single mutants of PTH1R ECL1. ……... 87
Figure 4.8: PTH(1-34) activates the mutant receptors …… 89
Figure 4.9: Changes in Ca^{2+} dependence for WT and mutant PTH1R ……... 92
Figure 4.10: Changes in binding affinity of PTH(1-34)E19AE22A in the presence and absence of 15 mM Ca^{2+} …… 94
Figure 5.1: Expression and purification of ^{15}N-PTH(1-34) …….. 105
Figure 5.2: Purification and characterization of ^{15}N-PTH(1-34). …… 106
Figure 5.3: Recombinant ^{15}N-PTH(1-34) activates PTH1R …… 107
Figure 5.4: 2D spectrum of ^{15}N-PTH(1-34) …….. 108
Figure 5.5: R_2 values for each residue of PTH(1-34). ……... 110
Figure 5.6: Changes in R_2 in the presence of PTH1R ……... 112
Figure 5.7: 15 mM Ca^{2+} does not affect the backbone structure of PTH(1-34) …… 113
Figure 5.8: Changes in PTH(1-34) R_2 in the presence of 15 mM Ca^{2+} PTH(1-34) ….. 115
Figure 5.9: Changes in R_2 values show the rigidity of PTH(1-34) in solution ……. 117

Figure 5.10: Changes in dynamics of residues of PTH(1-34) upon interaction with PTH1R …….. 120
Figure 6.1: Triblock molecules anchor into the lipid bilayer to interact with receptors..126
Figure 6.2: SPR platform to study ligand and G protein binding to PTH1R …… 128
Figure 6.3: The identity of the peptide N-terminus affects the activation of PTH1R... 132
Figure 6.4: SPR analysis of PTH(1-34) binding to PTH1R……...133

List of Tables

Table 1.1: Summary of family B GPCR physiology and drugs..…….. 4
Table 2.1: Binding affinity of PTH1R ligands …… 36
Table 2.2: Binding affinity of PTH(1-34) with divalent ion concentrations…….. 41
Table 3.1: Binding affinity of the tested PTH1R ligands …….. 63
Table 4.1: Binding affinity of PTH(1-34) to WT PTH1R and PTH1R mutants …… 77
Table 4.2: Binding affinity of PTH(1-34) to WT PTH1R and PTH1R mutants …… 80
Table 4.3: Binding affinity of PTH(1-34) to WT PTH1R and Ca^{2+}-sensing mutants …. 85
Table 4.4: Binding affinity of PTH(1-34) to WT PTH1R and PTH1R mutants …… 88
Table 4.5: Potency and efficacy of PTH(1-34) activation of WT and mutant PTH1R ... 89
Table 5.1: Common isotope in biological NMR experiments …… 98

Acknowledgements

The work presented in this thesis would not be possible without the support and guidance of so many people. I'd like to thank Dr. Elsa Yan for advising me and for allowing me to pursue many new directions of PTH1R ligand binding through new experimental techniques and collaborations. Thank you for challenging me to think critically and quantitatively about biological systems. Thank you to my thesis committee, Dr. Pat Loria and Dr. Don Engelman, for your guidance and advice throughout my dissertation work, which kept me focused and moving forward. Finally, thank you to my outside reader, Dr. Graham Ladds, for insightful comments and guidance throughout the writing process.

I'd like to thank the members of the Yan lab throughout my time here, who always provided help whenever I asked. I'm particularly grateful for Dr. Yingying Cai, who was an incredible labmate to work on the project with and for Ya-Na Chen's ability to listen well and keep me grounded. Jeremy, Ella and Allyson were incredible undergrads to work with and I wouldn't have made it through without your experimental help, energy and enthusiasm. I'm thankful for the members of the Loria lab for being so gracious and welcoming to me and for providing so much assistance with NMR. Your friendship and conversations always added a little fun into the workday. I'd also like to thank the Xiong lab for welcoming me in for coffee and snacks while providing help with protein expression and purification.

I couldn't have survived in New Haven without my friends in and out of the lab. I'm thankful for afternoon walks and ice cream trips with Sammie that kept me sane, for coffee runs with Cary, for trips to new and cool places with Sarah and for the many

friends who've shared meals, walks, movies and played softball. I'm incredibly grateful for Tyler, Laura and Jack who always shared delicious meals and even better company. I couldn't have survived without Molly, who listened so well and was always willing to hang out with delivery and wine. I'm also grateful for the community of McDougal Teaching Fellows at the Center for Teaching and Learning who shared so many laughs and so much support and for the many communities at Bethesda Lutheran church that welcomed me with open arms. Finally, I'd like to thank my family who are constantly supportive, each in their own ways. I would not have made it through this process without them!

Chapter 1: Introduction

The work presented in this introduction contains materials from the publication titled "Transmembrane signal transduction by peptide hormones via family B G protein-coupled receptors" published in *Frontiers in Pharmacology*.[1]

1.1 Overview of G protein-coupled receptors

G protein-coupled receptors (GPCRs), which form the largest protein superfamily of the vertebrate genome, play an important role in signal transduction by detecting extracellular stimuli and activating intracellular downstream pathways (Figure 1.1).[2] All GPCRs share a common seven-transmembrane helix topology, and mediate cellular responses through interactions with a variety of extracellular signals. The extracellular signals range from photons and small molecules to hormones and proteins, necessitating a wide structural and functional diversity of over 800 different GPCRs.[3] Despite this diversity, GPCRs share a general mechanism of activation. Ligand binding causes conformational rearrangements in the seven-transmembrane (7TM) domain that activate the G protein in the cytoplasmic region. G protein activation triggers various signaling cascades to mediate physiological processes (Figure 1.1). Since the ligand binding sites are highly specific, GPCRs have been heavily exploited as drug targets for over 40% of the current pharmaceutical drugs on the market, and estimated global sales of approximately $85 billion.[4, 5]

There are five GPCR subfamilies: families A-C, the Adhesion family and the Frizzled family (Figure 1.2). The largest family, family A, includes approximately 700 receptors that are activated by a wide variety of different ligands. In contrast, there are only 15 family B GPCRs, each of which bind to peptide ligands involved in many

metabolic processes (Table 1.1). Compared to GPCRs in other families, family B GPCRs have a relatively large N-terminus that is ~120 amino acids long (Figure 2.2). The family B GPCR N-terminus shares a conserved fold stabilized by three disulfide bridges, which is part of the ligand-binding site.

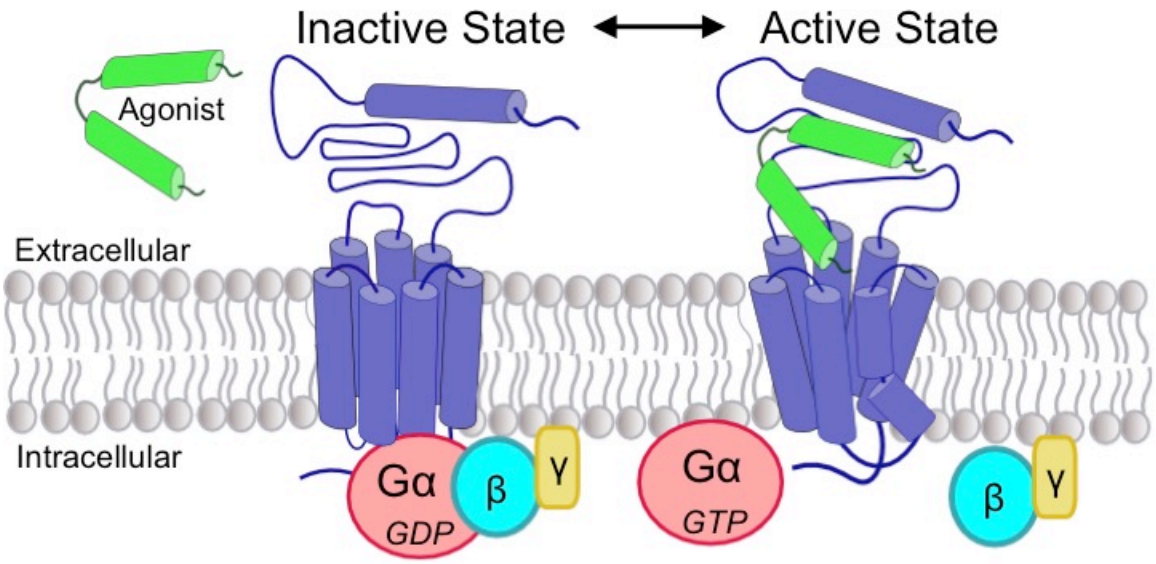

Figure 1.1. Simplified GPCR activation model. An agonist (green) binds the extracellular side of the GPCR (purple), which leads to conformational changes. This causes Gα subunit of the G protein heterotrimer to exchange GDP for GTP, leading to G protein activation and downstream signaling.

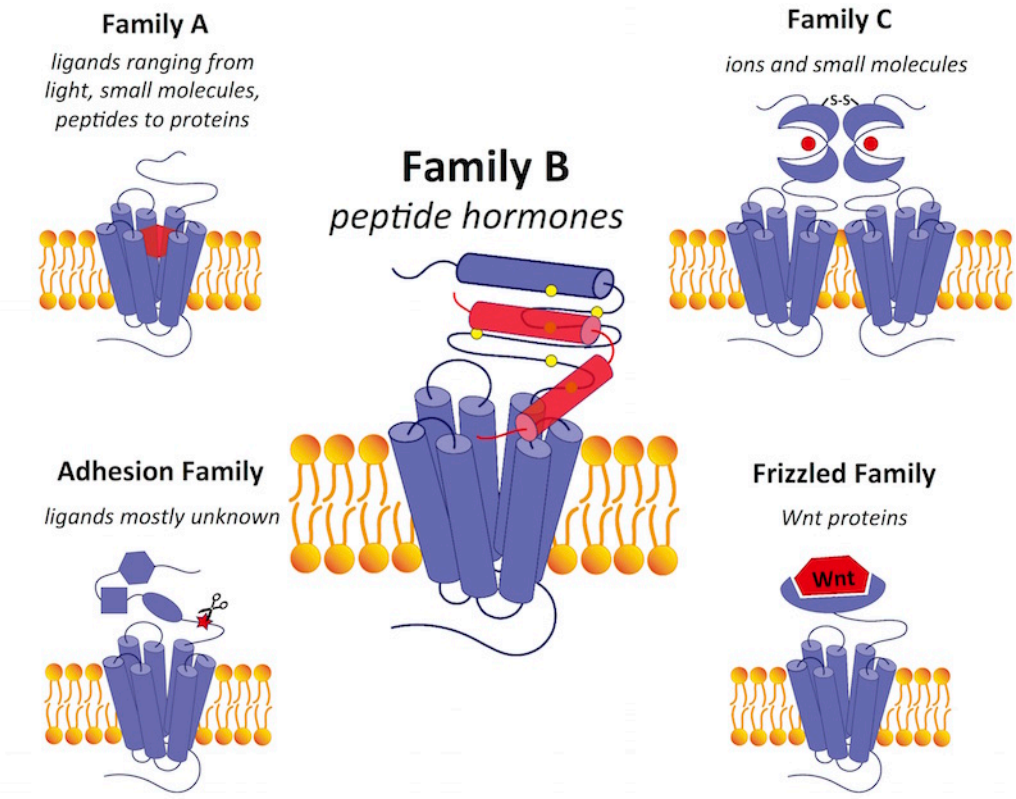

Figure 1.2: A comparison of GPCR families.[1] While all GPCRs share a common seven transmembrane helix fold, their extracellular domains and ligands vary widely. Family A GPCRs have a small extracellular domain and bind a wide range of diverse ligands in the transmembrane region. Family B GPCRs have a relatively large extracellular N-terminus (~120 amino acids) with a conserved structural fold stabilized by cysteine bonds used detect peptide hormones. Family C GPCRs form a dimer through a conserved disulfide linkage and have a large extracellular N-terminal ligand-binding region in the "Venus flytrap" fold for ligand binding. The adhesion and frizzled families have GPCR-like transmembrane-spanning regions fused together with one or several functional N-terminal domains. Ligands are shown in red. Scissors in the adhesion family indicate the autoproteolysis-inducing domain. Figure from [1].

Table 1.1: Summary of family B GPCR physiology and drugs. Table adapted from [1] as reviewed in [6-8]

Receptors	Ligands	Physiology	Disease(s)	Treatment
Calcitonin receptor family				
Calcitonin receptor	calcitonin	Ca^{2+} homeostasis	osteoporosis	Miacalcin, Fortical
Amylin receptors	amylin, amyloid-beta (Aβ)	Energy homeostasis	diabetes/obesity	Pramlintide
Calcitonin gene-related peptide receptor	α- and β-calcitonin gene-related peptide	Vasodilation and nociception	migraine	
Adrenomedullin receptors	adrenomedullin 1 and 2	Vasodilation	cardiovascular disease, cancer	
Glucagon receptor family				
Glucagon receptor	glucagon	Regulation of blood glucose	diabetes	Glucagon
Glucagon-like peptide 1 receptor	glucagon-like peptide 1	Insulin and glucagon secretion	diabetes	Exenatide Lixisenatide
Glucagon-like peptide 2 receptor	glucagon-like peptide 2	Gut mucosal growth	short bowel syndrome, Crohn's	Teduglutide
Gastric inhibitory polypeptide receptor	gastric inhibitory polypeptide	Insulin secretion, fatty acid metabolism	diabetes/obesity	
Corticotropin-releasing hormone receptors				
Corticotropin-releasing factor receptor 1	corticotropin-releasing factor, Urocortin I	Release of ACTH, stress responses	stress, IBS	Corticorelin
Corticotropin-releasing factor receptor 2	corticotropin-releasing factor, Urocortin II and urocortin III	Central stress responses, cardiac contractility	cancer, heart failure, hypertension	
Parathyroid hormone receptors				
Parathyroid hormone 1 receptor	parathyroid hormone	Ca^{2+} homeostasis	osteoporosis, hypopara-thyroidism	Teriparatide Preotact
	parathyroid hormone-related protein	Developmental regulator		
Parathyroid hormone 2 receptor	Parathyroid hormone, tuberoinfundibular peptide	Hypothalamic secretion, nociception	nociception	
Vasoactive intestinal polypeptide receptors				
Vasoactive intestinal polypeptide receptor 1 and 2	vasoactive intestinal polypeptide, PACAP	Vasodilation, neuroendocrine functions	inflammation, neurodegeneration	
Others				
Pituitary adenylate cyclase-activating polypeptide type I receptor	pituitary adenylate cyclase-activating polypeptide	Neurotransmission neuroendocrine functions	neurodegeneration, nociception, glucose homeostasis	
Growth-hormone-releasing hormone receptor	growth hormone-releasing hormone	Release of growth hormone	dwarfism, HIV-related lipodystrophy	Tesamorelin Sermorelin CJC-1295
Secretin receptor	secretin	Pancreatic secretion	autism, Schizophrenia, gastrinoma	

Although most drugs developed against GPCRs target family A receptors, family B GPCRs are becoming increasingly attractive drug targets for treatment of metabolic diseases.[5, 9] Nearly all family B GPCRs have been validated as drug targets for diseases such as cancer, osteoporosis, diabetes, cardiovascular disease, neurodegeneration, and migraine (Table 1.1).[6] However, it has been challenging to identify small-molecule therapeutics to target this family, with only a few peptide agonists approved by the FDA as drugs.[10] Most of these agonist drugs are derivatives of the family B cognate peptide ligands (Table 1.1). The challenge of identifying conventional small-molecule drugs lies in the lack of molecular information to locate druggable binding sites. Nevertheless, recent structural information has provided novel insights into the ligand binding and activation of family B GPCRs.

1.2 Peptide ligand binding and activation of family B GPCRs

1.2.2 Ligand binding to family B GPCRs

Family B GPCRs are activated by peptide hormones that range from 26 to 114 amino acids. Most ligands of family B GPCRs lack ordered structure in aqueous solutions, but form α-helical fragments upon binding to their cognate receptors, under structure-inducing in the presence of organic solvents or lipids, or upon crystallization.[11] It is widely accepted that the peptide hormones interact with family B GPCRs following the two-domain binding model, in which the peptide hormone's C-terminus binds to their cognate receptor's N-terminal domain and the N-terminus of the peptide hormone binds to the receptor's juxtamembrane, which is composed of the extracellular loops (Figure 1.3). Ligand binding causes conformational changes in the receptor's cytoplasmic domain

to activate a G protein, triggering a downstream signaling process.[12-15] Förster Resonance Energy Transfer (FRET) experiments measured the kinetics of the two domains of binding, further supporting the sequential nature of the model.[16]

The first step in the two-domain binding model - the C-terminus of the ligand binding to the N-terminal domain of receptors - is strongly supported by multiple crystal structures.[17-31] These structures reveal that the N-terminal domains contain a conserved three-layered α-β-βα fold with the helical segment of the peptide hormone primarily interacting in the middle layer to resemble a hotdog in a bun (Figure 1.3).[11, 12] Six conserved cysteine residues form three interlayer disulfide bonds that stabilize the α-β-βα fold (Figure 1.3). Additional hydrophobic packing interactions and hydrogen bonds stabilize the second and third layers of the fold.[32] Sequence conservation indicates the importance of these stabilizing interactions, which likely involve five partially conserved residues: Asp113, Trp118, Pro132 and Gly152 and Trp154 (PTH1R residues, Figure 1.3).[21] These conserved residues and the structural similarities of the three-layered fold form a structural foundation for the two-domain binding model. Of interest, the structure of the extracellular domain and the contacts with their cognate peptide hormone in the available full-length GPCR structures aligns well with the previously published crystal structures of the extracellular domain alone (Figure 1.3).[25-31]

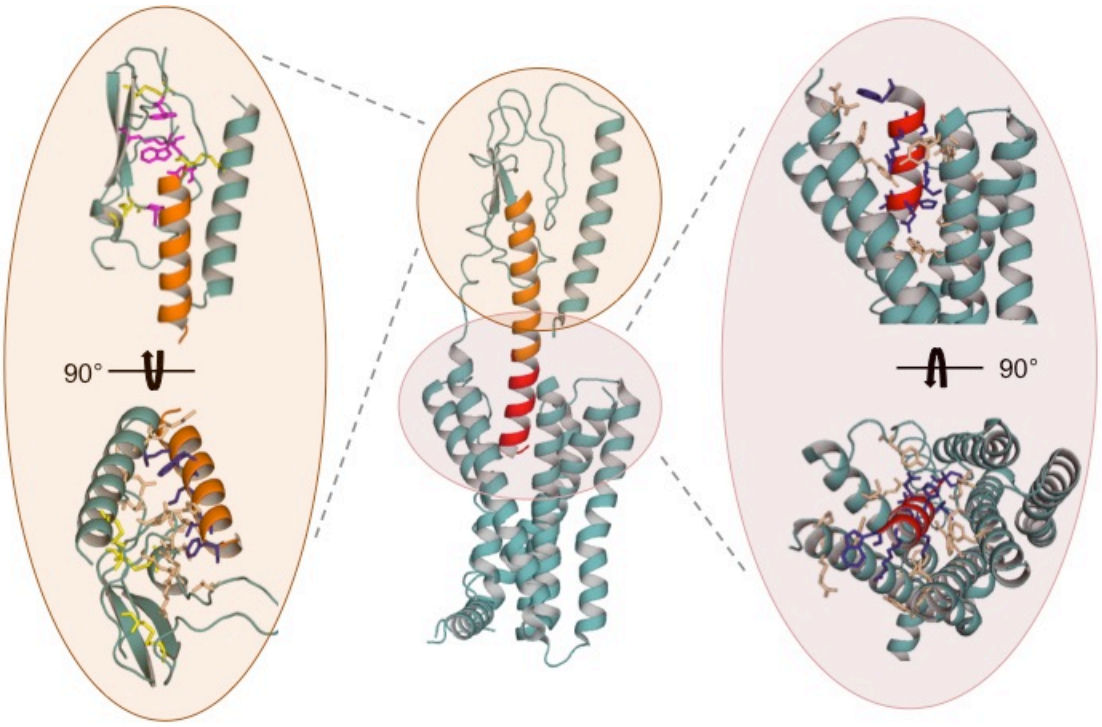

Figure 1.3: Two domain binding model of family B GPCRs. Evidence of the two-domain binding model from the crystal structure of PTH(1-34) bound to PTH1R (teal) resolved to 2.5 Å (PDBID: 6FJ3).[25] The first domain (orange) shows the interaction of PTH(15-34) with the N-terminal domain of PTH1R from the structure of the extracellular domain alone resolved to 1.95 Å (PDBID: 3CM4).[33] Conserved residues among family B GPCRs are shown in the top left as sticks with the residues of the hydrophobic core in pink and the 3 conserved disulfide bonds in yellow. The second domain (red) shows the interaction of PTH(1-14) with the juxtamembrane domain of the PTH1R, which activates the receptor. Interacting residues of PTH1R (tan) and PTH(1-34) (blue) are shown as sticks.

The second step of the two-domain binding model involves interactions between the N-terminus of the peptide and the juxtamembrane domain of the receptor as shown by the recent full-length structures.[25-31] In general, the mid-region of the peptide ligand makes contacts with the stalk and extracellular loops of the juxtamembrane domain. As the peptide inserts into the transmembrane domain (TMD), its α – helical structure runs parallel to helix 2 (Figure 1.3). Contacts between the N-terminal residues of the peptide and the GPCR helices 1, 2 and 7 are important for ligand binding. The structures show that these interactions are generally conserved between family B GPCRs.[25-31] Previous biochemical data from photoaffinity cross-linking identified specific contacts between the peptide ligand and the receptor, corroborating the interactions identified in the crystal structures.[34-37]

The structures of the full-length family B GCPRs showed the conformation of the receptors have an inherent flexibility, bringing the current understanding of the two-domain binding model into question.[25-31] From these structures, conformational changes that occur with both ligand binding and receptor activation are becoming evident. The new structural data combined with previous biophysical and biochemical studies have greatly increased our knowledge of the molecular mechanisms of family B GPCR ligand binding and activation.

We can combine the information from the structural studies, each of which shows a slightly different snapshot of the ligand binding process, to expand on the two-domain binding model. For instance, the structure of the glucagon receptor bound to a negative allosteric modulator shows the stalk region, which connects the extracellular domain (ECD) to helix 1 of the TMD forms a β-sheet structure with extracellular loop 1

(ECL1).[29] This interaction affects the position of the ECD relative to the transmembrane domain (Figure 1.4). Similar large conformational changes of the ECD upon ligand binding to the glucagon receptor were shown by molecular dynamics simulations and supported by Hydrogen-Deuterium Exchange Mass Spectrometry data.[38] Furthermore, the structure of the glucagon receptor with a glucagon analogue bound shows the β-sheet structure of the stalk and ECL1 is disrupted, with the stalk adopting a α-helical conformation (Figure 1.4). In this same structure, the α-helical structure of helix 2 extends on the extracellular side, which elevates the position of ECL1 for interactions with the mid-portion of the glucagon analogue. These changes cause a large rotation of the ECD compared to the glucagon receptor with no peptide ligand bound.[29] Thus, the authors proposed the dual-binding site trigger model of ligand binding, where peptide binding to both the ECD and the juxtamembrane domain trigger necessary changes for receptor activation (Figure 1.4).[30] While more structural information is necessary to support this new model, similar ligand binding interactions are observed in the structures of glucagon-like peptide 1 receptor (GLP1R) bound to GLP-1[30] or the agonist Exendin-5 (Ex-5),[26] and parathyroid hormone 1 receptor (PTH1R) bound to a PTH analogue.[25]

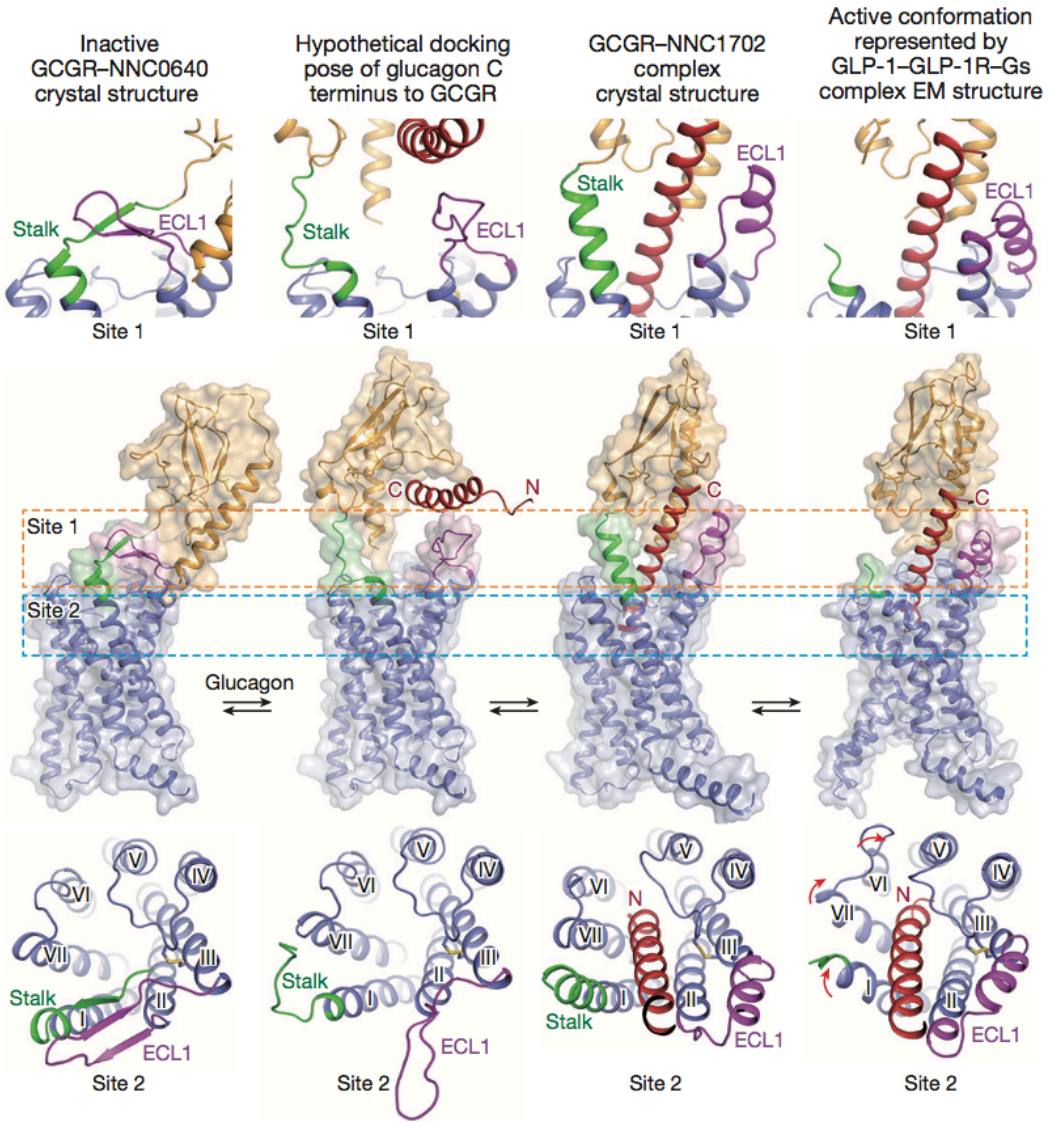

Figure 1.4: Dual binding site trigger for family B GPCRs.[30] Structural and computational data shows that upon the interaction of the C-terminus of the peptide ligand, conformational changes in the stalk (green) and ECL1(purple) allow for the insertion of the N-terminus of the peptide into the transmembrane domain. This triggers additional conformational changes in the juxtamembrane domain and shifts the position of transmembrane helices 1, 6 and 7 outwards to activate the receptor. Figure from [30]

1.2.2 Ligand binding induces conformation changes in the transmembrane domain

The transmembrane domain (TMD) of family B GPCRs serves as the bridge for communication between extracellular ligand binding and intracellular G protein coupling. Studying the variety of full-length family B GPCR structures allows for a more complete picture of the molecular mechanisms of receptor activation. First, the structural conservation in the family B GPCRs appears highest among the cytoplasmic half of TM helices with the extracellular half showing more divergence. This supports the idea that each receptor has a characteristic, highly selective ligand-binding site.[32] The structural similarity of the cytoplasmic half of the helices suggests conformational rearrangements associated with G protein binding upon activation may be more conserved because a large number of GPCRs interact with the same, less diverse G proteins.[26, 27, 31]

As discussed above, the extracellular side of the TMD interacts with the N-terminus of its peptide ligand. In particular, the N-terminus of the peptide, including the N-capping motif that is essential for receptor activation, reaches deep into the TMD. Previous studies showed the N-capping of the peptide is suggested to stabilize the receptor-peptide complex in the second step of the two-domain binding model.[11, 39] Early mutagenesis and photoaffinity studies on family B GPCRs including PTH1R and GLP1R, and the recent structural studies provide evidence supporting the deep insertion of the N-terminus of the peptide ligand.[14, 17, 18, 24, 36, 40-65] The deep insertion of peptide ligands into the TMD causes conformational changes that disrupt stabilized polar networks and allow for G protein binding and activation.[26, 27, 30] Each of the structures shows the conserved central polar network of $R^{2.60}$-$N^{3.43}$-$H^{6.52}$-$Q^{7.49}$, which stabilizes the inactive state along with the conserved HETX motif (Wootten numbering,[32] Figure 1.5). Peptide binding

interactions cause conformational changes that disrupt these networks, leading to a large outward movement of helix 6[26, 27, 30] at the conserved $P^{6.47}$-X-X-$G^{6.50}$ motif. This allows for the insertion of α5 of the $G\alpha_s$ ras-like domain into the receptor (Figure 1.5). These conformational changes are seen in the structure GLP-1R bound to the G_s heterotrimer and one of two different peptide agonists[26, 30] and the calcitonin receptor bound to the G_s heterotrimer and its cognate peptide ligand.[27]

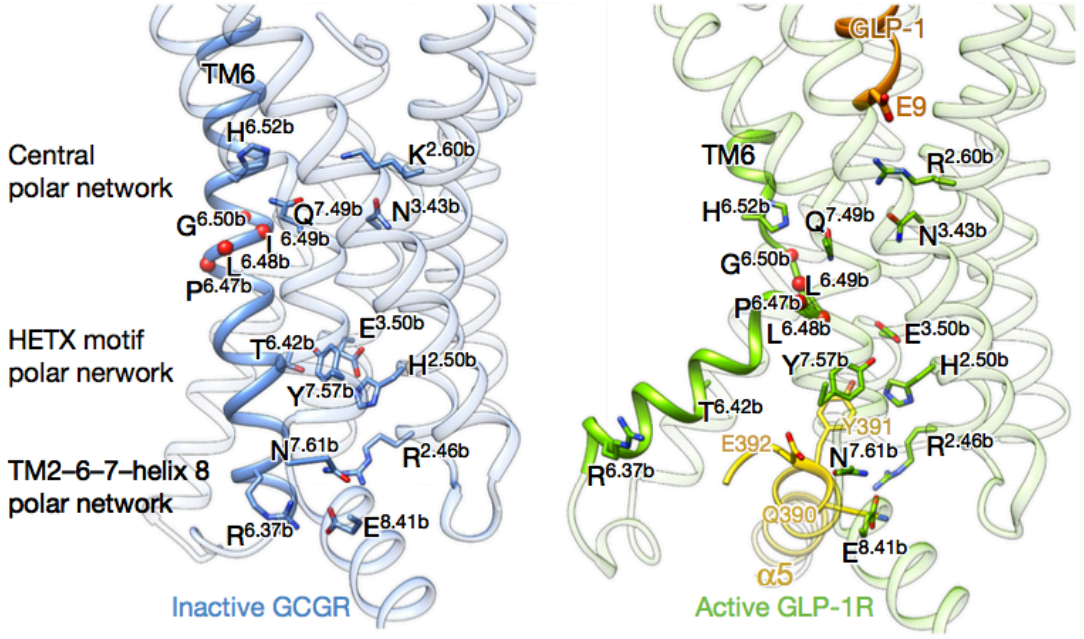

Figure 1.5: Structural comparison of an inactive and an active family B GCPR.[31] The residues of the conserved transmembrane domain networks are shown from the structure of inactive glucagon and active GLP-1R with GLP-1 (orange) bound and the α5 of G_α (yellow). GLP-1 binding disrupts the central polar network, which leads to an outward shift of TM6. This allows for the insertion of α5 the bound G_α subunit. Figure from [31]

1.2.3 G protein coupling and interactions with accessory proteins

Conformational changes in the TMD transduce signals from extracellular domains to intracellular domains, selectively activating various isoforms of G proteins that trigger specific downstream physiological responses.[66] Although intracellular loops have been suggested to be essential for G protein coupling in family B GPCRs, the specific interactions that govern the coupling between GPCRs and G proteins vary from receptor to receptor. Furthermore, most family B GPCRs can recognize multiple G proteins, such as G_s, $G_{q/11}$, and $G_{i/o}$, increasing the complexity of the signaling processes.[67] Many biochemical studies of family B GPCRs have investigated the effect of mutations and truncations in the intracellular loops on activation of different G protein subtypes.[68] Generally, intracellular loop 3 (ICL3) is the key determinant for family B GPCRs to activate G proteins of all types, including G_s, G_q, $G_{i/o}$ and G_{11} (Figure 1.6). The specific regions within each receptor that are responsible for selecting G proteins remain unclear, although accumulating evidence suggests that the N-terminal portion of ICL3 is essential for G_s coupling as well as G_q coupling in some receptors. In support of these biochemical studies, the structures of GLP-1R bound to G_s show extensive contacts between the heterotrimer and helices 2, 3, 5, 6, 7, 8, and all three intracellular loops (Figure 1.5).[31] However, because these structures are all bound to the G_s heterotrimer, the specific interactions between the receptors and different G proteins are still unknown.

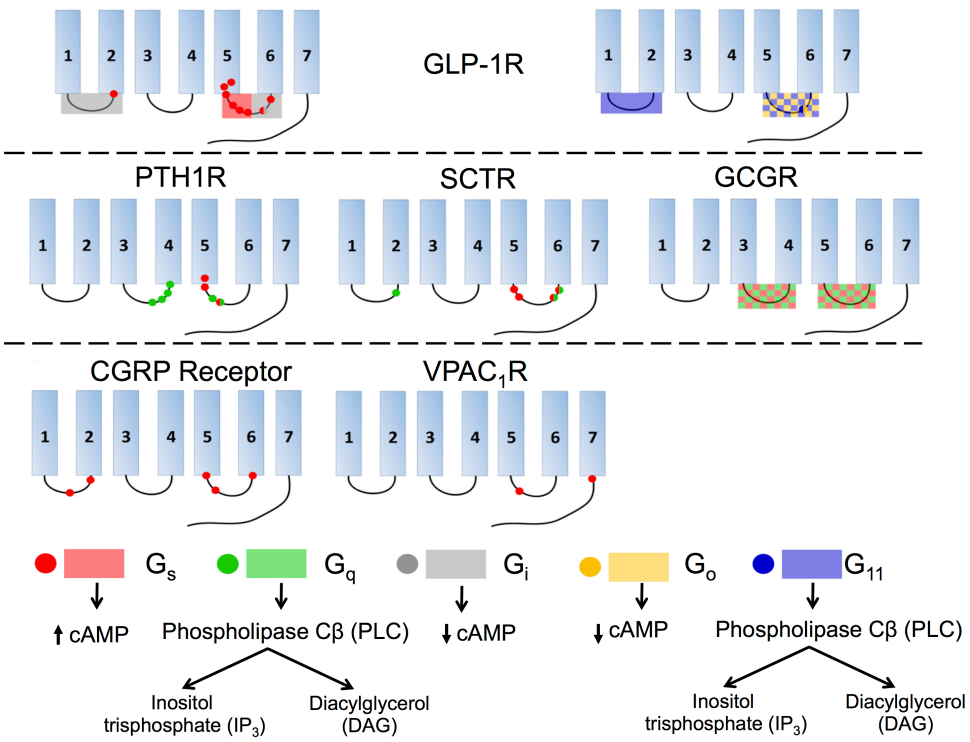

Figure 1.6: Interactions of various isoforms of G proteins with family B GPCRs.[1]

Red indicates G_s, green G_q, gray G_i, yellow G_o and blue G_{11}. Checkered boxes show two G proteins interact with the same loop. The red box on GLP1R ICL3 (top left) shows the N-terminal half of the loop associates with G_s and the C-terminal part of the ICL3 associates with G_i. Figure from [1].

The receptor's G proteins selectivity also depends on the binding of various ligands and accessory proteins. Family B GPCRs associate with a variety of accessory proteins that play important roles in modulating receptor functions, including cell surface expression of receptors, selectivity of hormone ligands, and selection of G protein signaling pathways.[69] These accessory proteins are diverse, including but not limited to receptor-activity-modifying proteins (RAMPs), PDZ domain-containing proteins, cytoskeleton proteins, chaperone molecules, and kinases.[69] Among the accessory proteins that interact with family B GPCRs, the RAMP family is the most extensively studied.[6, 70] There are three isoforms of RAMPs (RAMP 1, 2, and 3), which all have a single transmembrane domain and an 80-amino acid N-terminal domain folded into three helices.[71] Structural studies have shown the binding interface between RAMPs and family B GPCRs,[72] and RAMPs have been shown to modulate receptor trafficking,[73] the G protein coupling profiles[70] and the selectivity of ligands.[23, 71] Because the identification of accessory proteins and studies of their functional roles are still relatively novel, continuous efforts are necessary to explore the roles of these accessory proteins in the signaling processes of family B GPCRs.

While the specific interactions between the peptide hormone and the receptor govern the current understanding of the activation mechanisms of family B GPCRs, other factors influence ligand binding affinity and specificity for a given receptor. Many family B GPCRs bind more than one native ligand, with each ligand eliciting a distinct physiological response. Nonetheless, how the receptor distinguishes between these different pathways remains unclear. In addition, allosteric effects from regions of the receptors not directly involved in ligand binding add complexity to the molecular

mechanism of ligand recognition in family B GPCRs. This work builds on the foundation of structural and biochemical work on family B GPCRs to investigate the molecular mechanisms of parathyroid hormone 1 receptor (PTH1R) ligand binding and receptor activation.

1.3 The role of parathyroid hormone in bone remodeling and osteoporosis

Parathyroid hormone 1 receptor (PTH1R) is a family B GPCR expressed in bone and kidney cells, which binds to two endogenous peptide hormones: parathyroid hormone (PTH) and parathyroid hormone related peptide (PTHrP). PTH1R regulates serum Ca^{2+} and phosphate concentrations through the endocrine hormone PTH and tissue development through the paracrine signaling of PTHrP,[74] Truncated versions of both peptides, PTH(1-34) and PTHrP(1-36), have been shown to be full agonists of PTH1R.[75]

One mechanism of PTH serum Ca^{2+} regulation occurs through the action of the PTH1R receptor expressed in the bone on osteoblasts.[76] PTH binding to PTH1R activates cAMP signaling cascades, which induces bone formation by activating osteoblast precursor cells. It also produces receptor activator of nuclear factor-κB [77] ligand and macrophage colony stimulation factor (M-CSF). RANK ligand binds to its receptor, RANK, which is expressed on osteoclast precursor cells to promote osteoclast formation (Figure 1.7). In combination with the effects of M-CSF, this activates the bone resorption process to break down the bone matrix and increase serum Ca^{2+} concentrations.[78] In addition, PTH1R activation stimulates osteoprogerin (OPG) production, which acts a decoy receptor for RANK ligand.[79, 80] Therefore, OPG binds RANK ligand to prevent it from binding RANK on the osteoclast precursors, thus down-regulating the bone resorption process. PTH activation of PTH1R in the bone activates multiple pathways to

regulate the balance between bone formation and bone resorption, ultimately leading to an increase in bone turnover.[76]

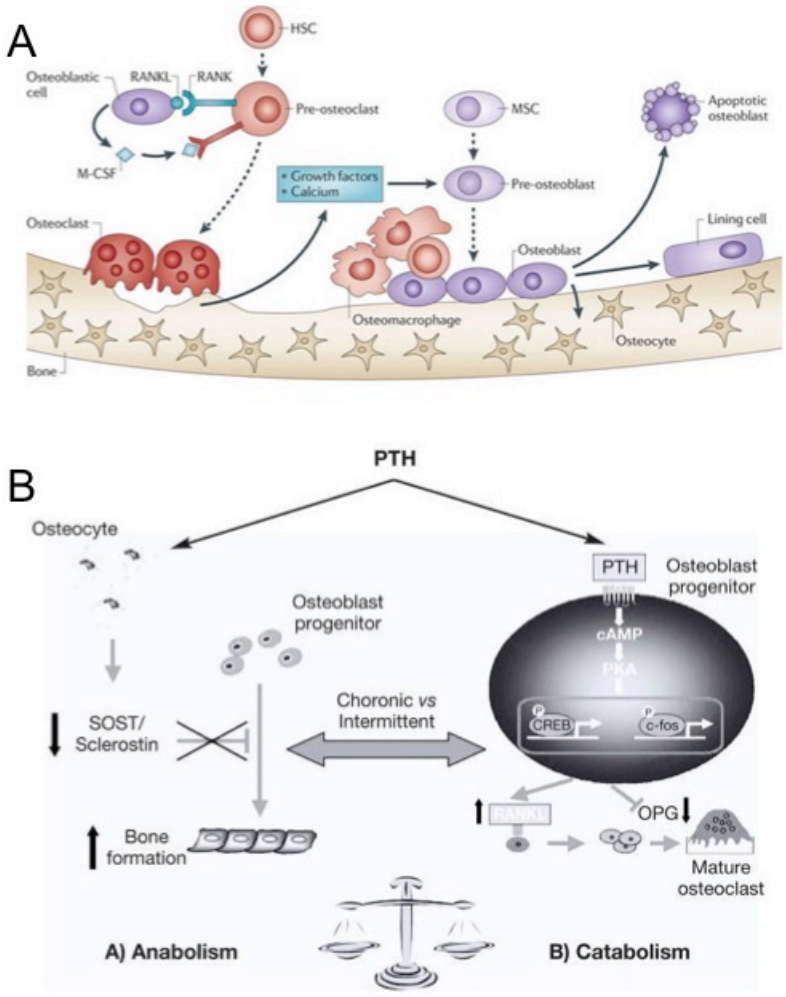

Figure 1.7: PTH regulation of the bone remodeling processing. *(A)*. The bone remodeling process is regulated by the action of osteoclasts causing bone resorption and osteoblasts, which mediate bone formation. Figure from [78]. The signaling between osteoblasts and osteoclasts is mediated by many factors including *(B)*. PTH activation of PTH1R expressed on osteoblasts. The actions of PTH1R depend on the duration of exposure to PTH, with intermittent exposure leading to bone formation and chronic exposure leading to activation of osteoclasts and bone break down. Figure from [76].

The mechanistic details regulating the balance between the anabolic bone formation and catabolic bone resorption processes induced by PTH are not fully understood. However, it is known that constant exposure to PTH leads to increased catabolic responses, which cause increased serum Ca^{2+}, while intermittent exposure to PTH leads primarily to an anabolic response (Figure 1.7B). As such, intermittent injections of PTH have been used as treatments for severe osteoporosis.[81, 82] Teraparatide, PTH(1-34), was one of the first peptide drugs approved for osteoporosis.[75, 83] Since then, abaloparatide, PTHrP(1-36) was also approved for osteoporosis treatment with clinical trials showing an increase in bone mass density compared to Teraparatide.[83-85] Despite the effectiveness of both PTH(1-34) and PTHrP(1-36) as treatment options, the molecular details of how these hormones interact with the receptor are poorly understood. This thesis aims to uncover the molecular details of ligand binding and activation of PTH1R in order to better understand how PTH regulates the bone remodeling process.

1.4 Overview and scope of dissertation

It is clear that family B GPCRs play important roles in metabolic disease through their interactions with peptide hormones. However, the particular mechanisms of ligand binding and G protein activation are poorly understood due to difficulty isolating enough receptors for structural and biophysical studies. Many attempts have been made to purify family B GPCRs, including purification from natural sources,[86] heterologous expression in multiple systems, such as *E. coli*,[87, 88] mammalian cells,[89-93] or insect cells;[25-31, 94] and cell-free synthesis systems.[95] Each of these expression and purification methods produced functional, purified receptors as demonstrated by their ability to bind to the ligand of

interest or activate G proteins. However, in most cases the purified receptors have not been used for biophysical studies to understand the conformational and dynamic changes in receptor structures during activation. In addition, many of these current purification methods focus on producing high quantities of very stable GPCRs for crystallographic studies, which require more stringent conditions than other biophysical techniques.

Recently, our laboratory developed a purification method for family B GPCRs, which directly purifies GPCRs into nanodiscs, which are disc-shaped particles containing a single layer of lipid bilayer that is stabilized by two membrane scaffold proteins.[90, 91] This method reduces the amount of contact of the receptor with detergent and eliminates the need to reconstitute the receptor from a detergent solubilized environment into lipid bilayers.[96] In nanodiscs, the receptor has both the extracellular and cytoplasmic domains available for molecular binding and interactions from the aqueous phase, enabling simultaneous assays for ligand binding and G protein activation.[97-100]

I applied this purification method to investigate the ligand binding and activation of PTH1R. I identified differences in the binding of PTH (1-34) and PTHrP(1-36) to PTH1R and determined that PTH(1-34) binding is affected by extracellular calcium while PTHrP(1-36) is not (Chapter 2). Through ligand binding studies of PTH(1-34) mutants, I proposed PTH(1-34) contains a built-in sensing mechanism for extracellular Ca^{2+} (Chapter 3). The observed Ca^{2+} dependence required residues of both PTH(1-34) and PTH1R, which suggests the presence of a weak binding Ca^{2+}-binding site (Chapter 4). Identifying and understanding how Ca^{2+} modulates of PTH(1-34) binding provides insight into the role of PTH1R activation on the bone remodeling process, which is

testable by future physiological studies of PTH1R activation during the bone remodeling process.

To better understand the details of hormone binding to PTH1R and the observed Ca^{2+}-modulation, I used protein NMR to study changes in the relaxation rate of each residue of PTH(1-34) (Chapter 5). This preliminary data shows changes in the dynamics of PTH(1-34) in the presence of PTH1R, identifying specific residues of PTH(1-34) that become more rigid in the presence of PTH1R. In combination with the structure of a PTH analogue bound to PTH1R, the changes in peptide dynamics under different conditions provide novel insights into the dynamics of peptide binding to a family B GPCR. Furthermore, to better understand PTH1R ligand binding and receptor activation, I developed new experimental methods to study allosteric interactions of PTH1R (Chapter 6). Finally, I summarized of the impact of my work presented in this thesis and the future directions (Chapter 7).

Chapter 2: PTH(1-34) binding to PTH1R shows calcium dependence

The molecular mechanisms of Family B GPCR structure and function are poorly understood because it is difficult to purify large quantities of functional receptors for structural and biophysical assays. To overcome this, we developed a protocol to purify parathyroid hormone 1 receptor (PTH1R) in nanodiscs, which are artificial lipid bilayers held together by two amphipathic, helical membrane scaffold proteins. This chapter uses the nanodisc purification protocol to study ligand binding to PTH1R. PTH1R binds truncated versions of two hormones: parathyroid hormone (PTH(1-34)) and parathyroid hormone related peptide (PTHrP(1-36)). Fluorescence anisotropy ligand binding assays show PTH(1-34), but not PTHrP(1-36), binds to PTH1R tighter in the presence of 15 mM Ca^{2+}. This chapter outlines work investigating this novel calcium dependent binding interaction of PTH(1-34) with PTH1R.

The work outlined in this chapter was published in the paper titled "Parathyroid hormone senses extracellular calcium to modulate endocrine signaling upon binding to the family B GPCR parathyroid hormone 1 receptor" in *ACS Chemical Biology*. [101] The work was performed in collaboration with many lab members. Dr. Yuting Lui collected the preliminary ligand binding and cellular activation data and with Dr. Pam Wang studied the binding of PTH(1-34) to the extracellular domain of PTH1R. Dr. Yingying Cai and Jeremy Sims performed PTH(1-34) binding assays in the presence of varying concentrations of divalent ions and Morgan E. Belina designed and performed flow cytometry ligand binding assays.

2.1 Introduction

There are 15 family B GPCRs with large extracellular domains that bind peptide hormone ligands (Figure 2.1), implicating these receptors in metabolic diseases, such as diabetes, obesity and osteoporosis.[1, 12, 32, 102] Among them, parathyroid hormone 1 receptor (PTH1R) is primarily expressed on bone and kidney cells and mediates cell signaling in response to extracellular stimuli, including two endogenous peptide hormones, parathyroid hormone (PTH) and parathyroid hormone-related peptide (PTHrP).[103] PTH1R regulates serum calcium and phosphate homeostasis via PTH, and tissue growth during embryonic development via PTHrP.[74] Truncated versions of these two hormones, PTH(1-34) and PTHrP(1-36), are full agonists of PTH1R.[75] Both truncated ligands bind PTH1R following the family B GPCR two domain-binding model, where the C-terminus of the peptide binds with high affinity to the receptor's extracellular domain and the N-terminus of the peptide interacts with the receptor's juxtamembrane domain to activate receptor signaling (Figure 2.1).[11, 12, 104, 105] Crystal structures show high affinity binding of the two ligands' C-terminal domain to the receptor's N-terminal extracellular domain and fluorescence studies show receptor activation, following the two domain-binding model.[20, 21, 33] However, this model is not sufficient to explain differences in how PTH(1-34) and PTHrP(1-36) interact with and signal through PTH1R.[106, 107]

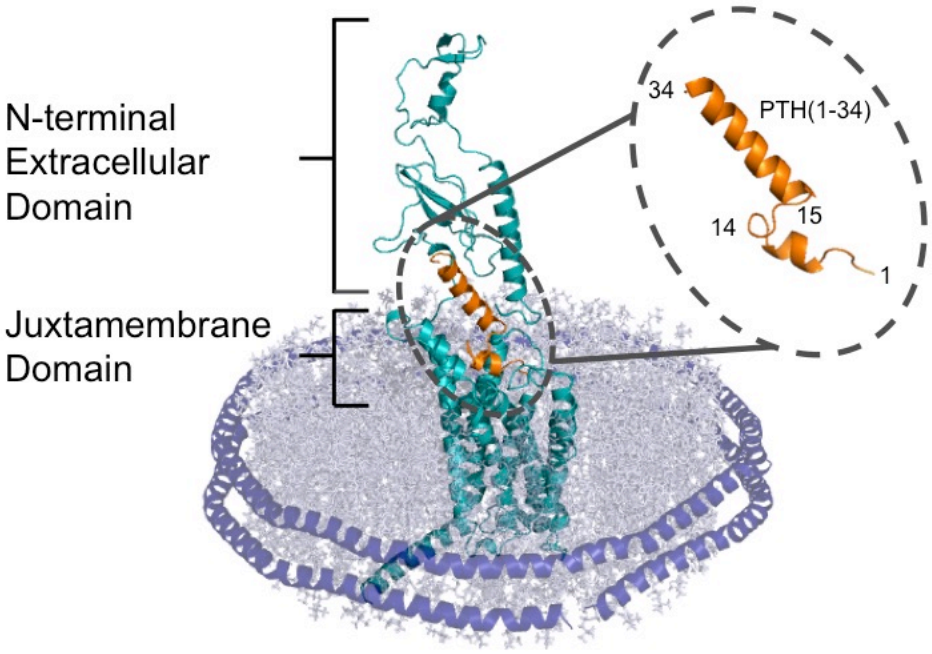

Figure 2.1: Model of PTH(1-34) bound to PTH1R shown in a nanodisc. The C-terminus of PTH(1-34) (orange) interacts with the extracellular domain of the PTH1R (teal), while the N terminus of the peptide hormone interacts with the juxtamembrane domain. The receptor is surround by a lipid bilayer (gray), which is held together with the alpha helical membrane scaffold protein MSP1E3D1 (purple). Dr. Heidi Hendrickson created this homology model of PTH1R in Dr. Victor Batista's group and provided the figure as described in Chapter 4.

Many studies have mutated residues of PTH(1-34) and PTHrP(1-36) in order to develop antagonists, agonists, or biased agonists for specific signaling pathways.[107-111] For instance, the N-terminally truncated peptide PTH(7-34) has been developed as a potent antagonist of PTH1R.[112] In addition, although PTH(1-14) and PTHrP(1-14) show very little binding affinity and efficacy, chemical modifications, such as incorporation of unnatural amino acids or covalent linkage to a lipid molecule, were shown to significantly enhance the efficacy of PTH(1-14) or improve the binding affinity to PTH1R.[110, 111, 113-116]

One specific function of PTH is to regulate bone remodeling, a process that replaces between 5-10% of total bone mass per year and repairs bone fracture and micro-damages to maintain bone health.[80, 117] Bone remodeling contains two processes, bone resorption and bone formation, during which the calcium concentration surrounding the bone tissue fluctuates between 1.5 and 40 mM.[118] An imbalance in regulation of bone remodeling can result in metabolic bone diseases, such as osteoporosis. Paradoxically, intermittent PTH exposure leads to bone formation while prolonged PTH exposure causes bone resorption.[82] Although the exact mechanism of PTH in bone remodeling is not fully understood, intermittent injections of PTH(1-34) and PTHrP(1-36) have been developed as the only FDA-approved hormone treatments for augmenting bone formation in severe cases of osteoporosis.[79, 81, 83-85, 119, 120] It remains largely unexplored how intermittent injection couples with fluctuation of calcium concentrations to achieve the therapeutic effect of PTH(1-34) in modulating bone remodeling for the treatment of osteoporosis.

To understand the therapeutic mechanism of PTH(1-34) and ligand-receptor interactions, PTH1R must be studied at the molecular level. Until recently, studies of PTH1R were primarily carried out in cells or membrane preparations due to the technical difficulty of purifying functional receptors.[87, 89, 90, 92-94, 121-123]

We recently introduced a new method for GPCR purification using nanodiscs, also known as nanoscale apoliprotein bound bilayers (NABBs) or high density lipoproteins (HDLs), which are nanometer-sized lipid bilayers surrounded by two α-helical membrane scaffold proteins (MSP) (Figure 2.1).[100, 124, 125] Using this method to purify PTH1R, we previously studied the ligand binding activity using fluorescence anisotropy and observed that the presence of 15 mM Ca^{2+} increases the binding affinity of PTH(1-34) by one order of magnitude. This chapter will investigate this Ca^{2+}-dependent binding of PTH(1-34) binding to PTH1R through ligand binding assays of PTH(1-34) and PTHrP(1-36) in the presence and absence of 15 mM Ca^{2+}. In order to determine the specificity of the observed Ca^{2+}-binding affect, I measured changes in PTH(1-34) binding in the presence of increasing concentrations of Mg^{2+} and Ca^{2+} and observed PTH(1-34) binding increased to a much greater extent in the presence of Ca^{2+}. Furthermore, I measured the ligand binding affinity of PTH(1-34) to the extracellular domain in the presence and absence of Ca^{2+} and found no change in affinity which suggests either the full length PTH1R or the lipids of the nanodisc are required for Ca^{2+} dependence. Titration curves of detergent purified PTH1R maintained Ca^{2+}-dependent binding of PTH(1-34), confirming that the lipid bilayer of the nanodisc is not required for the Ca^{2+} dependence. Finally, cell based assays showed extracellular Ca^{2+} decreased the amount of cAMP produced by PTH(1-34) activation of PTH1R. In combination, the work presented

in this chapters shows PTH(1-34) Ca^{2+}-dependent binding is specific to PTH(1-34) binding to PTH1R, does not occur with other divalent ions, requires the full length PTH1R and may decrease receptor activation.

2.2 Experimental Materials and Methods

Expression and purification of PTH1R. PTH1R was overexpressed in HEK293S *GnTI*$^-$ cell lines following previously published nanodisc purification protocols.[90] Briefly, PTH1R with the C terminal 1D4 epitope tag was cloned into tetracycline-inducible TetO-pACMV vectors.[126] The vectors were transiently transfected into HEK293S *GnTI*$^-$ cells and treated with 1mg/mL genetecin (AmericanBio, Natick, MA) for rounds of selection. The clonal cell line expressing the highest amount of PTH1R was determined by western blot using a mouse 1D4 monoclonal antibody (University of British Colombia). For purification, 10-cm plates of stable cells lines were induced with 2 μg/μL tetracycline and 0.55 mg/mL sodium butyrate for 48 hrs. The cells were harvested, lysed and the membrane fraction separated by sucrose density gradient ultracentrifugation (110,000 x g). The membrane pellet was solubilized with solubilization buffer (50 mM Tris-HCl pH 7.4, 150 mM NaCl, 5 mM $CaCl_2$, 5 mM $MgCl_2$, 2 mM EDTA, 10% glycerol and 0.5% n-Dodecyl-β-D-maltoside (DDM, ACROS Organics). Membrane scaffold protein (MSP1E3D1)[127] and detergent-solubilized 1-palmitoyl-2-oleoyl-*sn*-glycero-3-phosphocholine (POPC) were mixed with the solubilized membrane proteins, and Bio-beads were added to remove the detergent and initiate nanodisc assembly for 24 hrs. Nanodiscs containing PTH1R were separated from the mixture by single-step affinity purification against the 1D4 epitope.

Fluorescence anisotropy. Fluorescence anisotropy experiments measured the binding affinity between PTH1R-ND and the following peptide ligands: PTH(1-34), PTHrP(1-36). Each of the peptides was labeled with 5/6-fluorescein (FAM) (Figure 2.2) at Lys13, which is solvent exposed and does not perturb receptor binding.[20, 21, 33] The peptides were ordered from Neobiolabs (Woburn, MA), and were weighed and dissolved in anisotropy buffer (50 mM Tris-HCl pH 7.4, 150 mM NaCl, 3mM $MgCl_2$, and 100 μM EDTA). FAM-labeled peptides (50 nM) were titrated with various concentrations of PTH1R-ND (50nM-1000nM) and the anisotropy recorded using a PTI QuantaMaster C-61 two-channel fluorescence spectrophotometer at 30ºC with excitation/emission of 497 nm/518 nm and the slit width of 5 nm. In one experiment, each measurement was averaged over 30 seconds with one reading per second. To measure Ca^{2+}-dependent ligand binding, 15 mM $CaCl_2$ was added to the cuvette at each PTH1R-ND concentration and the fluorescence intensity was recorded again to determine the anisotropy. Each titration curve presented in Figure 1 is average of three or more experiments that were carried out using independent preparations of purified PTH1R-ND. $CaCl_2$ solutions were diluted in anisotropy buffer from a 1 M stock solution of $CaCl_2$ dihydrate, minimum 99.0% in ddH_2O (Sigma). $MgCl_2$ solutions were diluted in anisotropy buffer from 1 M $MgCl_2$ solution (AmericanBio).

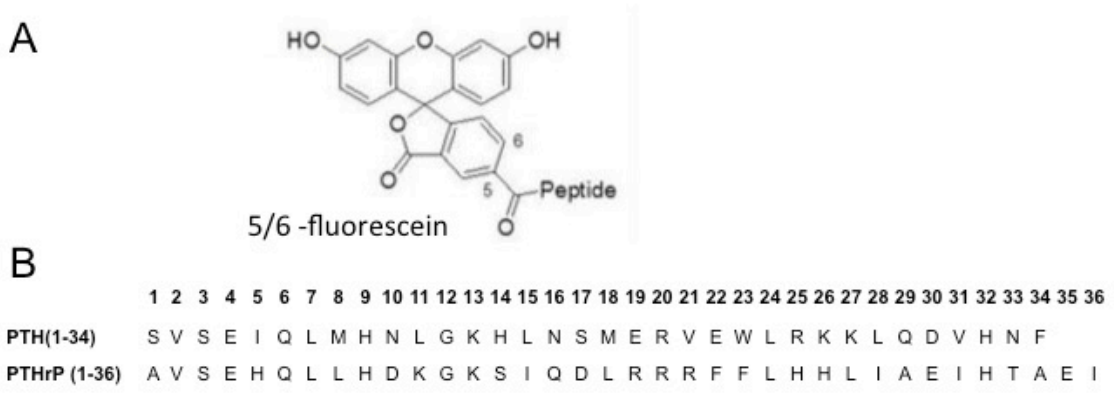

Figure 2.2: Fluorescent peptide design. *(A)*. Structure of 5/6-fluorescein conjugated to Lys13 of PTH(1-34) *(B)*. Sequence of PTH(1-34) and PTHrP(1-36).

Data Analysis. The dissociation constant (K_D) for the equilibrium of the peptide bound receptor (*RP*) dissociating into the free (*P*) and free receptors (*R*) is expressed by Eq. (2.1), which is related to the measured anisotropy values (*r*), as described in Eq. (2.2)[90]

$$K_D = \frac{[R][P]}{[RP]} \tag{2.1}$$

$$r = \frac{(K_D+C_R+C_P)-\sqrt{(K_D+C_R+C_P)^2-4C_RC_P}}{2C_P}\left(r_b + r_f\right) + r_f \tag{2.2}$$

where C_R is the concentration of PTH1R-ND; C_P is the concentration of peptide; r_b is anisotropy of the bound peptide; and r_f is the anisotropy of the free peptide.

In anisotropy assays, free peptides have low anisotropy due to their small size and fast rotation, while peptides bound to PTH1R-ND have high anisotropy due to the large size of the PTH(1-34)-PTH1R-ND complex and slower rotation. Since the size of molecular entities and photochemical properties of the fluorescence probe determine the values of anisotropy, the anisotropy of free peptides (r_f) are approximately the same for each peptide being studied, as is the anisotropy of those peptides bound to PTH1R-ND , as shown in the titration curves for the PTH1R-ND concentration at zero and saturated values. Thus, K_D can be determined by fitting the titration curves for each peptide under various conditions.

Flow Cytometry Titrations. 10 cm plates of HEK293S PTH1R stable cells lines were induced with 2 μg/μL tetracycline and 0.55 mg/mL sodium butyrate for 48 hrs. Cells were lifted from the plates with 1X PBS buffer with 2 mM EDTA. Cells were centrifuged and resuspended in Tris buffer with 1% BSA and counted using a hemocytometer. 400,000 cells were aliquoted into eppendorf tubes on ice. Different concentrations of

PTH(1-34) were added to each aliquot with or without 15 mM Ca^{2+}. Cells were incubated with PTH(1-34)-FAM for 5 minutes on ice and then sorted using an Accuri C6 Flow cytometer. As a control, uninduced cells were similarly harvested, incubated with the different concentrations of PTH(1-34)-FAM with or without Ca^{2+}, and sorted. For each PTH(1-34)-FAM condition, the mean fluorescence intensity was recorded. To determine the K_D of PTH(1-34) in the presence and absence of 15 mM Ca^{2+}, the data was fitted using the saturation binding equation for one site with total binding measured (Eq. 2.3),[128] where *X* is the concentration of PTH(1-34), *Y* is the mean fluorescence intensity measured, B_{max} is the maximum fluorescence of specific binding, *NS* is the non-specific binding, and the background is the measurement with no labeled ligand present. The value of *NS* was obtained from the slope of a linear equation fit to the data from uninduced cells and the background fixed as the mean fluorescence intensity of samples with no PTH(1-34)-FAM added.

$$Y = \frac{B_{max}*X}{(Kd+X)} + NS*X + Background \quad (2.3)$$

Expression and purification of the extracellular domain of PTH1R. The DNA constructs, pETDuet-1-MBP-PTH1R(ECD)-DsbC and pET15b-DsbC were provided by the Schepartz laboratory (Yale University). pETDuet-1 is a dual expression vector that expresses MBP-PTH1R ECD and the chaperone DsbC under two separate promoters.[21, 33] The maltose binding protein (MBP) was fused to the N-terminus of PTH1R ECD to provide additional stability. pET15b-DsbC is a single expression vector that expresses the chaperone DsbC. The His-tagged pET15b-DsbC construct was transformed into *E. coli*

Origami 2 cells, grown to OD_{600}~0.6 and induced for 4 hrs at 37°C with 0.4 mM IPTG. Cells were harvested and lysed by sonication. The clear lysate was incubated with Ni-NTA beads for 1.5 hrs at 4°C. The beads were then washed with 30 mM imidazole and the protein was eluted with 250 mM imidazole. All fractions containing DsbC were pooled and the His-tag was cleaved with biotinylated thrombin to yield pure DsbC. The biotinylated thrombin was removed by passing through streptavidin agarose, collect the supernatant and dialyze again the storage buffer (50 mM Tris-HCl, pH 7.5, 150 mM NaCl, 0.5 mM EDTA and 1 mM DTT).

Purification of MBP-PTH1R ECD was carried out as follows. Transformed *E. coli* Origami 2 cells were grown to OD_{600}~0.6 and induced overnight at 16°C with 0.4 mM IPTG. Cells were harvested and lysed by French press. The lysate was incubated overnight with Ni-NTA beads at 4°C. The beads were then washed with 25 mM imidazole and the protein was eluted with 250 mM imidazole. All fractions containing MBP-PTH1R ECD were pooled and subjected to a disulfide reshuffling reaction in 1 mM each of reduced and oxidized glutathione, 1 mg/ml MBP-PTH1R ECD and 0.4 mg/ml DsbC at 20°C for 20 h. The resultant mixture was incubated with Ni-NTA beads to remove DsbC. The sample was then concentrated and passed twice through a Sephadex 75 gel filtration column. The final pure protein (3.98 mg from a 3 L culture) was stored at -80°C in 50% glycerol.

Fluorescence polarization assays. Flu-PTH(1-34), PTH(1-34) with an N-terminal fluorescein, was prepared by the Schepartz lab. Direct binding experiments between MBP-PTH1R-ECD and Flu-PTH(1-34) were carried out as follows. First, 16 protein

solutions were prepared by 1:1 serial dilutions of MBP-PTH1R ECD in buffer (50 mM Tris-HCl, pH 7.4, 150 mM NaCl) starting with a 200 μM stock. Protein solutions at each concentration in a volume of 18 μL was then transferred in triplicate to a Corning® flat-bottom black polystyrene 384-well plate. Flu-PTH(1-34) (2 μL of a 250 nM stock solution) was then added to each well and incubated at room temperature for 3 hrs. Fluorescence polarization (excitation and emission of 485 nm and 530 nm, respectively) was recorded on an Analyst AD Fluorescence Plate Reader (LJL Biosystems, Sunnyvale, CA). The data were fitted using Eq. 2.4

$$F = F_L + \left(\frac{F_{LP}-F_L}{2[L]_T}\right) \cdot \left([L]_T + [P]_T + K_d - \sqrt{([L]_T + [P]_T + K_d)^2 - 4[L]_T[P]_T}\right) \quad (2.4)$$

where F is the measured fluorescence polarization, F_L is the fluorescence polarization of the free labeled ligand, F_{LP} is the maximum fluorescence polarization of the peptide-protein complex, $[L]_T$ is the total peptide concentration and $[P]_T$ is the total protein concentration.[129]

Detergent purification of PTH1R. PTH1R was overexpressed in HEK293S *GnTI*$^-$ cell lines as previously described.[90] For purification, 10-cm plates of stable cells lines were induced with 2 μg/μL tetracycline and 0.55 mg/mL sodium butyrate for 48 hrs. The cells were harvested in 1X PBS with protease inhibitor tablets (Roche Complete, EDTA free), centrifuged at 500 x g for 5 min and the cell pellet resuspended in 1 mL/plate of solubilization buffer (50 mM Tris-HCl pH 7.4, 150 mM NaCl, 5 mM $CaCl_2$, 5 mM $MgCl_2$, 2 mM EDTA, 10% glycerol and 0.5% n-Dodecyl-β-D-maltoside (DDM, ACROS Organics) for 3 hrs at 4°C. Solubilized membranes were centrifuged at ~110,000 x g to

precipitate cell debris. PTH1R detergent micelles were purified using a single step affinity purification against the 1D4 epitope.

Nanodisc Purification of GLP1R. GLP1R was purified in nanodiscs as described previously.[91] After nanodisc purification GLP1R was used for fluorescence anisotropy assays, as described above. GLP-1(7-37) was labeled with 5(6)-carboxyfluorescein (FAM) at position E21K and Ex-4 was labeled with FAM at L21K. Both FAM labeled peptides were obtained from the Keck Biotechnology Resource Laboratory at Yale University.

Cell-based cAMP assays. HEK293S cells expressing PTH1R were grown and induced in 48-well plates. After ~48 hrs induction, cells were washed with serum-free, Ca^{2+}-free media (Ca^{2+}-free DMEM and 0.2% BSA). Then, cells were treated with 120 μL of cAMP assay buffer (Ca^{2+}-free DMEM containing 200 uM IBMX, 1mg/ml BSA, 35 mM HEPES, pH 7.4), followed by the addition of 60 μL of binding buffer (50 mM Tris-HCl, pH 7.4, 100 mM NaCl, 5 mM KCl, 0.5% FBS and 5% heat-inactivated FBS) containing the peptides (concentrations indicated) and incubated for 30 minutes. Cells were lysed with the lysis buffer (0.1 M HCl and 0.5% Triton X-100), and the cAMP amount under each condition was determined using the Direct cAMP ELISA kit (Enzo Life Sciences).[130] Each point was measured in duplicate in each experiment and each curve represents an average of three experiments.

2.3 Results

2.3.1 Calcium increases PTH(1-34), but not PTHrP(1-36), binding to purified PTH1R

Figure 2.3 and Table 2.1 summarize the results of fluorescence anisotropy assays studying the effect of 15 mM Ca^{2+} on binding of PTH(1-34) and PTHrP(1-36) to PTH1R-ND. Since free peptides in solution have low anisotropy due to fast rotation and those bound to PTH1R-ND have high anisotropy due to slow rotation, fluorescence anisotropy can be used to study binding. In the experiments presented below, the concentration of peptides was kept constant at 50 nM and titrated with purified PTH1R-ND. The titration curve was fitted into a simple two-state equilibrium model, where the unbound state of the receptor interacts with a free peptide to form the bound state (see Experimental Methods). The measured anisotropy values are determined by the size of molecular entities and photochemical properties of fluorescence probe in its local environment.[131] Thus, the anisotropy of free peptides (r_f) were measured independently and the anisotropy of peptides bound to PTH1R-ND [130] were determined using multiple preparations of purified PTH1R-ND ($n \geq 3$) for each peptide. The titration curves can therefore be fitted into Eq (2.2), as described in the Methods section, to determine the dissociation constant (K_D). Figure 2.3 shows titration curve of the average anisotropy ($n \geq 3$) at each tested [PTH1R-ND] the fitted K_D are summarized in Table 2.1

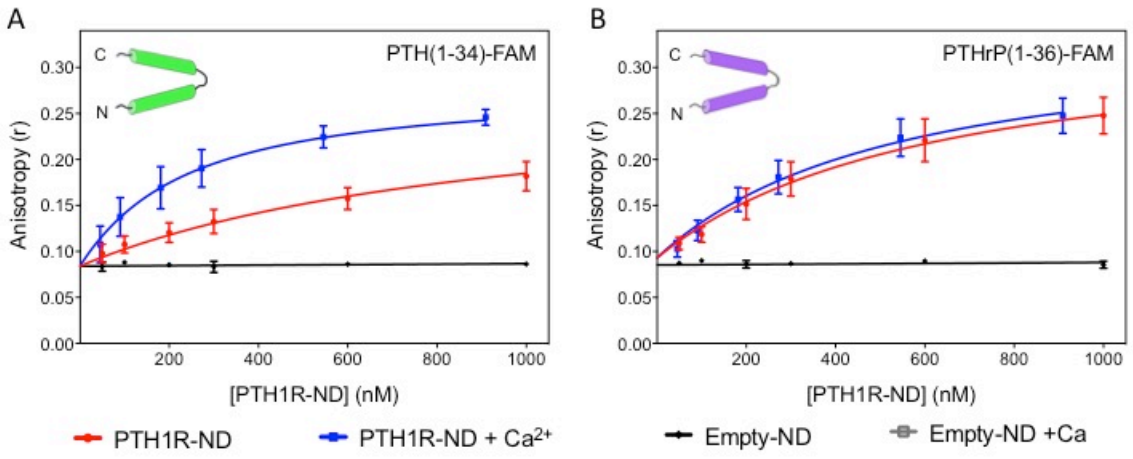

Figure 2.3: Binding of peptide ligands to PTH1R in nanodiscs. Titrations of *(A)*. PTH(1-34) and *(B)*. PTHrP(1-36) with PTH1R in nanodiscs (PTH1R-ND) with (blue) and without (red) addition of 15 mM Ca^{2+} and nanodiscs containing no PTH1R (empty-ND) with (gray) and without (black) addition of 15 mM Ca^{2+}. Data shown are the average of the following number of experiments: PTH(1-34) 0mM Ca^{2+} (n=11), PTH(1-34) 15 mM Ca^{2+} (n=3), PTHrP(1-36) 0 mM Ca^{2+} and 15 mM Ca^{2+} (n=4) with error bars showing standard deviation.

Table 2.1: Binding affinity of PTH1R ligands

	K_D (nM)		K_D (0 mM) /
Peptide	**0 mM Ca^{2+}**	**15 mM Ca^{2+}**	**K_D (15 mM)**
PTH(1-34)	1001 ± 41	204 ± 17**	4.9 ± 0.5
PTHrP(1-36)	568 ± 37	495 ± 31*	1.1 ± 0.1

*p<0.05 and **p<0.001 indicate significant difference in the fitted K_D values for the tested ligand in the presence and absence of 15 mM Ca^{2+}. The ratio K_D (0 mM)/K_D (15 mM) for PTH(1-34) is significantly different from the same ratio for PTHrP(1-36) $p < 0.0001$.

Figure 2.3A shows the titration of PTH(1-34) with PTH1R-ND. At constant concentration of PTH(1-34) (50 nM), the anisotropy increases with PTH1R-ND concentration. With the addition of 15 mM Ca^{2+}, the anisotropy increases more rapidly, and plateaus at a higher maximum anisotropy value (~ 0.25). Fitting the titration curves yields the K_D values of 1001 ± 41 nM (n= 11) with no additional Ca^{2+}, and 204 ± 17 nM (n = 3) with 15 mM Ca^{2+} ($p<0.001$), shown also in Table 2.1. As a control, we titrated PTH(1-34) with nanodiscs containing no receptors (empty-ND) with and without addition of 15 mM Ca^{2+} and the titrations show no change in anisotropy (black and gray, respectively), suggesting the observed binding is specific to the receptor and the Ca^{2+} effect is not due to nanodiscs. Hence, 15 mM Ca^{2+} increases the binding affinity of PTH(1-34) to PTH1R-ND by a factor of 4.9 ± 0.5.

Figure 2.3B shows the titration of PTHrP(1-36) at 50 nM with PTH1R-ND. In both the presence and absence of 15 mM Ca^{2+}, addition of PTH1R-ND increases the anisotropy value; however, the enhancement effect by Ca^{2+} is no longer observed. The control titrations (black and gray) using empty-ND in both the presence and absence of 15 mM Ca^{2+} do not show an increase in anisotropy, suggesting that the binding of PTHrP(1-36) is receptor specific. Fitting the titration curves yields K_D values of 568 ± 37 nM (n=4) without additional Ca^{2+}, and 495 ± 31 nM (n=4) with addition of 15 mM Ca^{2+} (Table 1). Hence, 15 mM Ca^{2+} does not show significant effect on the binding of PTHrP(1-36) to PTH1R-ND with a K_D ratio of 1.1 ± 0.1. The results from Figure 2.3 suggest that ligand binding to PTH1R-ND can be enhanced by 15 mM Ca^{2+} for PTH(1-34), but not PTHrP(1-36).

2.3.2 Calcium does not affect ligand binding to all family B GPCRs

Glucagon like peptide 1 receptor (GLP1R) is a family B GPCR expressed in pancreatic beta cells that is a validated drug target for type 2 diabetes.[132] GLP1R binds glucagon-like peptide 1 (GLP-1), which is secreted as GLP-1 (7-37).[133] In addition, the 39 amino acid peptide exendin-4 (Ex-4) has been developed as a GLP1R agonist for diabetes treatment.[91] To determine if the Ca^{2+}-sensing ability of PTH1R applies to other family B GPCRs, we purified GLP1R in nanodiscs for fluorescence anisotropy assays to test ligand binding in the presence and absence of 15 mM Ca^{2+}. Figure 2.4 shows the binding of GLP-1 and Ex-4 to GLP1R in nanodiscs. The addition of 15 mM Ca^{2+} does not significantly affect the binding affinity of both GLP-1 and Ex-4. These results highlight the uniqueness of the built in Ca^{2+}-sensing ability of PTH(1-34) in binding to PTH1R.

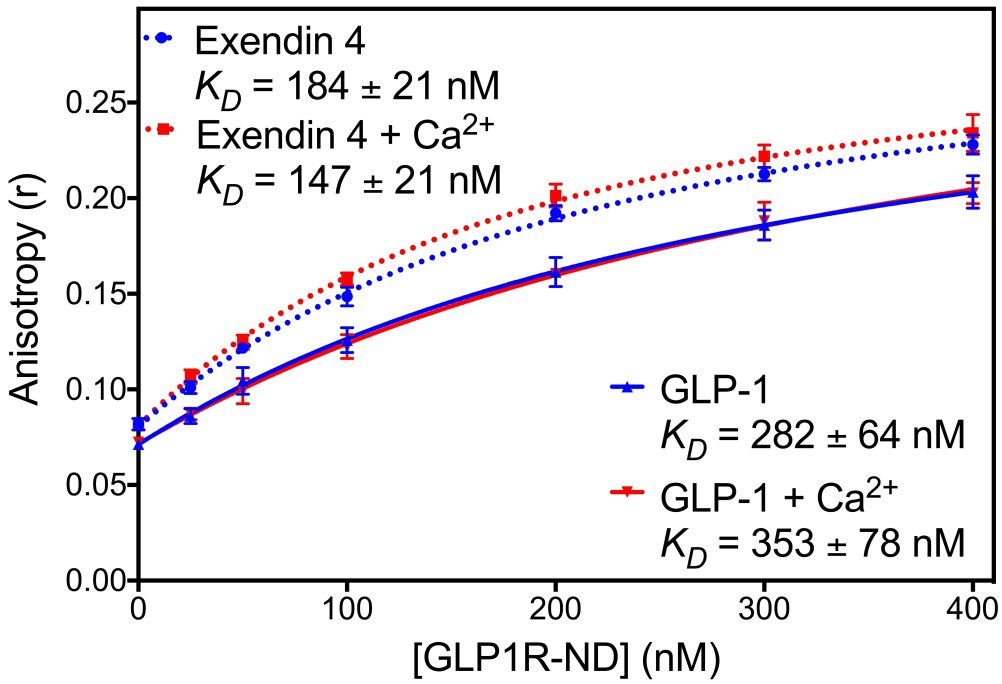

Figure 2.4: Ligand binding to GLP1R. Titration of 50 nM GLP-1 (solid lines) and 50 nM Exendin-4 (dotted lines) with GLP1R in nanodiscs (GLP1R-ND) in the presence (red) and absence (blue) of 15 mM Ca^{2+} show Ca^{2+} does not affect the K_D values of ligand binding to GLP1R ($p>0.05$). Fitted K_D values are indicated in the legend. Data shown are the average of 3 experiments with error bars showing the standard deviation.

2.3.3 Mg^{2+} and Ca^{2+} modulate PTH(1-34) binding to PTH1R differently

In order to directly compare the effect of divalent ions on PTH(1-34) binding to PTH1R-ND, I altered the reaction buffer conditions to exclude Mg^{2+} ions (previously 3 mM $MgCl_2$) and titrated 50 nM PTH(1-34) with PTH1R-ND in the new buffer (50 mM Tris-HCl pH 7.4, 150 mM NaCl, and 100 μM EDTA). I then repeated the titrations to test concentrations of both Ca^{2+} and Mg^{2+} from 0 to 100 mM. Figure 2.5 shows a stronger enhancement of ligand affinity by Ca^{2+} than Mg^{2+}. Fitting yields the K_D values for each concentration of Ca^{2+} and Mg^{2+} (Table 2.2). In the range of concentrations being tested (up to 100 mM), the K_D decreases less than two fold by addition of Mg^{2+} while about 10 fold by addition of Ca^{2+}, supporting selectivity of Ca^{2+} in enhancing binding of PTH(1-34) to PTH1R-ND ($p<0.0001$).

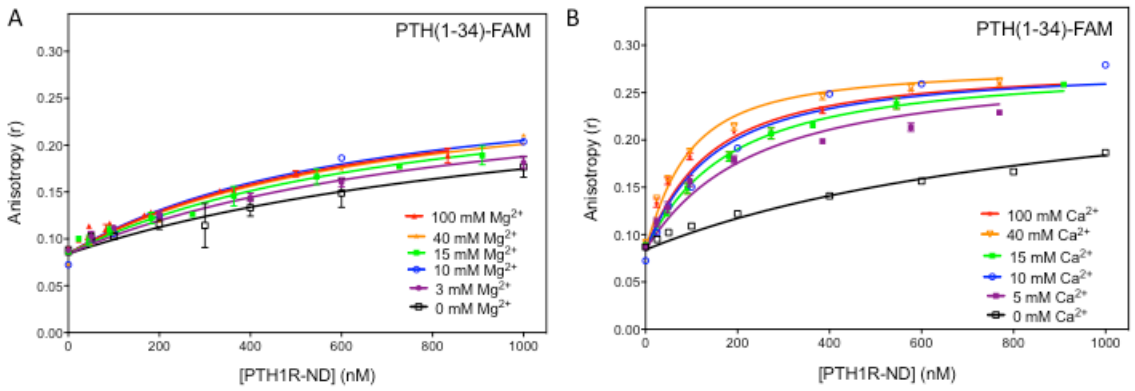

Figure 2.5: Specific Ca^{2+} effect on PTH(1-34) binding to PTH1R-ND. Titration of PTH(1-34)-FAM at 50 nM with PTH1R-ND in Mg^{2+}-depleted buffer (50 mM Tris-HCl pH 7.4, 150 mM NaCl, and 100 μM EDTA) at various concentration of *(A)*. Mg^{2+} and *(B)*. Ca^{2+}. Unless specified, each curve shows the average of three replicates with error bars showing standard deviation. The 10 mM Mg^{2+}, 40 mM Mg^{2+} and 10 mM Ca^{2+} titrations show a single experiment.

Table 2.2: Binding affinity of PTH(1-34) with divalent ion concentrations

Mg^{2+}		**Ca^{2+}**	
Concentration (mM)	K_D (nM)	Concentration (mM)	K_D (nM)
0 (n=6)	1132 ± 59	0 (n=6)	1132 ± 59
3 (n=4)	862 ± 36	5 (n=3)	200 ± 18***
10 (n=1)	600 ± 52	10 (n=1)	114 ±19
15 (n=7)	732 ± 23	15 (n=3)	146 ± 6***
40 (n=1)	650 ± 65	40 (n=4)	61 ± 4
100 (n=4)	628 ± 24	100 (n=4)	105 ± 6***

A one way ANOVA showed the K_D value for each concentration of Ca^{2+} is significantly different than K_D with 0 mM Ca^{2+} ($p<0.0001$), and the K_D value for each concentration of Mg^{2+} is significantly different than K_D with 0 mM Mg^{2+} ($p<0.0001$). ***t tests to compare the K_D values of equivalent concentrations for Mg^{2+} and Ca^{2+} showed $p<0.0001$ for the following comparisons: 3 mM Mg^{2+} and 5 mM Ca^{2+}, 15 mM Mg^{2+} and Ca^{2+}, and 100 mM Mg^{2+} and Ca^{2+}.

2.3.4 Full length PTH1R is required for calcium dependent binding

To explore the role of PTH1R in the Ca^{2+}-dependent binding of PTH(1-34), we used a fluorescence polarization assay to measure the K_D of PTH(1-34) binding to the extracellular domain (ECD) of PTH1R (a.a. 29-187), as used in previous studies.[131, 134-136] The peptide was labeled with fluorescein (Flu) at the N-terminus while the ECD of PTH1R was expressed as a soluble maltose-binding protein (MBP) fusion, MBP-PTH1R-ECD (Figure 2.6). A titration of Flu-PTH(1-34) at 25 nM with MBP-PTH1R-ECD increases the fluorescence polarization as a function of PTH1R-ECD concentration with and without 15 mM Ca^{2+}, yielding a K_D of 977 ± 66 nM, and 958 ± 45 nM, respectively. The results suggest that the ECD in isolation is not sufficient to observe Ca^{2+}-dependent binding of PTH(1-34), suggesting that the transmembrane region of the receptor and/or the lipid membrane is necessary for the observed Ca^{2+}-enhancement effect.

To determine if the lipid membrane is necessary for the Ca^{2+}-dependent binding, we purified PTH1R in detergent micelles for fluorescence anisotropy experiments. The receptor still shows calcium dependent binding in fluorescence anisotropy assays (Figure 2.7). The titration data does not reach saturation, suggesting that the PTH(1-34) binds with lower affinity to PTH1R purified in detergent micelles compared to PTH1R purified in nanodiscs. Thus, PTH1R appears to be less stable in detergent micelles compared to the nanodiscs. Because these titrations do no reach saturation, we are unable to determine the K_D values. However, we observe an increase in ligand binding in the presence of 15 mM Ca^{2+}. This result suggests the lipid bilayer is not required for the Ca^{2+}-sensing ability of PTH. The result also highlights the importance of nanodisc purification to stabilize PTH1R.

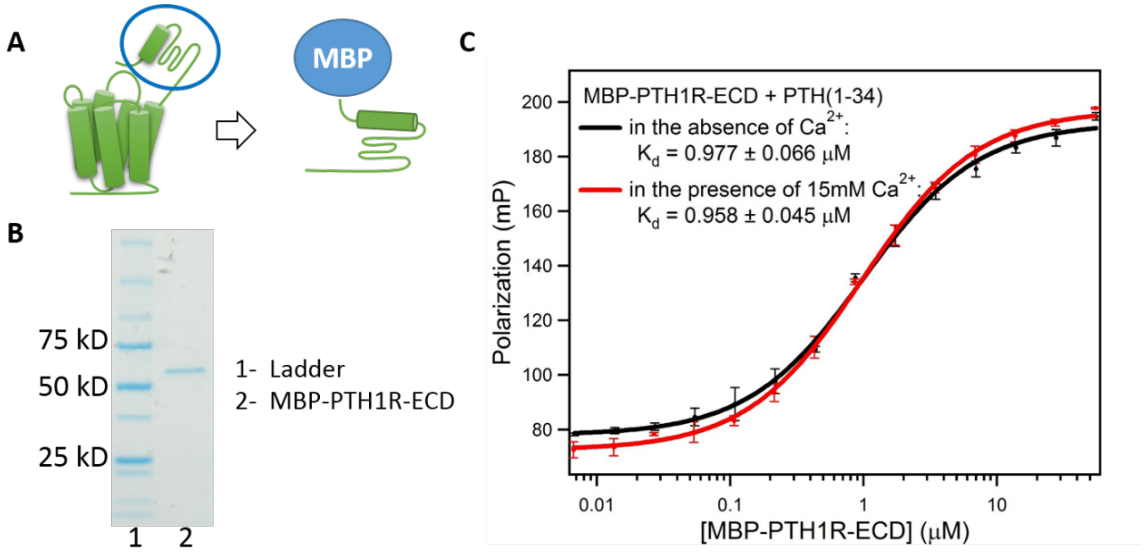

Figure 2.6: Binding of PTH(1-34) to the extracellular domain (ECD) of PTH1R. *(A)*. Construction of MBP-PTH1R-ECD. *(B)*. SDS-PAGE gel of MBP-PTH1R-ECD shows Lane 1, markers; lane 2, purified MBP-PTH1R-ECD (62 kD) *(C)*. Binding of PTH(1-34) to MBP-PTH1R-ECD measured by fluorescence polarization. Each curve shows the average of three fluorescence polarization experiments with error bars showing the standard deviation.

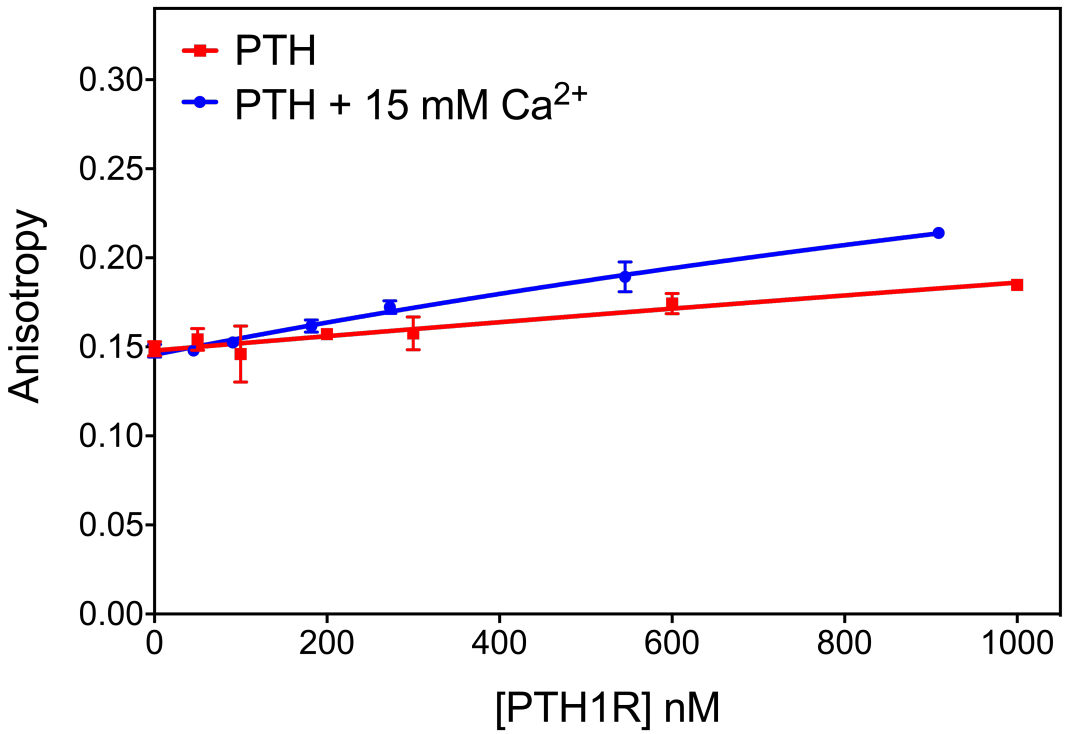

Figure 2.7: PTH(1-34) binding to PTH1R stabilized in detergent micelles. PTH(1-34) binds to PTH1R in solublization buffer (50 mM Tris-HCl, 150 mM NaCl, 5 mM $CaCl_2$, 5 mM $MgCl_2$, 4 mM EDTA, 10% glycerol, 1% n-Dodecyl-β-D-maltoside (DDM)) with (red) and without (blue) 15 mM Ca^{2+}. Each curve shows 3 replicates, with error bars showing the standard deviation.

2.3.5 PTH(1-34) binds to PTH1R on the cell surface with Ca^{2+} dependence

To confirm PTH(1-34) binding to PTH1R is calcium-dependent in a cell-based environment, we implemented a flow cytometry assay, as reported by Bajaj *et al*. [128, 137, 138] We used HEK293S cells overexpressing PTH1R and PTH(1-34)-FAM to measure the mean fluorescence intensity of PTH(1-34) bound to individual HEK293S cells at various concentrations of PTH(1-34) in the presence and absence of 15 mM Ca^{2+}. The results show that the mean fluorescence intensity increases as the concentration of PTH(1-34) increases for both 0 mM Ca^{2+} and 15 mM Ca^{2+} while control experiments using uninduced HEK293 cells without PTH1R overexpression show a relatively small linear increase in fluorescence intensity (Figure 2.8). These results suggest PTH(1-34) binds to PTH1R expressed on the cell surface. The experiments were repeated five times using five separate batches of HEK293S cells grown on different days. The five experiments consistently show that the increase in mean fluorescence intensity as a function of PTH(1-34) concentration occurs with a steeper slope and to a higher maximum intensity for 15 mM Ca^{2+} than for 0 mM Ca^{2+} (Figure 2.8). The titration curves were fitted with a saturation binding model as described in the Methods section to obtain the average (n = 5) K_D values of 122 ± 50 nM with 0 mM Ca^{2+} and 34 ± 17 nM with 15 mM Ca^{2+}, suggesting tighter binding in the presence of 15 mM Ca^{2+} ($p<0.05$). The results support that PTH(1-34) binding to PTH1R in a cell based environment can be enhanced by 15 mM Ca^{2+}, corroborating the results of anisotropy measurements shown in Figure 2.3.

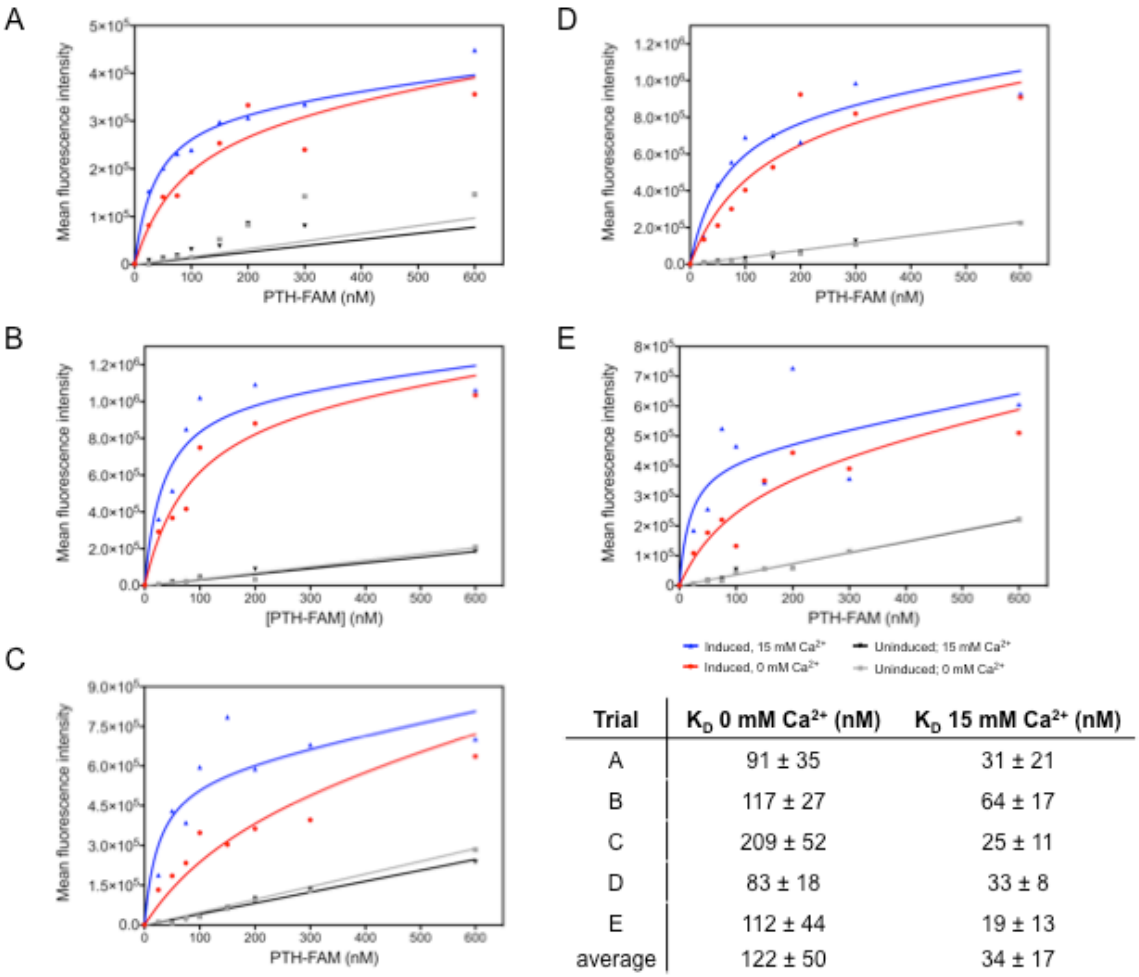

Trial	K_D 0 mM Ca^{2+} (nM)	K_D 15 mM Ca^{2+} (nM)
A	91 ± 35	31 ± 21
B	117 ± 27	64 ± 17
C	209 ± 52	25 ± 11
D	83 ± 18	33 ± 8
E	112 ± 44	19 ± 13
average	122 ± 50	34 ± 17

Figure 2.8: Flow Cytometry titrations of HEK293S cells. Increasing concentrations of PTH(1-34)-FAM were titrated with HEK293S cells induced to overexpress PTH1R in the presence (blue) and absence (red) of 15 mM Ca^{2+}. As a control PTH(1-34)-FAM was titrated with uninduced HEK293S cells in the presence (black) and absence (gray) of 15 mM Ca^{2+}. Each panel represents a single trial using the same batch of HEK293S cell culture performed on the same day. The fitted K_D values for each trial are shown in the table.

2.3.6 Extracellular Ca^{2+} affects PTH(1-34) activation of PTH1R

Ligand binding to PTH1R activates G protein signaling cascades, leading to the production of cAMP. To determine if the calcium dependent binding of PTH(1-34) affects the activation of PTH1R, I performed cAMP assays in the presence and absence of 15 mM Ca^{2+} (Figure 2.9). The addition of 15 mM Ca^{2+} did not affect the potency of PTH(1-34) in activating PTH1R. Control experiments to test the effect of 15 mM Ca^{2+} on cAMP production in the absence of PTH(1-34) show that the cAMP produced decreases from 6.8 ± 2.6 to 0.8 ± 0.2 pmol/mg total protein upon addition of 15 mM Ca^{2+} (Figure 2.9 inset). Upon PTH(1-34) stimulation of PTH1R, the maximum cAMP produced was 276 ± 67 and 154 ± 42 pmol/mg total protein in the absence and presence of 15 mM Ca^{2+}, respectively ($p<0.05$). Thus, these results suggest that although 15 mM Ca^{2+} increases PTH(1-34) binding to PTH1R, it decreases PTH(1-34) activation of PTH1R. However, it is still important to consider a portion of this decrease could be due to the effect of 15 mM Ca^{2+} alone on cAMP production of the cells.

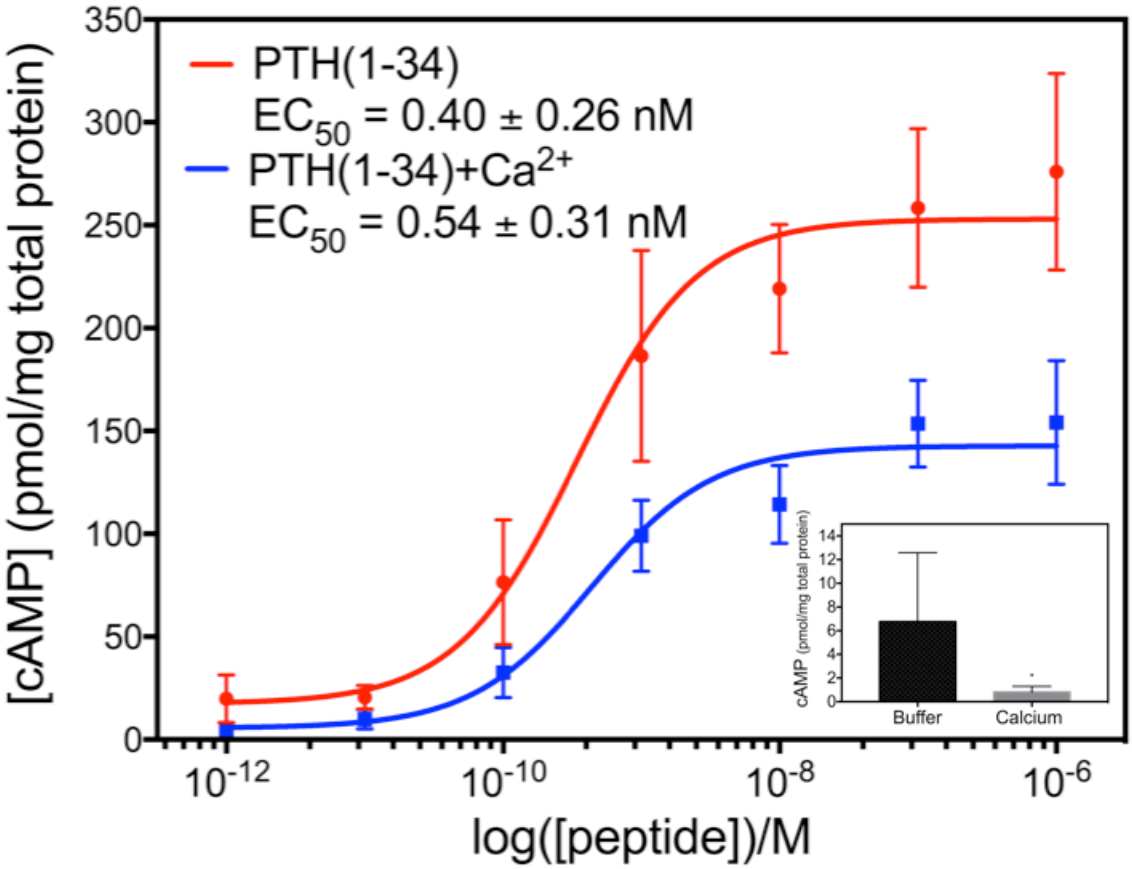

Figure 2.9: PTH(1-34) activates PTH1R in the presence and absence of 15 mM Ca^{2+}. HEK293S cells expressing PTH1R were stimulated with indicated concentrations of PTH(1-34) with 0 mM Ca^{2+} (red) and 15 mM Ca^{2+} (blue) for 30 minutes before harvesting to measure the concentration of cAMP. The addition of 15 mM Ca^{2+} does not change the potency of PTH(1-34) but does decrease the efficacy of PTH(1-34). Dose response curves show the average of 3 experiments with error bars showing standard deviation. Inset shows decrease in cAMP production by 15 mM Ca^{2+} in the absence of PTH(1-34) (n=3) with error bars showing standard deviation($p<0.05$).

2.4 Discussion and conclusions

Using our nanodisc purification method, I observed and investigated the effect of Ca^{2+} on peptide binding to PTH1R-ND. I showed the binding affinity of PTH(1-34), but not PTHrP(1-36), is enhanced 5-fold by 15 mM Ca^{2+}, indicating a built-in mechanism of PTH(1-34) for sensing Ca^{2+} in millimolar concentrations. Such high Ca^{2+} concentrations are relevant in the physiological context of bone remodeling, during which extracellular Ca^{2+} concentrations reach as high as 40 mM.[118] Flow cytometry titrations of HEK293S cells expressing PTH1R show PTH(1-34) binding increases with extracellular Ca^{2+} concentrations in a cellular context, confirming the results from our nanodisc titrations. In addition, PTH(1-34) shows no Ca^{2+}-dependent binding to the extracellular domain (ECD) of PTH1R in isolation, suggesting that the presence of the full receptor is necessary for PTH(1-34) to sense Ca^{2+} in millimolar concentrations. Cell-based cAMP assays show that 15 mM Ca^{2+} decreases the amount of cAMP produced by PTH(1-34) activation of PTH1R. This decrease is greater than that observed when 15 mM Ca^{2+} is added to the cells in the absence of PTH(1-34), suggesting high calcium concentrations may attenuate PTH(1-34) activation of PTH1R. Finally, adjusting the reaction buffer to remove divalent ions shows PTH(1-34) binding affinity is affected by Ca^{2+} concentrations from 5 to 100 mM while the same Mg^{2+} concentrations do not greatly affect PTH(1-34) binding affinities, demonstrating the effect is specific to Ca^{2+}. Our results show that PTH(1-34) has the unique ability to sense Ca^{2+} in millimolar concentrations. The results highlight the remarkable implication that PTH(1-34) has two signaling functions: one in endocrine signaling for PTH1R activation and one in sensing extracellular Ca^{2+} concentrations.

We previously reported a 20-fold enhancement in PTH(1-34) binding to PTH1R-ND with the addition of 15 mM Ca^{2+} based on analysis of titrations under the same conditions but using concentrations of PTH1R-ND only up to 300 nM due to a limited yield of purification.[90] In the current study, we optimized the expression level of the inducible cell lines that stably express PTH1R by additional rounds of antibiotic selection.[139, 140] The optimized cell lines increased the yield 10-fold, reaching 0.75 μg per 10-cm plate of cell culture. The increased yield allowed us to use higher concentration of PTH1R-ND (~1000 nM) in each titration for more reliable data analysis in determining K_D.

In order to better understand the Ca^{2+}-dependent binding of PTH(1-34), I investigated components of PTH1R that might contribute to Ca^{2+}-dependent binding. Because the two domain binding model suggests that C-terminal fragment interacts with the extracellular domain (ECD) of the receptor, we tested the binding of PTH(1-34) to the ECD (Figure 2.6). The results show PTH(1-34) binding to the ECD in isolation shows no Ca^{2+} dependence, which suggests the presence of the transmembrane domain is crucial for the Ca^{2+}-sensing of PTH(1-34). We also obtained experimental data to show that the Ca^{2+}-dependent PTH(1-34) binding to PTH1R does not depend on the lipid bilayer. Using detergent solubilized PTH1R, fluorescence anisotropy assays still show that 15 mM Ca^{2+} can enhance binding of PTH(1-34) (Figure 2.7). The lack of Ca^{2+}-dependent binding using the ECD of PTH1R adds to the growing evidence of allosteric interactions between the two domains of binding for PTH(1-34),[141] thus expanding our understanding of ligand binding in family B GPCRs.

Prior to our studies, the Ca^{2+}-sensing ability of PTH(1-34) was unobservable likely due to the limitations of cell based assays and other purification methods. To determine if PTH1R activation is affected by 15 mM Ca^{2+}, we performed cell-based cAMP accumulation assays to measure PTH(1-34) activation of PTH1R in the presence and absence of 15 mM Ca^{2+}. We observed that 15 mM Ca^{2+} does not significantly affect the potency of PTH(1-34); however, it decreases the amount of cAMP produced from 276 ± 67 to 154 ± 42 pmol/mg total protein (Figure 2.9). The observed decrease in cAMP production in the presence of 15 mM Ca^{2+} potentially provides an a novel understanding about the physiological relevance of the PTH(1-34)'s Ca^{2+}-sensing ability. Physiologically, PTH(1-34) is released into circulation when Ca^{2+} levels are low, leading to bone resorption and Ca^{2+} release. However, PTH(1-34) has opposing effects depending on the duration of exposure. Prolonged exposure to PTH(1-34) breaks down bones to release Ca^{2+} while intermittent exposure leads to increased bone denisty.[80, 81, 119] Despite the importance of PTH(1-34) used as a drug for osteoporosis, the molecular mechanisms defining this paradoxical signaling of PTH are unknown.

While our results do not shed light on the underlying paradox of PTH(1-34)'s role in bone remodeling, they do provide interesting insights. For instance, our ligand binding results show tighter binding of PTH(1-34) in the presence of very high Ca^{2+} and our cAMP results show decreased cAMP production of PTH(1-34) activation of PTH1R with 15 mM Ca^{2+}. Thus, it is possible that the observed Ca^{2+}-dependent binding of PTH(1-34) increases its binding affinity to PTH1R while negatively regulating PTH1R activation to decrease cAMP production. This initial hypothesis requires future

experiments to determine if 15 mM Ca^{2+} affects other aspects of PTH1R signaling in more physiologically relevant experimental systems.

In conclusion, we have highlighted a novel, built-in Ca^{2+}-sensing ability of PTH(1-34), one of two ligands that binds to PTH1R. We determined that the Ca^{2+}-sensing ability of PTH(1-34) requires the full length PTH1R, and is specific to Ca^{2+}. Sequence alignments allowed us to hypothesize the Ca^{2+}-sensing ability of PTH(1-34) involves residues of PTH(1-34) and PTH1R, which will be discussed in chapters 3 and 4. Future studies aided by molecular modeling to investigate these interactions as well as domains of PTH1R that contribute to Ca^{2+}-dependent ligand binding will help elucidate the molecular mechanisms of the ligand binding in PTH1R, facilitating studies to uncover the intricate role of PTH in the bone remodeling process.

Chapter 3: PTH(1-34) senses extracellular calcium to regulate binding and activation of PTH1R

Chapter 2 detailed our investigation into the specificity and general requirements for Ca^{2+}-dependent binding of PTH(1-34) to PTH1R. In order to better understand the mechanisms underlying this Ca^{2+}-dependent binding, this chapter focuses on regions of PTH(1-34) required for this Ca^{2+} dependence. First, we created a pair of chimeric PTH/PTHrP hormones to test if the N-terminus or C-terminus of PTH(1-34) is important for the Ca^{2+}-dependent binding. We found the C-terminal PTH residues 15-34 are required for Ca^{2+} -dependent binding. Furthermore, sequence alignment of PTH(1-34) and PTHrP(1-36) identified two non-conserved glutamic acid residues in the C-terminus of PTH(1-34). Mutating these two residues to alanine decreased the magnitude of the Ca^{2+}-dependent binding but did not remove it. Thus, we hypothesize other residues of PTH(1-34) or PTH1R are also involved to coordinate the Ca^{2+}-dependent binding. These results propose a built-in Ca^{2+}-sensing mechanism of PTH1R, creating a novel understanding of ligand binding interactions to family B GPCRs.

The work outlined in this chapter was published in the paper titled "Parathyroid Hormone Senses Extracellular Calcium To Modulate Endocrine Signaling upon Binding to the Family B GPCR Parathyroid Hormone 1 Receptor" in *ACS Chemical Biology*. [101]

3.1 Introduction

The observed Ca^{2+}-dependent binding of PTH(1-34) is novel for a peptide hormone and unique among family B GPCRs. However, studies have shown cations are important modulators of family A and family C GPCRs. For example, crystal structures show a conserved Na^{+}-binding site that shifts the conformational equilibrium of many family A GCPRs towards the inactive state.[142] In addition, the presence of high concentrations of divalent cations shifted the conformational equilibrium of the Adenosine 2A receptor towards the active state if agonist was present.[142] Furthermore, two family C GPCRs, the calcium sensing receptor (CaSR),[143] and the metabotropic glutamate receptor (mGluR),[144] are modulated by extracellular Ca^{2+}. However, the mechanism of the Ca^{2+} effect on these receptors is distinct from the Ca^{2+}-sensing ability of PTH(1-34). For instance, Ca^{2+} alone activates the CaSR with an EC_{50} value of around 4 mM and binds to a distinct and conserved binding site in CaSRs.[145] The mechanism of the Ca^{2+} effect on mGluR is distinct because Ca^{2+} binds to a specific binding site that include 3 acidic residues of mGluR which modulates the effect of glutamate and other ligands.[146] In contrast to the specificity of Ca^{2+} on PTH(1-34) binding, the Ca^{2+} modulation of mGluR occurs for multiple, small molecule ligands.[146] The existing work studying the effects of Ca^{2+} on the function of family A and family C GPCRs highlights the importance of continued investigation of PTH(1-34) Ca^{2+}-dependent binding to PTH1R. Understanding the molecular details of this effect may provide novel insights into broader GPCR structure and function.

Although the observed Ca^{2+} -dependent binding is specific PTH(1-34), both PTH(1-34) and PTHrP(1-36) have been studied in order to investigate difference in

signaling between the two peptide hormones. Sequence alignment shows that PTH(1-34) and PTHrP(1-36) share 70% similarity and 30% identity (Figure 2.2). Crystal structures (Figure 3.1) show that the C-terminus of both peptides, PTH(15-34) and PTHrP(15-36), are bound to the extracellular domain structurally overlap with backbone root-mean-square deviation (RMSD) of 0.357 Å,[20, 21] suggesting the observed difference in Ca^{2+} dependence is not due to major changes in molecular interactions. Combining the available structural studies with sequences alignment identified non-conserved, negatively charged residues of PTH(1-34) that might be important for Ca^{2+}-dependent binding. This chapter outlines the design and characterization of PTH(1-34) mutants, which identified the novel, built-in Ca^{2+}-sensing ability of PTH(1-34). These studies highlight the uniqueness of a single hormone with dual functions of sensing the extracellular environment and carrying endocrine signals.

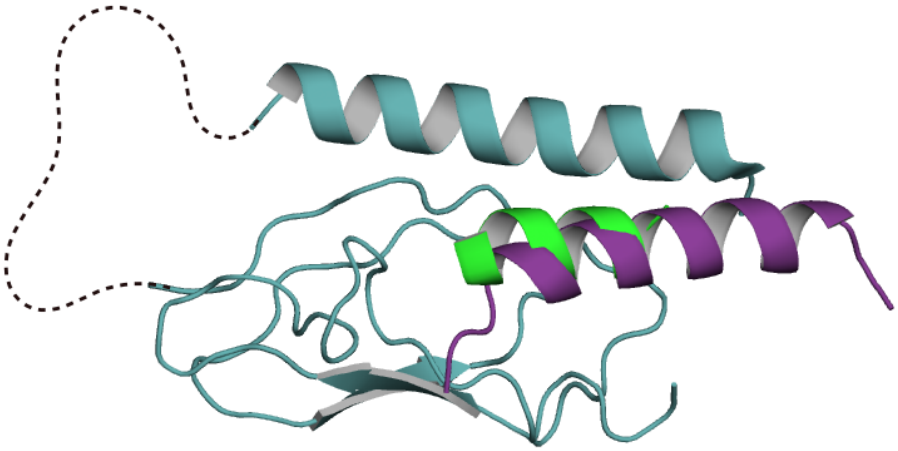

Figure 3.1. Structural alignment of PTH(15-34) and PTHrP(15-36) binding. The structure of the extracellular domain (teal) bound to PTH(15-34) resolved at 1.95 Å (PDB ID: 3C4M, green)[33] and PTHrP(15-36) resolved at 1.94 Å (PDB ID: 3H3G, purple)[20] show the C-terminus of the hormones interact with the extracellular domain similarly, with the largest difference in the C-terminal residues.

3.2 Experimental Materials and Methods

Circular Dichroism Spectroscopy. Tested peptides were prepared in anisotropy buffer (50 mM Tris-HCl pH 7.4, 150 mM NaCl, 3mM $MgCl_2$, and 100 μM EDTA). Ellipticity was measured using a Jasco-J810 spectrophotometer in a quartz cuvette with a 2-mm path length. Each spectrum was repeated 2 times and averaged with a step size of 0.5 nm and a bandwidth of 1.0 nm. Molar ellipticity was calculated from millidegrees using the equation: Molar ellipticity = M*100/(path length*concentration).

Expression and purification of PTH1R. PTH1R was expressed and purified as described in chapter 2.

Fluorescence anisotropy. Fluorescence anisotropy experiments were performed and analyzed as described in chapter 2, with the following peptide ligands: PTH(1-34), PTH(1-36), PTH(1-14)PTHrP(15-36), PTHrP(1-14)PTH(15-36) and PTH(1-34)E19AE22A. Each of the peptides was labeled with 5/6-fluorescein (FAM) at Lys13 (Neobiolabs, Woburn, MA).

Cell-based cAMP study. Cell based cAMP studies were performed as described in Chapter 2 with the following change in binding buffer (50 mM Tris-HCl, pH 7.4, 100 mM NaCl, 5 mM KCl, 2 mM $CaCl_2$, 0.5% FBS and 5% heat-inactivated FBS).

3.3 Results

3.3.1. Design and characterization of mutants ligands to investigate the PTH(1-34) Ca^{2+} dependence

Because PTH(1-34), but not PTHrP(1-36) shows Ca^{2+}-dependent binding, I analyzed a sequence alignment of the two peptides. The canonical Ca^{2+}-binding site is the EF-Hand, which coordinates Ca^{2+} ions through negatively charged Glu and Asp residues.[147, 148] As neither PTH nor PTH1R contain and EF hand sequence, I identified negatively charged residues in PTH(1-34) that were not conserved in PTHrP(1-36) at position 19 and 22 (Figure 3.2). I created the double mutant, PTH(1-34)E19AE22A mutant to remove two non-conserved glutamic acids. Furthermore, it is well accepted the peptide hormones bind to family B GPCRs following the two-domain binding model.[12, 32] To investigate if Ca^{2+}-dependent binding required only one of the domains of PTH(1-34) biding to PTH1R I created two chimeric ligands. These two chimeras contain the N-terminal (1-14) and C-terminal (15-34 or 15-16) fragments of the two native peptides that bind to the extracellular and transmembrane domains, respectively, according to the two domain-binding model.

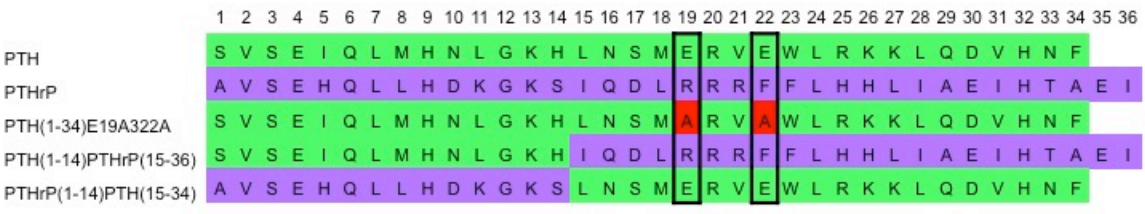

Figure 3.2: Sequence alignment of the PTH and PTHrP ligands under study. PTH residues (green) PTHrP residues (purple), and E19A and E22A mutations (red).

To determine if the chimeric and mutant ligands affected the peptide's secondary structure, I collected circular dichroism (CD) spectra of each of the five tested ligands (Figure 3.3). The observed spectra show expected characteristics of defined secondary structures. The CD spectra of the chimera, PTHrP(1-14)PTH(15-34), which does not bind to PTH1R-ND, shows similar helical content to PTH(1-34). In addition, the spectra of PTH(1-14)PTHrP(15-36) shows similar negative peaks as the PTHrP(1-34) spectra. Thus, the CD spectra show the chimeric and mutant ligands have a defined secondary structure that is influenced primarily by the identity of the C-terminal residues.

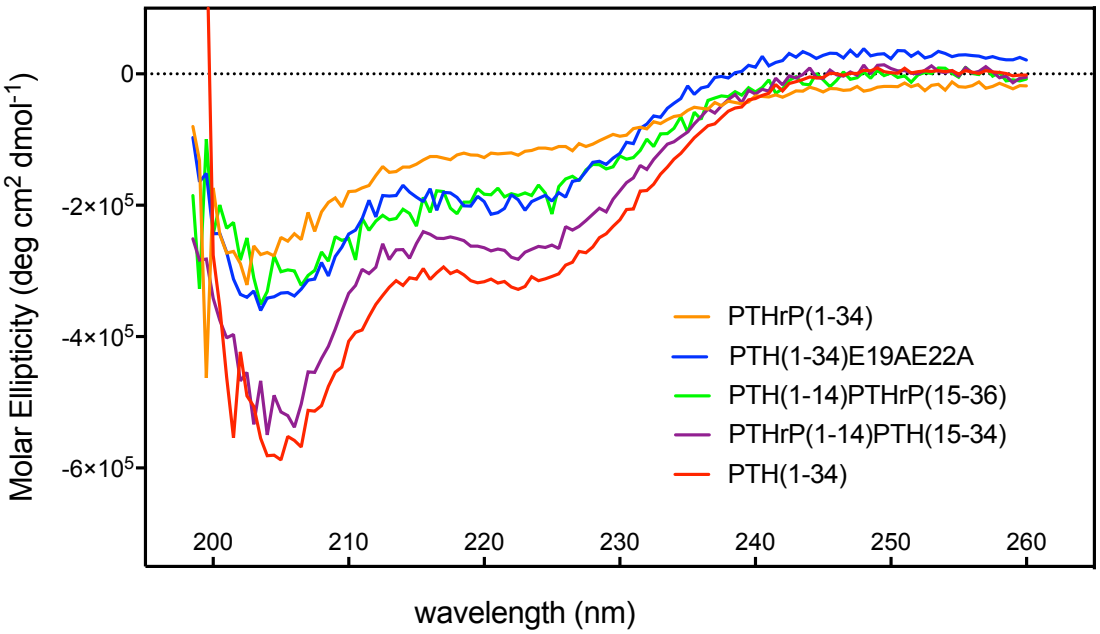

Figure 3.3: Chimeric and mutant peptides maintain their secondary structures. Each of the tested peptides showed defined secondary structures with peaks characteristic of a α-helix at 208 nm and 222 nm or random coil at 200 nm. Each spectrum was repeated twice.

3.3.2. Mutant ligands bind to PTH1R in the presence and absence of calcium

Fluorescence anisotropy assays measured the effect of 15 mM Ca^{2+} on binding of the E19AE22A mutant of PTH(1-34), and two chimeras, PTH(1-14)PTHrP (15-36) and PTHrP(1-14)PTH(15-34) to PTH1R-ND. The peptide concentration was kept constant at 50 nM and titrated with purified PTH1R-ND with the resulting titration curve fitted into a simple two-state equilibrium model, as described above. Figure 3.4 shows the titration curves of the average anisotropy (n≥3) at each tested [PTH1R-ND] the fitted K_D are summarized in Table 3.1.

Figure 3.4B shows the titrations of the E19AE22A mutant of PTH(1-34). Adding PTH1R-ND without Ca^{2+} (red) or with 15 mM Ca^{2+} (blue) steadily increased anisotropy. Addition of 15 mM Ca^{2+} leads to a slightly more rapid increase in anisotropy. The fitted K_D values are 224 ± 18 nM (n = 3) with no additional Ca^{2+}, and 82 ± 6 nM (n =3) with 15 mM Ca^{2+}. As controls, titrating the mutant ligand with empty-ND with (gray) and without additional 15 mM Ca^{2+} shows no binding. Addition of 15 mM Ca^{2+} increases the binding affinity of the mutant to PTH1R-ND by 2.7 ± 0.3 fold (Figure 3.4B, Table 3.1). The results show that the double mutation partially abolishes the Ca^{2+} enhancement.

Figure 3.4C shows the titrations of PTH(1-14)PTHrP(15-36), which does not contain the E19 and E22 residues in the C-terminal domain of PTH(1-34) that contribute to the Ca^{2+} effect shown in Figure 3.4B. Both in the presence and absence of 15 mM Ca^{2+}, the anisotropy values increase with the concentration of PTH1R-ND. Fitting the curves yields the K_D values of 114 ± 5 nM (n = 3) without additional Ca^{2+} and 76 ± 4 nM (n = 3) with the addition of 15 mM Ca^{2+} (Figure 3.4C, Table 3.1). The peptide shows no binding to empty-ND regardless of addition of 15 mM Ca^{2+} (black and gray, Figure 3.4C). The

results show that the chimera largely eliminates the Ca^{2+} effect of PTH(1-34), suggesting that the segment PTH(15-34) likely contains residues responsible for binding to Ca^{2+}, in agreement with the results of the E19AE22A mutant of PTH(1-34).

Figure 3.4D shows the titrations of the second chimera, PTHrP(1-14)PTH(15-34). Surprisingly, adding PTH1R-ND to PTHrP(1-14)PTH(15-34) in both the presence and absence of 15 mM Ca^{2+} leads to only a slight increase in anisotropy, to ~ 0.10 (red) at the highest concentration PTH1R-ND (1000 nM) used in the titration. The maximum anisotropy value does not change from r_f (0.084 ± 0.002), indicating insignificant binding. In the context of the two domain ligand binding model, it is widely accepted that the ligand binding affinity mostly comes from the interaction between the C-terminal domain of the peptide and the extracellular domain of the receptor (K_D in the 1 mM regime)[20, 21] while the binding of the N-terminal domain of the peptide to the juxtamembrane domain of the receptor is relatively weak (K_D in the 100 mM region)[114, 149] Hence, it is surprising that the presence of N-terminal domain PTHrP(1-14) almost abolishes the binding of the C-terminal domain PTH(15-34), although this observation is in agreement with observations reported by Gardella and coworkers.[141] The results suggest more complicated ligand binding interactions than the widely accepted two domains binding model, implying possible allosteric modulations between receptor's extracellular and transmembrane domains via interactions with the peptide ligands.

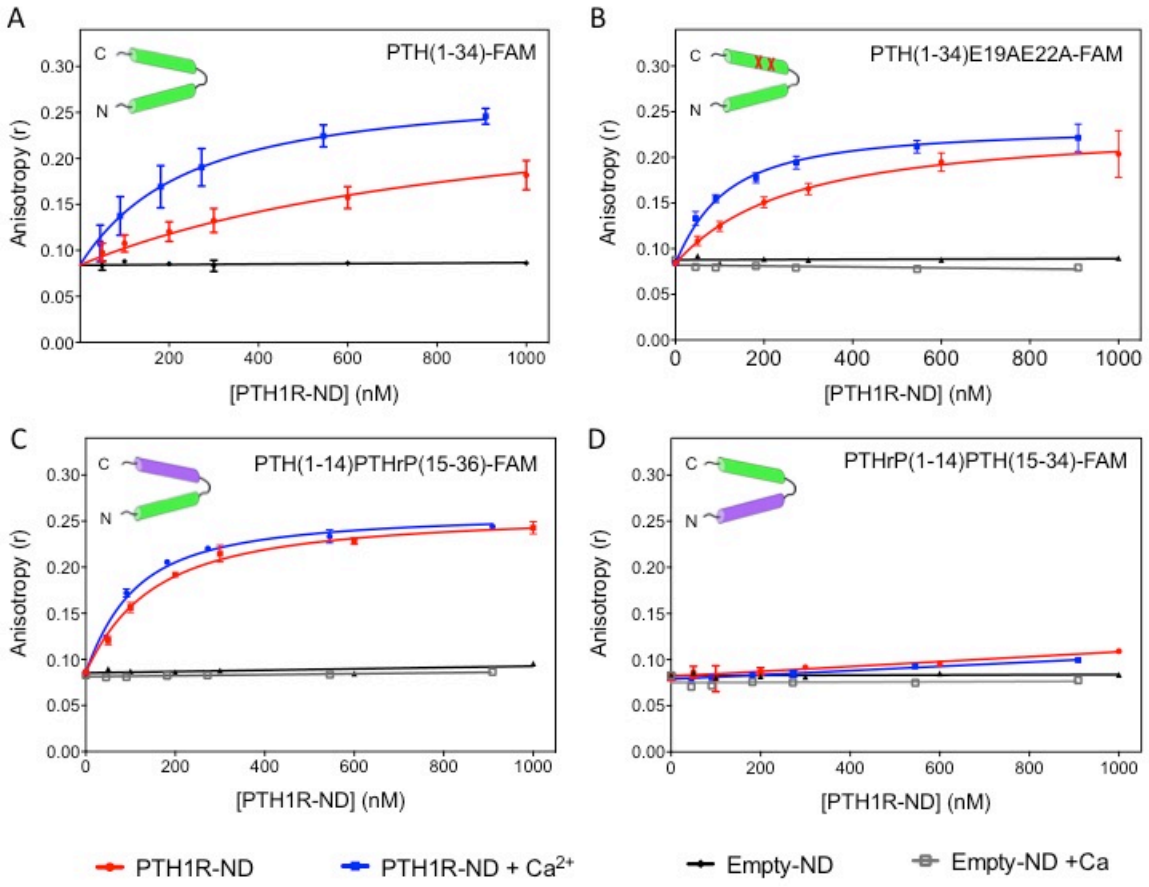

Figure 3.4: Binding of mutant peptide ligands to PTH1R. Titrations of *(A)*. PTH(1-34); *(B)*. PTH(1-34)E19AE22A; *(C)*. PTH(1-14)PTHrP(15-36) and *(D)*. PTHrP(1-14)PTH(15-34) with PTH1R-ND with (blue) and without (red) addition of 15 mM Ca^{2+} or nanodiscs containing no PTH1R (empty-ND) with (gray) and without addition of 15 mM Ca^{2+} (black). Each data point in the titration curves is an average of more than three experiments with error bars showing standard deviation and each experiment was performed using independent preparations of purified PTH1R-ND.

Table 3.1: Binding affinity of the tested PTH1R ligands

	Total Charges	K_D (nM)		K_D (0 mM) /
Peptide	**+ / - (net charge)**	**0 mM Ca^{2+}**	**15 mM Ca^{2+}**	**K_D (15 mM)**
PTH(1-34)	7 / 4 (+3)	1001 ± 41	204 ± 17**	4.9 ± 0.5
PTHrP(1-36)	10 / 5 (+5)	568 ± 37	495 ± 31 *	1.1 ± 0.1
PTH(1-34)E19AE22A	7 / 2 (+5)	224 ± 18	82 ± 6 **	2.7 ± 0.3
PTH(1-14)PTHrP(15-36)	9 / 4 (+4)	114 ± 5	76 ± 4	1.5 ± 0.1
PTHrP(1-14)PTH(15-34)	9 / 5 (+4)	No binding	No binding	NA

*p<0.05 and **p<0.001 indicate significant difference in the fitted K_D values for the tested ligand in the presence and absence of 15 mM Ca^{2+}. The ratio K_D(0 mM)/K_D(15 mM) for PTH(1-34) is significantly different from the same ratio for all of the other tested ligands $p < 0.0001$.

3.3.3. Mutant ligands activate PTH1R in cAMP assays

In order to test the bioactivity of all peptides under study, cell-based cAMP accumulation assays were performed. Upon ligand binding, PTH1R undergoes a conformational change that activates G proteins. The activated G protein then initiates a signaling cascade that causes cAMP production. Thus, cAMP production was measured in stable HEK293S cells overexpressing PTH1R. All of the peptides were able to activate PTH1R (Figure 3.5). Of the tested ligands, PTH(1-34) has the best potency with an EC_{50} = 0.3 ± 0.1 nM. PTH(1-14)PTHrP(15-36) and PTH(1-34)E19AE22A share similar potency values with EC_{50} = 1.7 ± 0.9 nM and EC_{50} = 3.7 ± 1.0 nM, respectively. PTHrP(1-36) and PTHrP(1-14)PTH(15-34), which shows no binding in our fluorescence anisotropy assay, both activate PTH1R at least 10 time worse, with EC_{50} = 9.4 ± 4.3 nM and EC_{50} = 12.0 ± 4.0 nM, respectively.

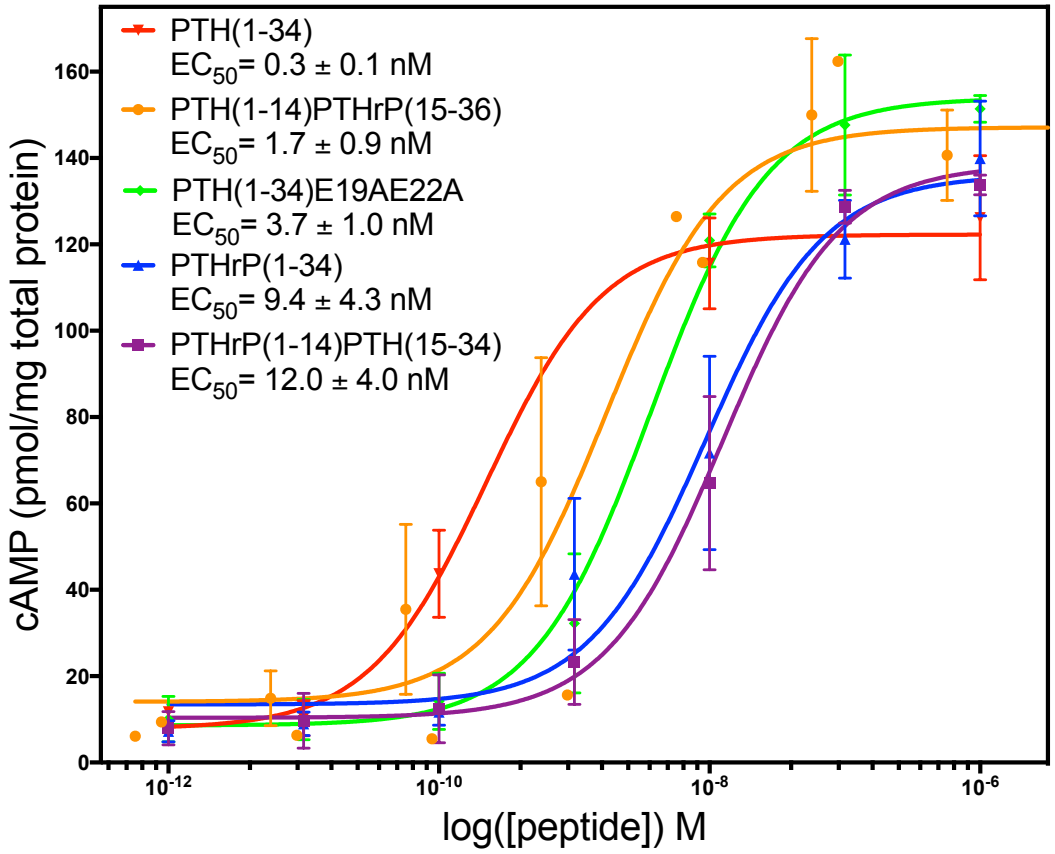

Figure 3.5: Chimeric and mutant peptides activate PTH1R to produce cAMP. HEK293S cells stably expressing PTH1R produce cAMP upon stimulation for 20 minutes with the mutant and chimeric ligands. Each point is an average of 3 different experiments with the error bars showing SEM.

3.4 Discussion and conclusions

Through these studies we determined that the Ca^{2+}-dependent binding requires the C-terminal residues of PTH(15-34), specifically the negatively charged residues Glu19 and Glu22. The results from each tested peptide mutant uncover novel information about both the binding and Ca^{2+}-sensing mechanisms of PTH(1-34).

From the results of the double mutant titration and a comparison of the Ca^{2+} and Mg^{2+} effect, we propose that ligand binding to PTH1R is modulated by a combination of electrostatic interactions and specific Ca^{2+} binding. The E19AE22A mutant removed two non-conserved, negatively charged residues of PTH(1-34) (Figure 3.2), which decreased the Ca^{2+}-dependent peptide binding to PTH1R-ND from 4.9 ± 0.5 fold to 2.7 ± 0.3 fold. In addition, the binding of PTH(1-34)E19AE22A (K_D = 224 ± 18 without 15 mM Ca^{2+} and K_D = 82 ± 6 with 15 mM Ca^{2+}) is tighter than that of wild type PTH(1-34) (K_D =1001 ± 41 without 15 mM Ca^{2+} and K_D = 204 ± 17 with 15 mM Ca^{2+}). The enhanced binding of the mutant is attributed to electrostatic interactions with PTH1R, which has a total of 30 negatively charged residues (Glu or Asp) on the extracellular side (Figure 3.6). The WT PTH(1-34) has a net charge of +3 while the PTH(1-34)E19AE22A mutant has a net charge of +5. Hence, the increase in net positive charges in the mutant can enhance electrostatic interactions with the negatively charged ECD of receptor for a higher binding affinity, which aligns with the Shimizu *et al*. (2002) report of enhanced binding of PTH(1-34)E19R to PTH1R in competitive, radiolabeled ligand binding assays.[150] More importantly, the addition of 15 mM Mg^{2+} has a much lower impact on the binding affinity of PTH(1-34) than the addition of 15 mM Ca^{2+} has. Therefore, our report of enhancement effect of PTH(1-34) binding to PTH1R is not merely electrostatic but specific to Ca^{2+}.

The titration curves of the two chimeric peptides show that residues 15-34 are needed for the Ca^{2+}-dependent binding of PTH(1-34). The results of the PTH(1-14)PTHrP(15-36) titrations show a 1.5 ± 0.1 -fold change in binding with the addition of 15 mM Ca^{2+}, corroborating the double mutant results by implicating residues 15-34 of PTH for Ca^{2+}-sensing (Figure 3.4C). Thus, we expected that the chimera PTHrP(1-14)PTH(15-34) containing the PTH(15-34) would retain the Ca^{2+}-sensing ability of PTH(1-34). However, we observed no binding to PTH1R-ND in both the presence and absence of 15 mM Ca^{2+} (Figure 3.4D). We performed control experiments using circular dichroism spectroscopy and determined this lack of binding is not due to loss of secondary structure of PTHrP(1-14)PTH(15-34) (Figure 3.3). Gardella *et al*. (1995) also observed that PTHrP(1-14) is incompatible with the fragment PTH(15-34), likely because the combination of the two fragments disrupts important allosteric interactions between the N- and C-terminus of PTH(1-34) through PTH1R.[141] In our studies, we further showed that even the addition of 15 mM Ca^{2+} cannot rescue the binding of PTHrP(1-14)PTH(15-34). This loss of binding affinity (Figure 3.4D) highlights the complex nature of the interactions of PTH(1-34) and PTHrP(1-36) with PTH1R. Understanding these interactions may provide a new understanding of the Ca^{2+}-sensing ability of the PTH(1-34) and allostery in family B GPCRs.

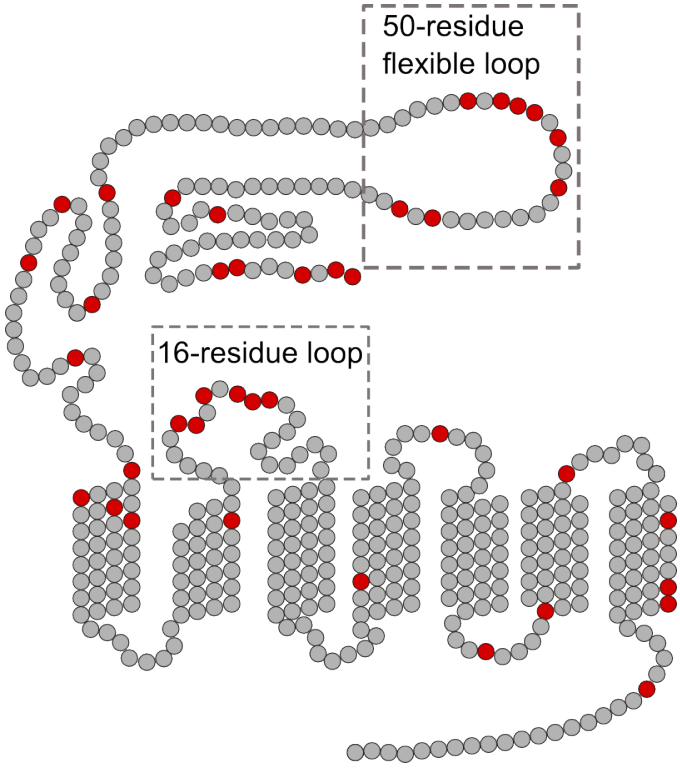

Figure 3.6: Extracellular domain of PTH1R has a high density of negatively charged residues. Snake plot of PTH1R shows negatively charged residues in red, which are clustered towards the extracellular side of the receptor. Two regions of PTH1R not conserved in family B GPCRs are boxed: the 50-residue flexible loop contains 8 negatively charged residues and the 16-residue extracellular loop 1 contains 6 negatively charged residues.

A recent structure of the full length PTH1R bound to a PTH(1-34) analogue (ePTH) resolved to 2.5 Å shows interactions of ePTH with PTH1R.[25] The structure showed the C-terminal resides of ePTH interacts with the extracellular domain of PTH1R similarly to the previously published crystal structure of PTH(15-34) bound to the extracellular domain of PTH1R.[25, 33] While the crystal structure of the extracellular domain shows residues E19 and E22 to be solvent exposed, the structure of full length PTH1R, shows possible interactions for E22. The authors show E22 is involved in a hydrogen bond network through a water molecule with R25 of the peptide and L174 of the stalk region of the extracellular domain. However, this does not negate the hypothesis that E19 and E22 play a role in Ca^{2+}-dependent binding because this structure is a single snapshot a thermostablized receptor.[25] Due to likely conformational flexibility, it is possible that E22 participates in the identified hydrogen bond network in this particular conformation and the presence of extracellular Ca^{2+} disrupts this interaction to favor a different conformation. Thus, further structural and biophysical studies of PTH1R are necessary to identify the mechanisms of the built-in Ca^{2+}-sensing of PTH(1-34).

Chapter 4: Residues of PTH1R modulate the calcium-sensing ability of PTH(1-34)

Chapter 3 highlighted the importance of negatively charged residues in the C-terminus of PTH(1-34) for the observed Ca^{2+}-sensing ability. However, mutating the two non-conserved glutamic acid residues in PTH(1-34) at positions 19 and 22 decreased, but did not completely abolish the Ca^{2+} effect. In this chapter, I identified two, non-conserved loops of PTH1R with a high density of negatively charged residues. I mutated the residues in those loops in order to determine their effect on the Ca^{2+}-sensing ability of PTH(1-34). Fluorescence anisotropy ligand binding assays showed that PTH1R mutations in a non-conserved region of extracellular loop 1 significantly decreased the Ca^{2+}-dependent binding, while mutations in the non-conserved region of the extracellular domain showed a smaller effect on Ca^{2+}-dependent binding. In combination with the mutant PTH(1-34), we observed complete abolition of Ca^{2+} dependence. Thus, we propose that residues of PTH(1-34)E19AE22A and the extracellular loop of PTH1R interact with Ca^{2+} to form a weak binding site.

This work was performed with Allyson Ho, who made the mutant PTH1R DNA vectors, created stable cell lines, and measured the activation and ligand binding of D251A and E252A PTH1R. Shavanie Prashad measured the activation of the 8pt PTH1R and 6pt PTH1R in cell based cAMP assays. The PTH1R homology model was created by Dr. Heidi Hendrickson in collaboration with Dr. Amendra Fernando and Dr. Lucky Ahmed from Dr. Victor Batista's group and Dr. Yingying Cai.

4.1 Introduction

To investigate the molecular mechanism of Ca^{2+} binding, we analyzed the sequence of both the ligand and receptor. We found that PTH(1-34) and PTH1R do not contain a canonical Ca^{2+} binding EF-hand motif, which is typically a sequence of 9 residues providing 7 ligands to coordinate a Ca^{2+} ion with affinity from nM to μM.[147, 148] Previous studies have identified weak Ca^{2+}-binding sites in proteins that do not have a conserved motif but involved negatively charged residues and backbone carbonyls.[151, 152] The weak Ca^{2+} binding we observe with PTH(1-34) in the mM range involves not only E19 and E22 but also likely other negatively charged or polar residues of PTH1R. The observation that Ca^{2+} does not affect PTH(1-34) binding to the PTH1R extracellular domain (ECD) alone supports the hypothesis that both PTH(1-34) and PTH1R are needed for the Ca^{2+} effect (Figure 2.5). Moreover, sequence analysis shows that PTH1R contains a high density of glutamic and aspartic acid residues on the extracellular side of the receptor (Figure 3.6). In particular, PTH1R contains a 50-residue flexible loop on the ECD. This loop is not present in other family B GPCRs, but contains 8 negatively charged residues (Figure 4.1). In addition, the 16-residue extracellular loop 1 (ECL1) also includes 6 negatively charged residues (Figure 4.1). In the recent structure of full-length PTH1R, both the extra-long ECL1 and the 50-residue ECD loop were disordered due to likely flexibility. We hypothesize these negatively charged residues on the extracellular side of PTH1R can potentially coordinate with E19 and E22 of PTH(1-34) in sensing Ca^{2+} in the millimolar range, a concentration relevant in bone remodeling.[118]

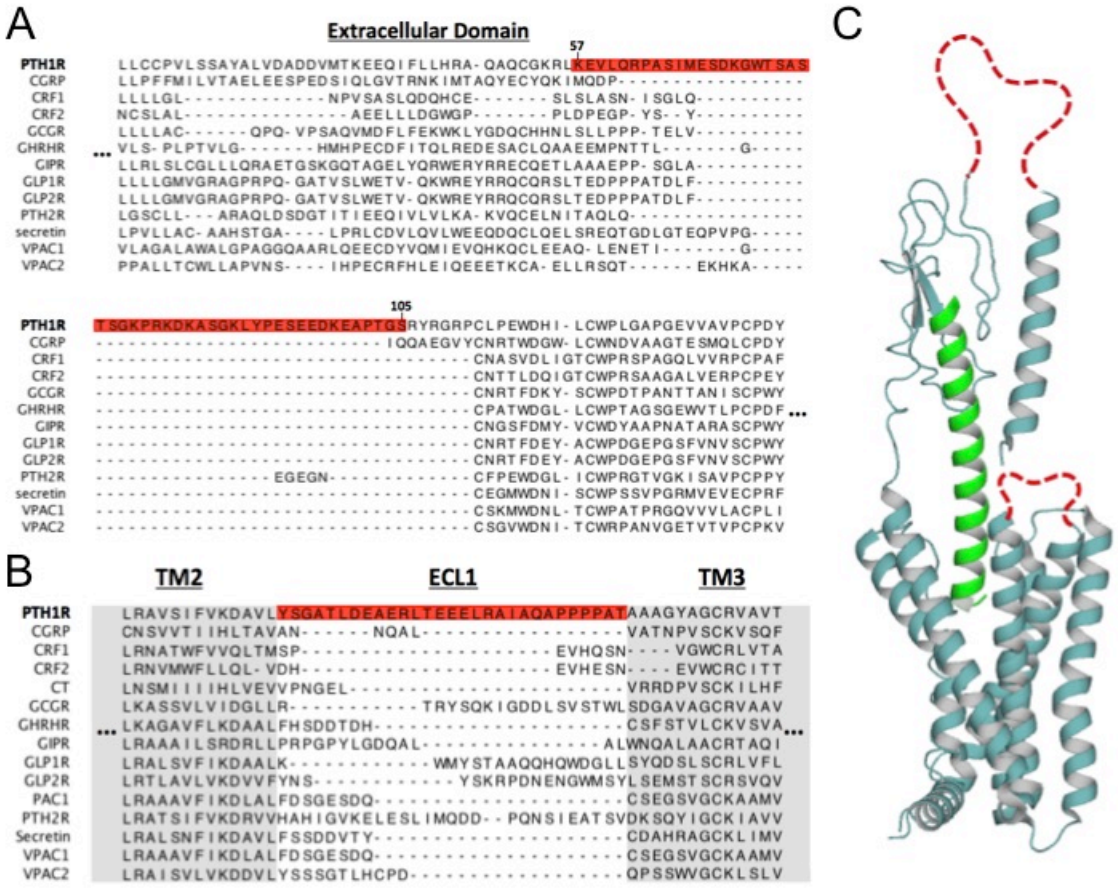

Figure 4.1: Sequence alignment of family B GPCRs. (*A)*. ECD and (*B)*. ECL1 shows two regions of PTH1R (red) that are not present in other family B GPCRS. (*C)*. The crystal structure of PTH1R (teal) bound to a PTH analogue (green) resolved to 2.5 Å does not contain the identified loops in the ECD and ECL1 PTH1R because the loops are likely disordered (red dashed lines) (PDB ID: 6FJ3).[25]

The work presented in this chapter describes the design and expression of PTH1R mutants in HEK293S stable cell lines. These cell lines were used to express the desired mutant PTH1R for nanodisc purification and fluorescence anisotropy ligand binding assays with PTH(1-34) and PTH(1-34)E19AE22A. Results from these ligand binding assays show that ligand binding of PTH(1-34) still exhibits a partial response to extracellular Ca^{2+}. However, titrations with PTH(1-34)E19AE22A show almost no Ca^{2+} response. These results show that residues of PTH(1-34) and PTH1R form a weak Ca^{2+}. binding site. While previous studies on family A GPCRs have proposed allosteric regulation by divalent ions[142] this is the first work to show Ca^{2+} modulates ligand binding of a family B GPCR through specific residues of the ligand and receptor.

4.2 Experimental Materials and Methods

Mutant receptor constructs. The PTH1R mutant of interest with the C-terminal 1D4 epitope tag was cloned into tetracycline-inducible TetO-pACMV vectors.[126, 139] The vectors were transiently transfected into HEK293S *GnTI*$^-$ cells and treated with 1mg/mL genetecin (AmericanBio) for rounds of selection. The clonal cell line expressing the highest amount of PTH1R was determined by western blot and detergent purification using a mouse 1D4 monoclonal antibody (University of British Colombia).

Expression and purification of PTH1R. PTH1R was expressed and purified as described in chapter 2.

Fluorescence anisotropy. Fluorescence anisotropy experiments were performed and analyzed to measure the binding affinity as described in chapter 2, using 20 nM PTH(1-34)-FAM or PTH(1-34)E19AE22A-FAM.

Cell-based cAMP study. Cell based cAMP assays to determine the EC_{50} values for the activation each mutant receptor with PTH(1-34) were performed as described in chapter 3.

Construction of the Computational Model. A structural model of the PTH1R receptor was constructed using the SWISS-MODEL workspace.[153-158] Homology models of the transmembrane and extracellular domain loops were combined with the extracellular domain crystal structure to create a complete model of PTH1R(24-487). The PDB entries 4L6R[159] and 3H3G[20] served as templates for the transmembrane domain (TMD) and extracellular domain (ECD), respectively. The homology models for the TMD and ECD were attached at residue V171 of PTH1R, and the orientation of the ECD was optimized and validated based on agreement with previously published experimental data of PTH(1-34) and PTH1R mutations.[52, 160, 161] The PTH1R and PTH(1-34) hormone ligand (PDB ID: 1HPH)[162] were prepared in the Schrodinger's Maestro 10.2.010 software package.[163] The PTH(1-34) ligand was docked in the PTH1R receptor using the BioLuminate protein-protein docking software (version 2.4.015, Schrodinger, New York, NY). The docked pose was selected based on bound position within the TMD of PTH1R and orientation predicted by experimental data,[161, 164, 165] and one pose was selected that fulfilled both of these criteria.

4.3 Results

4.3.1 Stable cell lines express PTH1R mutants

Sequence alignment of the 15 family B GPCRs shows PTH1R has two non-conserved segments, one in the extracellular domain (ECD) (residues 57-105) and one in extracellular loop 1 (ECL1, residues 240-282) (Figure 4.1). Both of these segments contain a high density of negatively charged Glu and Asp residues with 8 in the ECD and 6 in the ECL1 segment. To determine if the residues in the ECD and the residues in ECL1 are important for Ca^{2+}-dependent binding, I made 3 PTH1R constructs with the indicated acidic residues mutated to alanine: the 8 ECD residues (8pt), the 6 ECL1 residues (6pt) and all 14 residues (14pt). I generated stable cells lines for these 3 constructs and determined the expression levels of the 6pt and the 8pt constructs to be 40% and 80% of the WT PTH1R, respectively (Figure 4.2). These expression levels appeared to be enough to proceed for nanodisc purification. However, the expression of the 14pt construct appeared to be 10% of the wild type. In order to obtain enough of the 14pt purified receptor, we would need to harvest from at least 90 10 cm plates, which is technically not feasible.

To investigate the effect of each negative charge in the non-conserved portion of ECL1, we generated stable cell lines for the individual mutations (D251A, E252A, E254A, E258A, E259A, E260A), performed additional selections to optimize receptor expression and measured expression levels using western blots. We determined the expression levels of each mutant ranged from 50% - 150% of the WT PTH1R (Figure 4.2B).

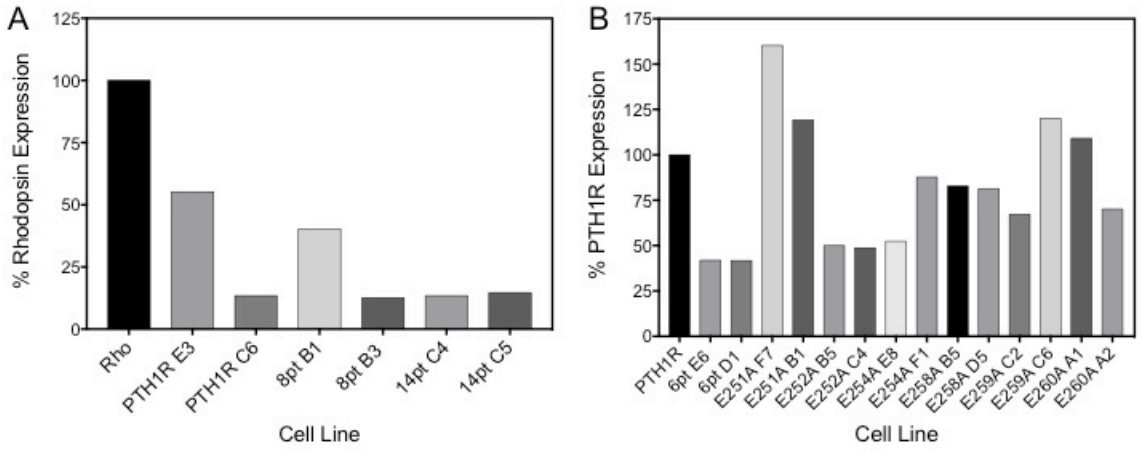

Figure 4.2: Expression levels of established stable cell lines. Expression levels quantified from western blots of cell lines (*A)*. relative to previously established Rhodopsin stable cell line and (*B)*. relative to the PTH1R E3 cell line. Each bar shows quantification from a single experiment.

4.3.2 Calcium affects PTH(1-34) binding to PTH1R mutants

In order to determine the effect of the alanine scanning mutations on the Ca^{2+}-sensing ability of PTH(1-34) binding, we purified each mutant in nanodiscs for fluorescence anisotropy experiments. I titrated 20 nM of PTH(1-34)-FAM with the desired receptor and fit the resulting titration curve to the binding equation for fluorescence anisotropy. Previous experiments with PTH1R used 50 nM PTH(1-34)-FAM. The titrations here used a lower concentration of ligand (20 nM) and 0 mM Mg^{2+} in the anisotropy buffer in order to observe the most accurate binding affinities. PTH(1-34) bound WT PTH1R with K_D = 716 ± 83 nM with 0 mM Ca^{2+} and K_D = 98 ± 11 nM with 15 mM Ca^{2+} (Figure 4.3A, Table 4.1). The ratio between the K_D values (0 mM Ca^{2+} / 15 mM Ca^{2+}) is 7.3 ± 1.2 (Table 4.1).

Titrating PTH(1-34) with the 8pt PTH1R mutant yielded K_D = 668 ± 48 nM with 0 mM Ca^{2+} and K_D = 123 ± 11 nM with 15 mM Ca^{2+} (Figure 4.3B, Table 4.1). The ratio between the K_D values (0 mM Ca^{2+} / 15 mM Ca^{2+}) is 5.4 ± 0.6 (Table 4.1). This decreased ratio compared to WT PTH1R shows the negatively charged residues of the flexible loop on the extracellular domain may play a role in Ca^{2+}-dependent binding.

The titration of PTH(1-34) with the 6pt PTH1R mutant yielded K_D = 442 ± 62 nM with 0 mM Ca^{2+} and K_D = 123 ± 17 nM with 15 mM Ca^{2+} (Figure 4.3C, Table 4.1). The ratio between the K_D values (0 mM Ca^{2+} / 15 mM Ca^{2+}) is 3.4 ± 0.7 (Table 4.1). These results suggest that the residues in the 6pt loop affects the binding of PTH(1-34) and the Ca^{2+}-dependent binding of PTH(1-34). However, we do not see a complete abolishment of the Ca^{2+} dependence of PTH(1-34), which suggests that additional residues of either PTH1R or PTH(1-34) are involved in Ca^{2+}-dependent binding . Due to low expression rates of the 14pt PTH1R mutant, we were unable to purify high enough quantities to determine the binding affinity of PTH(1-34) to the receptor. Thus, the potentially additive effect of having both the 8pt and the 6pt mutants together was not tested.

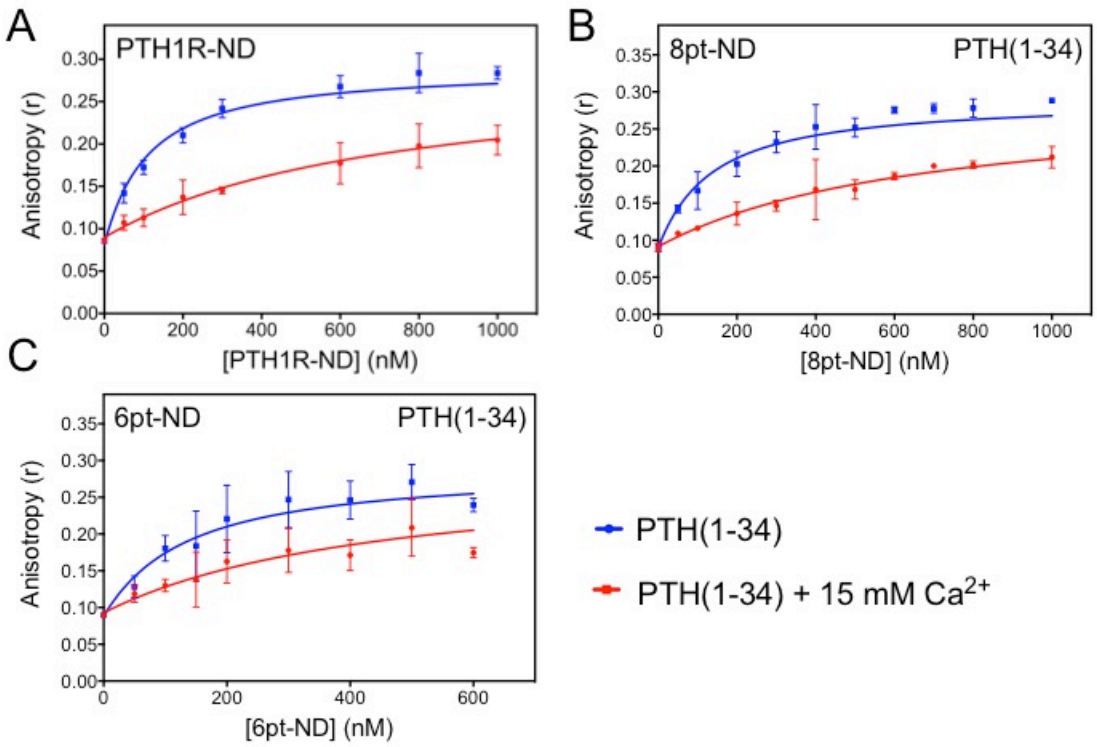

Figure 4.3: Mutant PTH1R binds PTH(1-34). Fluorescence anisotropy titrations of 20 nM PTH(1-34)-FAM with (*A*). WT PTH1R, (*B*). 8pt PTH1R and (*C*). 6pt PTH1R with 0 mM Ca^{2+} (red) and 15 mM Ca^{2+} (blue). PTH(1-34) binds to each receptor and this binding is affected by the presence of 15 mM Ca^{2+}. Each titrations shows n=3 with error bars showing the standard deviation.

Table 4.1: Binding affinity of PTH(1-34) to WT PTH1R and PTH1R mutants

	K_D (without Ca^{2+}) nM	**K_D (with Ca^{2+}) nM**	**Ratio (with/without)**
PTH1R	716 ± 83	98 ± 11	7.3 ± 1.2
8pt PTH1R	668 ± 48	123 ± 11	5.4 ± 0.6
6pt PTH1R	442 ± 62*	123 ± 17	3.4 ± 0.7 **

*p<0.05 and **p<0.001 indicate significant difference in the value for the 6pt PTH1R mutant compared to WT PTH1R. For each receptor, the K_D values with Ca^{2+} are significantly different from K_D values without Ca^{2+} $p < 0.001$.

4.3.3 Calcium shows differential effects on PTH(1-34)E19AE22A binding to PTH1R mutants

As outlined in chapter 3, we hypothesized that the built-in Ca^{2+}-sensing ability of PTH(1-34) involved residues of both PTH(1-34) and PTH1R. The results in sections 3.3.2 and 4.3.2 support this, because mutations to negatively charged residues of PTH(1-34) or PTH1R show partial abolishment of the Ca^{2+}-sensing ability of PTH(1-34). To test our hypothesis that both are involved, I performed ligand binding assays of PTH(1-34)E19AE22A with the 6pt PTH1R and 8pt PTH1R mutants.

First, titrating 20 nM of PTH(1-34)E19AE22A with the WT PTH1R mutant yielded K_D = 338 ± 58 nM with 0 mM Ca^{2+} and K_D = 246 ± 45 nM with 15 mM Ca^{2+} (Figure 4.4A, Table 4.3). The ratio between the K_D values (0 mM Ca^{2+} / 15 mM Ca^{2+}) is 1.3 ± 0.4 (Table 4.2). These values are different than those presented in section 3.3.2 both because other divalent ions were removed from the anisotropy buffer and the concentration of PTH(1-34)E19AE22A was decreased to 20 nM for more accurate assays.

The binding of 20 nM of PTH(1-34)E19AE22A with the 8pt PTH1R mutant showed K_D = 447 ± 55 nM with 0 mM Ca^{2+} and K_D = 307 ± 37 nM with 15 mM Ca^{2+} (Figure 4.4B, Table 4.2). The ratio between the K_D values (0 mM Ca^{2+} / 15 mM Ca^{2+}) is 1.5 ± 0.3 (Table 4.2). This shows that the combination of PTH(1-34)E19AE22A and the 8pt ECD mutant show similar Ca^{2+}-dependent binding as PTH(1-34)E19AE22A binding to WT PTH1R.

Finally, to study the effect of the 6pt PTH1R we titrated 20 nM of PTH(1-34)E19AE22A with the 6pt PTH1R mutant and observed K_D = 338 ± 58 nM with 0 mM

Ca^{2+} and K_D = 246 ± 45 nM with 15 mM Ca^{2+} (Figure 4.4C, Table 4.2). The ratio between the K_D values (0 mM Ca^{2+} / 15 mM Ca^{2+}) is 1.3 ± 0.4 (Table 4.2). These values are similar to PTH(1-34)E19AE22A binding to WT and 8pt PTH1R.

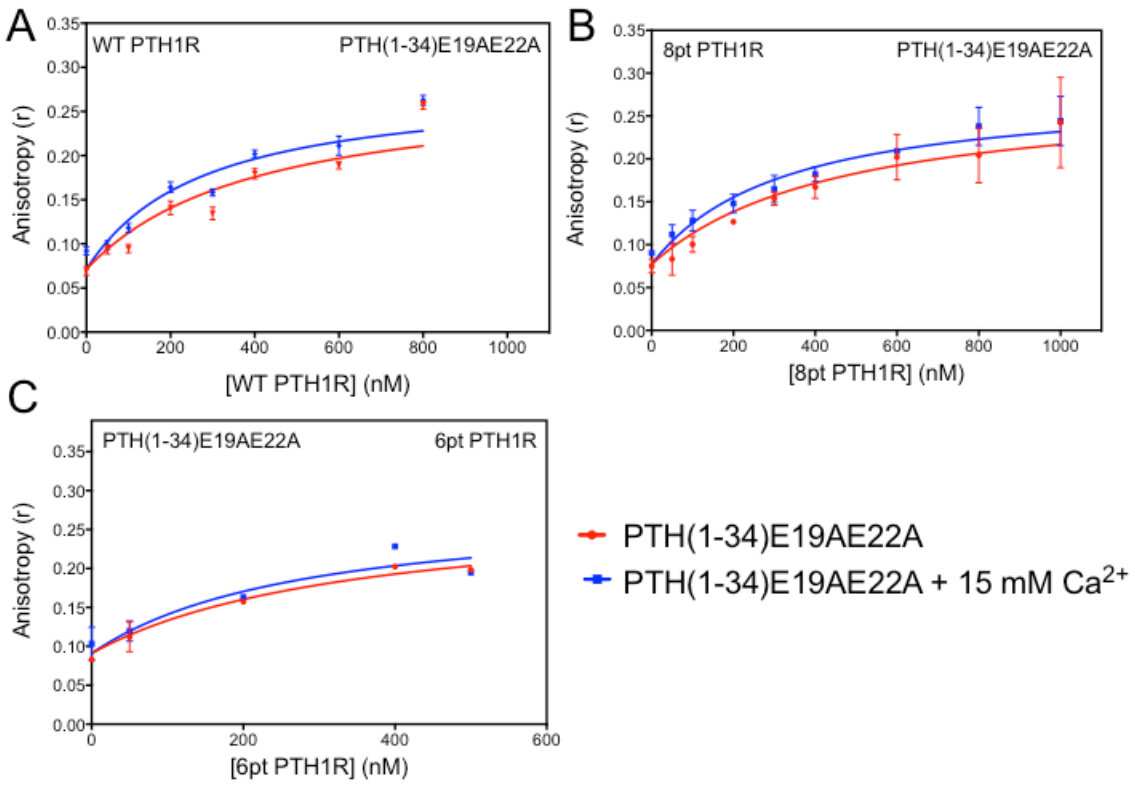

Figure 4.4: PTH(1-34)E19AE22A binds to PTH1R mutants. Fluorescence anisotropy titrations of 20 nM of PTH(1-34)E19AE22A-FAM with *(A.)* WT PTH1R (n=1) *(B)*. 8pt PTH1R (n=2) and *(C)*. 6pt PTH1R (n=2) with 0 mM Ca^{2+} (red) and 15 mM Ca^{2+} (blue) with error bars showing standard deviation.

Table 4.2: Binding affinity of PTH(1-34) to WT PTH1R and PTH1R mutants

	K_D (without Ca^{2+}) nM	**K_D (with Ca^{2+}) nM**	**Ratio (with/without)**
PTH(1-34)			
PTH1R	716 ± 83	98 ± 11	7.3 ± 1.2
8pt PTH1R	668 ± 48	123 ± 11	5.4 ± 0.6
6pt PTH1R	442 ± 62	123 ± 17	3.4 ± 0.7
PTH(1-34)E19AE22A			
PTH1R	389 ± 78	259 ± 52	1.5 ± 0.4
8pt PTH1R	447 ± 55	307 ± 37	1.5 ± 0.3
6pt PTH1R	333 ± 58	264 ± 45	1.3 ± 0.4

4.3.4 Residues of PTH1R extracellular loop 1 regulate Ca^{2+} dependence

In order to identify specific residues of PTH1R important for the Ca^{2+}-sensing ability of PTH(1-34), we collaborated with the Batista group to build a homology model of PTH1R using the crystal structure of the transmembrane domain of CRF1R published in 2015.[166] Using a docking algorithm, they docked PTH(1-34) into the homology model in order to predict possible binding interactions of PTH(1-34) with PTH1R (Figure 4.5). When studying the location of the 8pt and 6pt mutations on PTH1R, we observed that the flexible loop on the ECD is spatially distinct from the hormone-binding site. However, the mutated residues in ECL1 are much closer, and indeed might interact with Ca^{2+} during peptide binding. Thus, we hypothesized that a single negatively charged residue of ECL1 is important for the Ca^{2+}-sensing ability of PTH(1-34). To test this hypothesis we created single alanine scanning mutants of the each of the 6 acidic residues in the 6pt PTH1R mutation with the goal of identifying specific residues of PTH1R ECL1 that are important for PTH(1-34) Ca^{2+}-sensing ability.

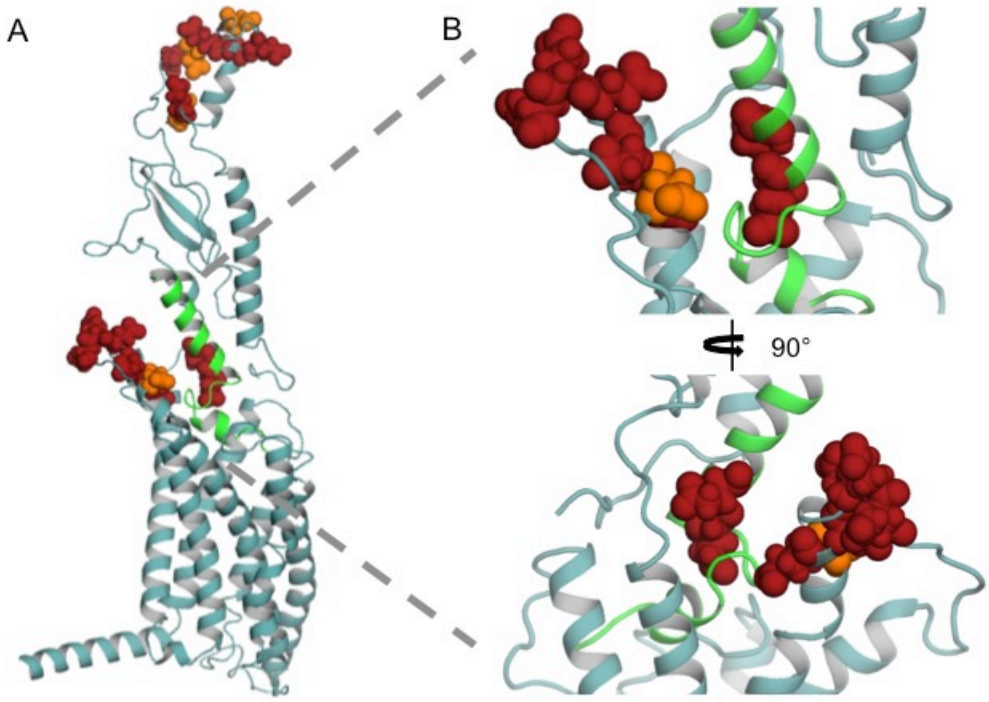

Figure 4.5: Homology model of PTH(1-34) bound to PTH1R. (*A)*. Homology model of PTH1R (teal) and docked PTH(1-34) shown in green. The 8pt ECD and 6pt ECL1 Glu (red) and Asp (orange) residues that were mutated are shown as spheres. (*B)*. The 6 negatively charged residues of ECL1 are in close proximity to the non-conserved glutamic acid resides of PTH(1-34). The homology model was created by Dr. Heidi Hendrickson of Dr. Victor Batista's group.

Each of the PTH1R ECL1 single mutants bound PTH(1-34) and showed partial Ca^{2+} dependence in the presence of 15 mM Ca^{2+}. When titrated with 20 nM of PTH(1-34)-FAM, D251A PTH1R bound to PTH(1-34) with K_D = 224 ± 27 nM with 0 mM Ca^{2+} and K_D = 47 ± 10 nM with 15 mM Ca^{2+} (Figure 4.6A, Table 4.3). The ratio between the K_D values (0 mM Ca^{2+} / 15 mM Ca^{2+}) is 4.8 ± 1.3 (Table 4.3). These dissociation constants in the present and absence of 15 mM Ca^{2+} are significantly lower than both WT PTH1R and the parent 6pt ECL1 PTH1R, which means tighter binding.

PTH(1-34) binds E252A PTH1R with K_D = 800 ± 90 nM with 0 mM Ca^{2+} and K_D = 161 ± 21 nM with 15 mM Ca^{2+} (Figure 4.6B, Table 4.3). The ratio between the K_D values (0 mM Ca^{2+} / 15 mM Ca^{2+}) is 4.9 ± 0.8 (Table 4.3). The binding affinities are within the same order of magnitude of WT PTH1R and the 6pt PTH1R mutant, which suggests that they are not important for PTH(1-34) binding or its Ca^{2+}-sensing ability.

When titrated with PTH(1-34), the binding affinity of E254A PTH1R was calculated to be K_D = 375 ± 95 nM with 0 mM Ca^{2+} and K_D = 102 ± 28 nM with 15 mM Ca^{2+} (Figure 4.6C, Table 4.3). The ratio between the K_D values (0 mM Ca^{2+} / 15 mM Ca^{2+}) is 3.7 ± 1.0 (Table 4.3). PTH(1-34) binds E254A PTH1R tighter than WT PTH1R in the absence of Ca^{2+}, but binds WT PTH1R with the same order of magnitude in the presence of 15 mM Ca^{2+}.

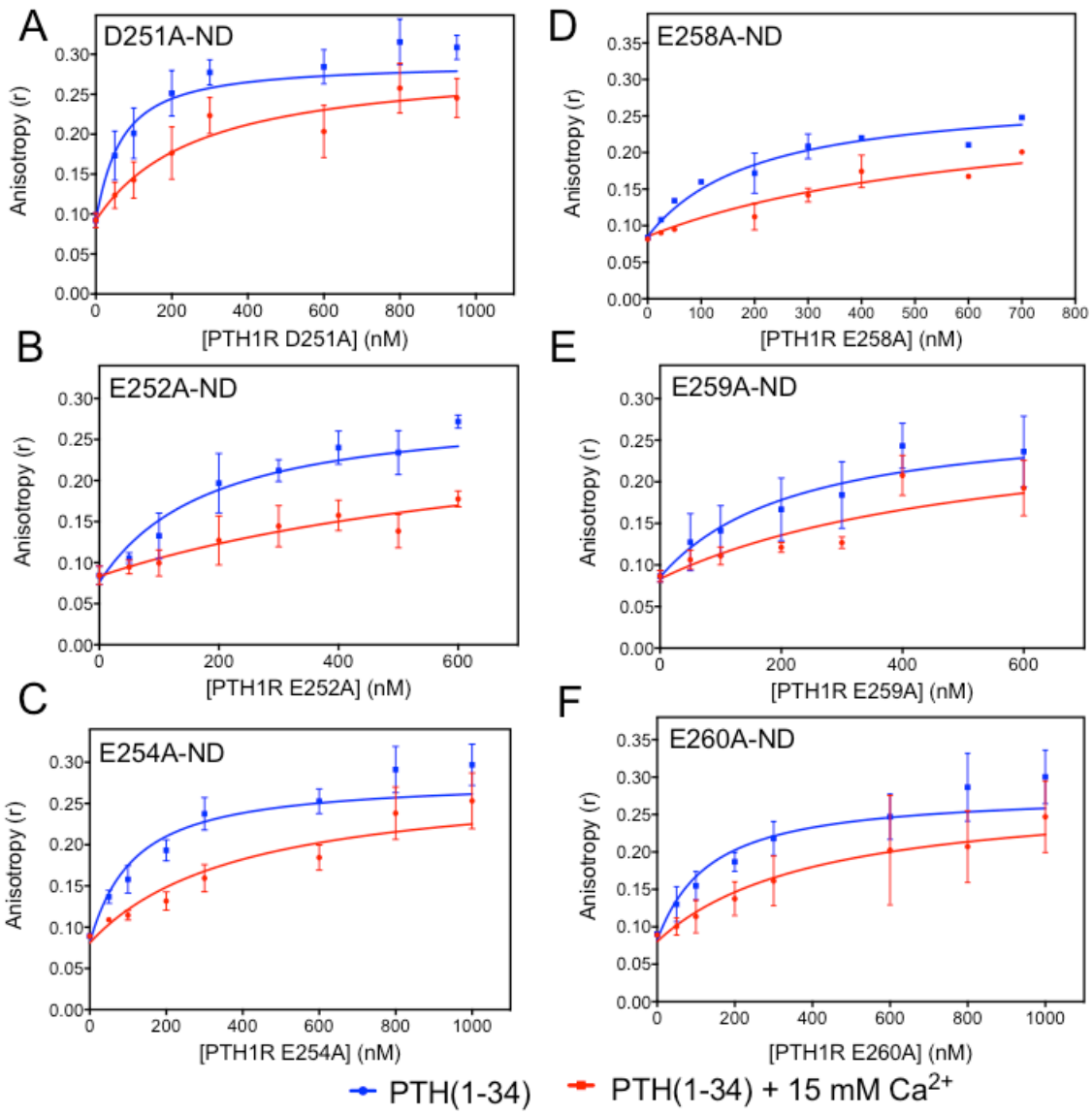

Figure 4.6: **Single mutants of PTH1R ECL1 bind PTH(1-34).** Fluorescence anisotropy titrations of 20 nM PTH(1-34)-FAM with (*A*). D251A PTH1R, (*B*). E252A PTH1R, (*C*). E254A PTH1R, (*D*). E258A PTH1R (n=2), (*E*). E259A PTH1R or *(F)*. E260A PTH1R with 0 mM Ca^{2+} (red) and 15 mM Ca^{2+} (blue). PTH(1-34) binds to each receptor, and the addition of Ca^{2+} increases the anisotropy for each mutant. Each titration shows an average of 3 experiments unless indicated with error bars showing the standard deviation.

Table 4.3: Binding affinity of PTH(1-34) to WT PTH1R and Ca^{2+}-sensing mutants

	K_D (without Ca^{2+}) nM	K_D (with Ca^{2+}) nM	Ratio (with/without)
PTH1R	716 ± 83	98 ± 11	7.3 ± 1.2
8pt ECD	668 ± 48	123 ± 11	5.4 ± 0.6
6pt ECL1	442 ± 62*	123 ± 17	3.4 ± 0.7 **
D251A	224 ± 27***	47 ± 10	4.8 ± 1.3
E252A	800 ± 90	161 ± 21	4.9 ± 0.8
E254A	375 ± 95**	102 ± 28	3.7± 1.0**
E258A (n=2)	649 ± 88	188 ± 22**	3.1 ± 0.7**
E259A	553 ± 106	209 ± 56**	2.6 ± 0.9**
E260A	392 ± 95**	237 ± 49	4.4 ± 1.3*

*p<0.05, **p<0.001 and ***p<0.0001 indicate significant difference in the value for the PTH1R mutant compared to WT PTH1R. For each receptor, the K_D values with Ca^{2+} are significantly different from K_D values without Ca^{2+} $p < 0.05$.

E258A, E259A and E260A are the three residues in ECL1 spatially closest to the docked PTH(1-34) in the homology model of PTH1R. In that same model, these residues are close to the C-terminus of PTH(1-34) which section 3.3.2 has shown is necessary for Ca^{2+}-dependent binding.[101] PTH(1-34) binds E258A PTH1R with K_D = 586 ± 98 nM with 0 mM Ca^{2+} and K_D = 192 ± 27 nM with 15 mM Ca^{2+} (Figure 4.6D, Table 4.3). The ratio between the K_D values (0 mM Ca^{2+} / 15 mM Ca^{2+}) is 3.1 ± 0.7 (Table 4.4). PTH(1-34) binds E259A PTH1R with K_D = 553 ± 125 nM with 0 mM Ca^{2+} and K_D = 209 ± 56 nM with 15 mM Ca^{2+} (Figure 4.6E, Table 4.3). The ratio between the K_D values (0 mM Ca^{2+} / 15 mM Ca^{2+}) is 2.6 ± 0.9 (Table 4.3). PTH(1-34) binding to E260A PTH1R shows K_D = 392 ± 95 nM with 0 mM Ca^{2+} and K_D = 121 ± 28 nM with 15 mM Ca^{2+} (Figure 4.6F, Table 4.3). The ratio between the K_D values (0 mM Ca^{2+} / 15 mM Ca^{2+}) is 3.2 ± 0.9 (Table 4.3). The E258A PTH1R, and E259A PTH1R mutants show similar binding

affinities to PTH(1-34). E260A PTH1R shows tighter binding, but all 3 single mutants show have similar effects on the Ca^{2+}-sensing of PTH(1-34).

To determine if single residues show similar abolishment of Ca^{2+}-sensing of PTH(1-34)E19AE22A to the 6pt and 8pt PTH1R mutant, I performed titrations with 20 nM PTH(1-34)E19AE22A-FAM and PTH1R E258A, PTH1R E259A and PTH1R E260A. These three mutants were chosen because they showed the greatest reduction in Ca^{2+}-sensing ability of the six ECL1 mutations. The preliminary data shows PTH(1-34)E19AE22A binds to each of the single mutant receptors with no change in binding affinity in the presence and absence of 15 mM Ca^{2+}. PTH(1-34)E19AE22A binds E258A PTH1R with K_D = 354 ± 52 nM without Ca^{2+} and K_D = 290 ± 42 nM with 15 mM Ca^{2+} (Figure 4.7A, Table 4.4). The ratio between the K_D values (0 mM Ca^{2+} / 15 mM Ca^{2+}) is 1.2 ± 0.2 (Table 4.4). The titrations of PTH(1-34)E19AE22A with E259A PTH1R with K_D = 318 ± 53 nM without Ca^{2+} and K_D = 350 ± 58 nM with 15 mM Ca^{2+} (Figure 4.7B, Table 4.4). The ratio between the K_D values (0 mM Ca^{2+} / 15 mM Ca^{2+}) is 0.9 ± 0.1 (Table 4.4). Finally, the binding of PTH(1-34)E19AE22A to E260A PTH1R shows K_D = 358 ± 37 nM without Ca^{2+} and K_D = 224 ± 23 nM with 15 mM Ca^{2+} (Figure 4.7C, Table 4.4). The ratio between the K_D values (0 mM Ca^{2+} / 15 mM Ca^{2+}) is 1.6 ± 0.2 (Table 4.4). The K_D ratios indicate the Ca^{2+} sensitivity of each receptor mutant and are all similar in binding to PTH(1-34)E19AE22A.

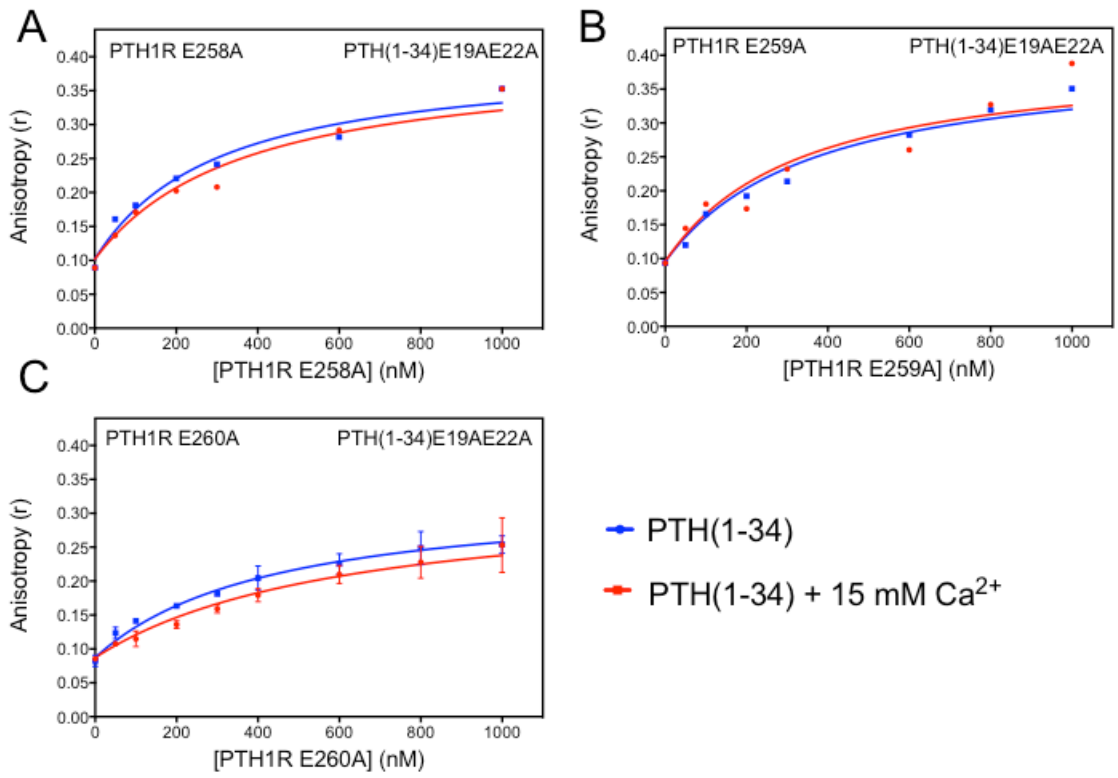

Figure 4.7: PTH(1-34)E19AE22A binding to single mutants of PTH1R ECL1. Fluorescence anisotropy titrations of 20 nM PTH(1-34)E19AE22A-FAM with (*A*). E258A PTH1R (*B*). E259A PTH1R, or (*C*). E260A PTH1R with 0 mM Ca^{2+} (red) and 15 mM Ca^{2+} (blue). PTH(1-34)E19AE22A binds to each receptor with decreased sensitivity to 15 mM Ca^{2+}. Each point of the titration shows the average of 2 experiments with error bars showing the standard errors.

Table 4.4: Binding affinity of PTH(1-34) to WT PTH1R and PTH1R mutants

	K_D (without Ca^{2+}) nM	K_D (with Ca^{2+}) nM	Ratio (with/without)
PTH(1-34)			
PTH1R	716 ± 83	98 ± 11	7.3 ± 1.2
6pt PTH1R	442 ± 62	123 ± 17	3.4 ± 0.7
E258A (n=2)	649 ± 88	188 ± 22	3.1 ± 0.7
E259A	553 ± 106	209 ± 56	2.6 ± 0.9
E260A	392 ± 95	237 ± 49	4.4 ± 1.3
PTH(1-34)E19AE22A			
PTH1R	389 ± 78	259 ± 52	1.5 ± 0.4
6pt PTH1R	333 ± 58	264 ± 45	1.3 ± 0.4
E258A PTH1R	354 ± 52	290 ± 42	1.2 ± 0.2
E259A PTH1R	318 ± 53	350 ± 58	0.9 ± 0.2
E260A PTH1R	358 ± 37	224 ± 23	1.6 ± 0.2

4.3.5 PTH(1-34) activates PTH1R mutants in cAMP assays

For many GPCRs, the ligand binding affinity does not directly reflect the level of receptor activation. Thus, in order to determine if the mutant receptors were still activated by PTH(1-34), I performed cell based cAMP accumulation assays. These assays measure the amount of cAMP produced by stable cell lines expressing the receptor of interest. Each of the single mutants of PTH1R ECL1 was activated by PTH1R to produce cAMP (Figure 4.8). D251A, E258A and E259A showed similar EC_{50} values to WT PTH1R, with the other mutants showing slightly higher EC_{50} values, indicating worse potency (Table 4.5). In particular, preliminary data from the 6pt PTH1R show PTH(1-34) activates this mutant more than an order of magnitude worse that WT PTH1R (Table 4.5).

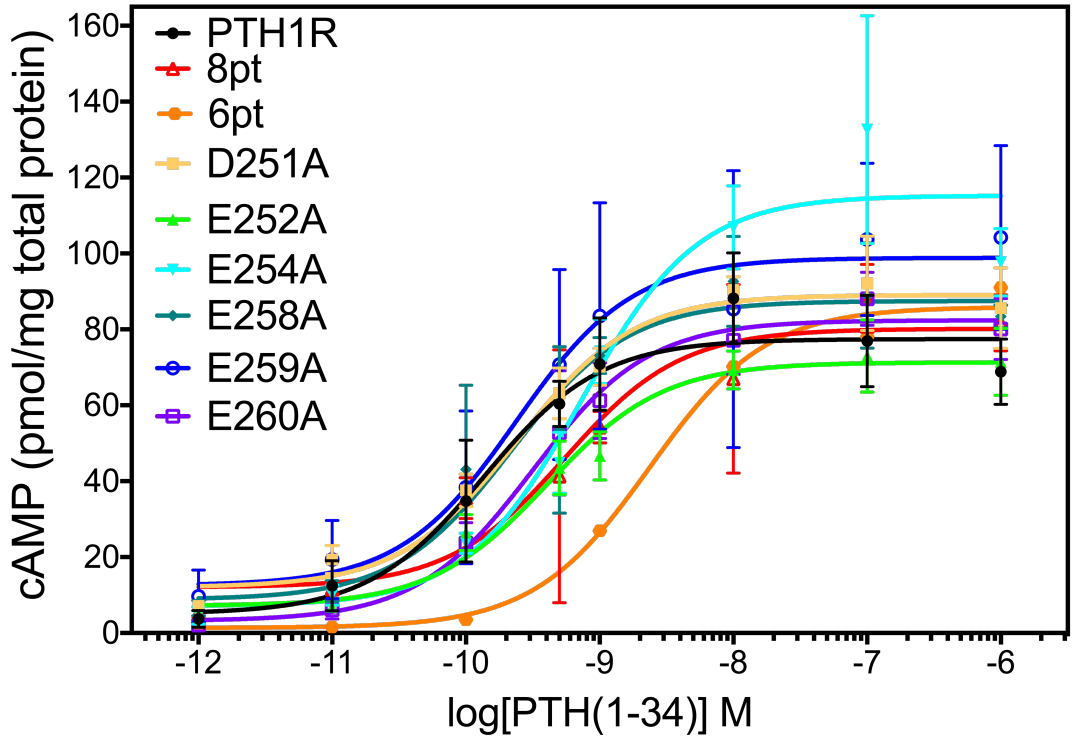

Figure 4.8: PTH(1-34) activates the mutant receptors. Cell based cAMP assays measure pmols of cAMP produced by each PTH1R mutant after stimulation with different concentrations of PTH(1-34). n=3 for each tested mutant except the 6pt PTH1R (n=3) and error bars show the standard deviation.

Table 4.5: Potency and efficacy of PTH(1-34) activation of WT and mutant PTH1R

Receptor	Log(EC_{50}) M	EC_{50} (nM)	Max cAMP produced (pmols)
WT PTH1R	-9.87 ± 0.14	0.14	77.5 ± 3.0
8pt ECD	-9.26 ± 0.21**	0.55	80.2 ± 5.5
6pt ECL1	-8.63 ± 0.10***	2.4	86 ± 2.9
D251A	-9.62 ± 0.09	0.24	89.1 ± 2.4
E252A	-9.40 ± 0.09*	0.41	71.3 ± 2.3
E254A	-9.13 ± 0.13***	0.73	115.2 ± 5.3
E258A	-9.66 ± 0.16	0.22	87.5 ± 4.3
E259A	-9.63 ± 0.22	0.24	98.9 ± 6.3
E260A	-9.50 ± 0.10*	0.31	82.4 ± 2.7

*p<0.05, **p<0.001 and ***p<0.0001 indicate significant difference in EC_{50} for the PTH1R mutant compared to WT PTH1R

4.4 Discussion and conclusions

Ligand binding to family B GPCRs has long been studied through mutational analysis, as reviewed in [1]. In addition, crystal structures of truncated ligands bound to the extracellular domain of their cognate receptors have revealed many of the important interactions crucial for ligand binding.[17-31] In the case of PTH1R, ligand binding has been studied almost exclusively through mutational analysis of residues PTH(1-34) in order to develop more effective drugs for osteoporosis.[107-111] However, less is known about the important residues of PTH1R. The data presented here show that K_D values for each PTH1R mutant are different in the presence and absence of 15 mM Ca^{2+}, providing new insights into the ligand binding interactions of PTH1R. By analyzing the K_D values for each receptor mutant with or without Ca^{2+} we begin to understand the way PTH(1-34) binds to PTH1R and how the presence of high concentrations of Ca^{2+} affects this binding.

Figure 4.9A shows the K_D values of PTH(1-34) in the presence and absence of Ca^{2+}, highlighting two important relationships. First, we can compare K_D values of PTH(1-34) binding to each of the receptor mutants in the absence of Ca^{2+} (black bars). From this, we observed no significant change in K_D for PTH(1-34) binding to 8pt PTH1R compared to WT PTH1R, showing the negatively charged residues of the non-conserved loop in the extracellular domain likely do not interact with PTH(1-34) during the ligand binding. In contrast, PTH(1-34) binds 6pt PTH1R about 2 fold tighter than WT PTH1R, suggesting these negatively charged residues may fine tune the ligand binding interactions. Of interest, only 3 of the 6 single ECL1 mutants showed significantly tighter binding of PTH(1-34) compared to wild-type, with the E252A, E258A and E259A mutants showing no significant change in K_D. Thus, E252A, E258A and E259A likely do

not provide important contacts with PTH(1-34) during the ligand binding process in the absence of Ca^{2+}. In contrast, the D251A mutant showed significantly tighter binding in the absence of Ca^{2+}, which suggests the residue repels a portion of PTH(1-34) during binding. It is possible the removal of just one or two negative charges in ECL1 causes a major change in the interaction of PTH(1-34) with PTH1R. Specifically, ECL1 is highly flexible which may affect the position of the ECL1 negatively charged residues as PTH(1-34) interacts with PTH1R, fine-tuning the interaction depending on the receptor environment. This is further supported by the fact that none of the PTH1R mutants significantly increases in the K_D of PTH(1-34) binding with 0 mM Ca^{2+}. Thus, the residues tested are not necessary for PTH(1-34) binding to PTH1R, but are likely involved in more complicated allosteric interactions that affect the conformational dynamics upon ligand binding and receptor activation.

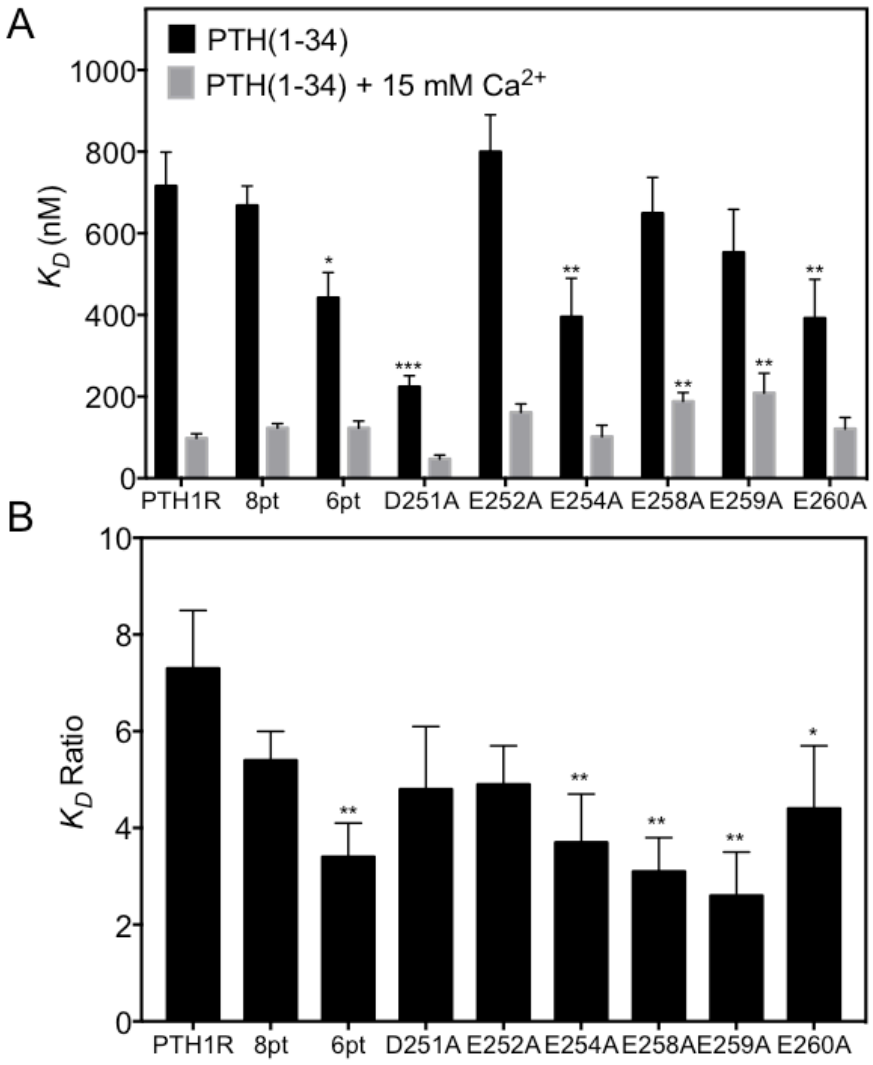

Figure 4.9: Changes in Ca^{2+} dependence for WT and mutant PTH1R. *(A)*. K_D values of PTH(1-34) binding with 0 mM Ca^{2+} (black) and 15 mM Ca^{2+} (gray) Significant differences in K_D values of the mutant to WT PTH1R with 0 mM Ca^{2+} are above the black bars and with 15 mM Ca^{2+} are above the gray bars. *(B)*. The ratio of PTH(1-34) K_D with 15 mM Ca^{2+} to the K_D with 0 mM Ca^{2+}. Each bar shows data from at least 3 experiments, with error bars showing the standard deviation. P values were calculated using an ordinary one-way Anova comparing each mutant to WT PTH1R (* $p<0.05$, ** $p<0.01$, ***$p<0.0001$).

In the presence of 15 mM Ca^{2+} many of the mutants show similar binding to PTH(1-34) with only E258A and E259A showing significantly increased K_D values (Figure 4.9A, gray). Because E258A and E259A significantly decreased the binding of PTH(1-34) in the presence of 15 mM Ca^{2+}, it is likely these two residues are particularly important for the Ca^{2+} dependent binding to occur. Thus, E258 and E259 may interact with residues of PTH(1-34) and/or with Ca^{2+} ions for tighter binding of PTH(1-34) in the presence of 15 mM Ca^{2+}.

Figure 4.9B shows that the receptor mutants affect PTH(1-34) binding differently in the presence and absence of Ca^{2+}. We analyzed the changes in the ratio of K_D with 0 mM Ca^{2+} / K_D with 15 mM Ca^{2+}, which indicates each receptor's sensitivity to Ca^{2+} (Figure 4.9B). PTH1R has the highest K_D ratio, meaning that mutant receptors with decreased ratios show less Ca^{2+}-dependent binding. The K_D ratios of the 8pt, D251A and E252A mutants were not significantly different than the K_D ratio of WT PTH1R, which suggests these residues are not important for Ca^{2+}-dependent binding of PTH(1-34) (Figure 4.9B). However, the 6pt PTH1R and 4 of the single mutants showed significantly decreased K_D ratios, indicating their importance in Ca^{2+}-dependent binding. Residues E254, E258, E259 and E260 are in a flexible loop of ECL1, which is disordered in the crystal structure and shown to be flexible region in the homology model (Figure 4.5). It is possible the presence of 15 mM Ca^{2+} causes a slight conformational changes in ECL1 that changes the binding affinity of PTH(1-34). This is supported by the crystal structure of a PTH(1-34) analogue bound to PTH1R, where ECL1 was too flexible to resolve.[25]

To determine if residues of PTH(1-34) and PTH1R are both necessary for Ca^{2+} modulation of ligand binding, I measured the binding affinity of PTH(1-34)E19AE22A to five of the PTH1R mutants. Preliminary data shows no major differences in the binding of PTH(1-34)E19AE22A to WT PTH1R or its mutants in the presence and absence of 15 mM Ca^{2+} (Figure 4.10). It is important to note this preliminary data needs to be replicated in order to make stronger conclusions about the effect of PTH1R mutants on PTH(1-34)E19AE22A binding. However, these initial results suggest that Ca^{2+} modulates the interaction of PTH(1-34) with PTH1R through the negatively charged residues of PTH1R primarily in the ECL1.

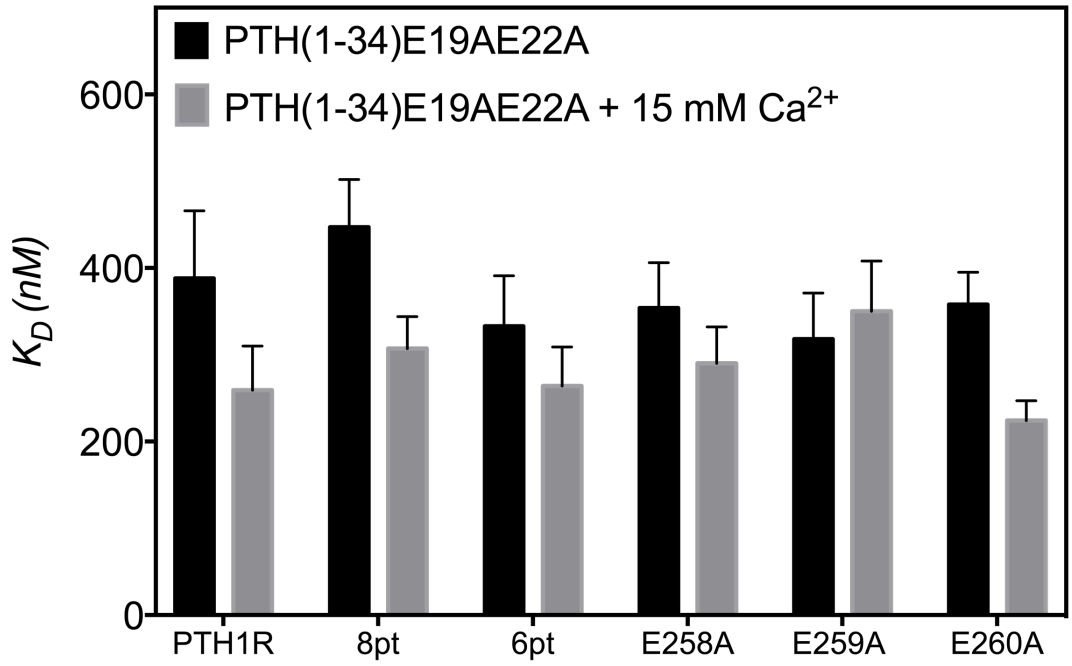

Figure 4.10: Changes in binding affinity of PTH(1-34)E19AE22A in the presence and absence of 15 mM Ca^{2+}. K_D values from fitted anisotropy curves show the binding of PTH(1-34)E19AE22A with 0 mM Ca^{2+} (black) and 15 mM Ca^{2+} (gray). Data shown from 2 experiments, except for WT PTH1R (n=1) and error bars show the standard deviation.

The results presented here identify residues of PTH1R that are important in forming one or more weak Ca^{2+}-binding site(s) with PTH(1-34). I hypothesize that this binding site primarily involves residues of the ECL1, specifically E254, E258, E259 and E260 and two residues of PTH(1-34), E19 and E22 (Figure 4.5). This weak binding site significantly increases the binding affinity of PTH(1-34) in the presence of 15 mM Ca^{2+}. It is possible the weak Ca^{2+}-binding site causes a conformational change in ECL1 upon PTH(1-34) binding. Previous structural studies of family B GPCRs show conformational changes in ECL1 upon ligand binding and receptor activation.[29, 30] Although each receptor has a slightly different conformation, the consistent changes in the secondary structure and location of ECL1 upon ligand binding highlight its importance in ligand binding interactions.[26, 30, 31] Future studies will investigate the mechanism of the Ca^{2+} binding to PTH(1-34) and PTH1R to determine possible conformational changes that occur. In addition, the physiological effect of Ca^{2+} binding to PTH(1-34) and PTH1R is currently unknown. Future experiments are necessary in order to determine the effect of extracellular Ca^{2+} on the activation and signaling of PTH1R.

Chapter 5: Solution NMR studies show ligand binding dynamics to PTH1R

Previous chapters focused on biochemical studies of ligand binding and activation of PTH1R, leading to the conclusion that residues of the extracellular loop 1 of PTH1R and PTH(1-34) form a weak binding site for Ca^{2+}. To better understand the molecular details of this interaction, we decided to study PTH(1-34) binding to PTH1R using solution NMR. In particular, we measured changes in the transverse relaxation rates (R_2) of each residue of ^{15}N-PTH(1-34) with and without PTH1R present. Changes in the R_2 values indicate changes in flexibility on a residue-by-residue basis. Previous solution NMR structures of ^{15}N-PTH(1-34) show the N-terminal residues of PTH(1-34) are disordered, while the C-terminal residues are in an α-helix. The measured R_2 values for ^{15}N-PTH(1-34) show the C-terminal residues exhibits elevated R_2 values, which confirms the increased rigidity attributable to the C-terminal α-helix. In the presence of PTH1R, changes in R_2 values signify a binding interaction with PTH1R that alters the dynamic motions in PTH. The changes in R_2 observed in the presence of PTH1R matched interactions in the crystal structure PTH analogue bound to PTH1R. This preliminary data highlights the success of the novel method development of solution NMR to study changes in peptide dynamics upon binding to PTH1R. With this new system, we will be able to study changes in PTH dynamics as it binds to PTH1R and its mutants under many different conditions.

This work was performed in collaboration with Dr. Pat Loria's group. Dr. Kyle East and Apala Chaudhuri provided assistance and training in operating the magnet and data

analysis. Sol Chang of Dr. Alana Schepartz's group provided assistance in developing HPLC purification methods.

5.1 Introduction

To best understand the binding mechanism of PTH binding to PTH1R, it is necessary to examine conformational changes of the ligand and receptor during binding. While the nanodisc purification produces sufficient quantities of stable proteins for biophysical assays, it is still difficult to obtain sufficient quantities for structural studies. Therefore, we decided to pursue solution NMR experiments to study changes in the dynamics of PTH as it interacts with PTH1R.[167-170]

Solution NMR experiments are an excellent tool that can be used to study molecular interactions with atomistic detail.[167-170] The principles of NMR spectroscopy are based on the concept that atoms can have a spin, referred to with the spin quantum number *I*.[171, 172] The nuclear spin has a unique spin angular momentum and a magnetic moment (μ), both of which have direction and magnitude.[171] NMR experiments commonly probe spin- ½ nuclei such as ^{1}H, ^{13}C and ^{15}N. When placed in a static magnetic field, B_0, a spin will precess around the external field vector with a characteristic frequency called the Larmor frequency (ω).[171] The magnitude of this frequency is proportional to the strength of the magnetic field and the gyromagnetic ratio (γ), which is the nuclei specific ratio of the magnetic moment to the angular momentum of the nuclei (Table 5.1).

Table 5.1: Common isotopes in biological NMR experiments.
Adapted from [171]

Isotope	Gryomagentic ratio (γ, 10^6 rad s^{-1} T^{-1})	Natural abundance
^{1}H	267.522	~100%
^{13}C	67.283	1.1%
^{15}N	-27.126	0.37%

When placed in an external magnetic field (B_0), the spins of the nuclei align to the direction of the field (Z-axis). A radio frequency (rf) pulse is applied to generate a B_1 field, bringing the magnetic moments into the transverse plane (X, Y plane). The effective field strength (B_{eff}) experienced by the nucleus depends on the external field strength and the local contributions to the chemical environment (intermolecular interactions, dipolar coupling).[173] This shielding effect is known as the chemical shift, which affects the precession of the magnetic moment.[174] Because the Larmor frequency is dependent on the strength of the magnetic field and the magnetic environment surrounding the nucleus, the chemical shift measures the difference between the observed precession frequencies from a calculated, theoretical value. Chemical shifts are different for nuclei in different magnetic environments, providing information about protein structure and dynamics.[173-175] As the magnetic moment precesses orthogonal to the main B_o field, it generates a current that is detected and measured by a receiver coil. The signal detected is the time-dependent oscillation of the magnetic field, which decreases as the magnetic moment relaxes back to the orientation of the bulk magnetic field on the Z-axis. The decay and relaxation of the perpendicular magnetization is free induction decay (FID). Performing a Fourier Transform of the FID yields the precession frequency of each nuclei, which is the primary data of the NMR experiment.[170] Important information about biological samples can be obtained by varying the sequences of rf pulses to probe different nuclei and resonances.[176, 177]

After the application of an rf pulse, the magnetization relaxes in two distinct ways, longitudinal (spin-lattice) relaxation or transverse (spin-spin relaxation).[176, 178] The longitudinal relaxation (T_1) is the relaxation from the x-y plane back to the z-axis and is

measured by the rate $R_1 = 1/T_1$. T_1 is affected by properties such as the temperature, molecular weight and fast molecular motions in the same time scale as the Larmor frequency. A short T_1 value means the magnetization recovers quickly, which means the NMR acquisition time can be quicker as the spin system achieves Boltzmann equilibrium more quickly. The transverse relaxation (T_2) is due the spins relaxing in the x-y plane and losing phase coherence and is measured by the rate $R_2 = 1/T_2$. Molecular motions and the size and shape of the macromolecule affect R_2, which provides valuable information about the dynamics and structure of the protein sample.[171, 179, 180]

Solution NMR studies of proteins usually utilize two-dimensional (2D)[181, 182] or three-dimensional (3D)[183] experiments to study the interactions of two or three nuclei. Many 2D experiments probe ^{1}H-^{15}N or ^{1}H-^{13}C labeled samples, while 3D experiments often require ^{1}H-^{15}N-^{13}C labeled samples to determine important structural information. A standard 2D experiment is the heteronuclear single quantum correlation (HSQC),[184] which studies the correlation between the chemical shift of protons and the chemical shift of ^{13}C or ^{15}N. The ^{1}H-^{15}N HSQC experiment exploits the two-bond J-coupling interaction between chemically bonded H and N atoms. The HSQC experiment uses INEPT[185] pulse sequences to transfer magnetization from the proton to ^{15}N, where the chemical shift evolves, and then the magnetization is transferred from the ^{15}N back to the proton. The 2D spectra will show a peak for each backbone amide and any N-H side chains.

In the work presented below, I used spin-echo pulse sequences including varying durations of the delay times.[186-188] As the delay time increases, the decay of the NMR signal intensity will decrease, which means the intensity of each peak will decrease in a single exponential fashion. We can fit the change in peak intensity vs. delay time to

determine the R_2 values of each reside of the protein of interest. This chapter will describe the use of R_2 measurements of ^{15}N-PTH(1-34) to study changes in dynamics as it interacts with PTH1R.

Solution NMR has been used for many years to study the conformation of PTH(1-34) in different conditions. Initial solution NMR work on PTH(1-34) used proton NMR, including 2D ^{1}H-^{1}H experiments, to determine possible structures of PTH(1-34) and PTHrP(1-36).[162, 189-191] Previous work highlights the possibility of different structures of the hormone depending on the buffer system, with the structure of PTH(1-34) in an aqueous buffer system showing primarily disordered structure, with a short α-helical region at the C-terminus.

More recent work used purified ^{15}N-PTH(1-34) from *E. coli* for 2D NMR experiments.[192-195] The 2D NMR experiments probed interactions of ^{15}N-PTH(1-34) with an engineered PTH1R receptor mimetic,[192] changes in ^{15}N-PTH(1-34) flexibility in the presence of lipid micelles,[195] and the binding of the Zn(II) coordination complex to the N-terminus of PTH(1-34).[194] These studies provide an important foundation for the study of conformational dynamics of PTH(1-34) and its interaction partners. However, the changes in PTH(1-34) dynamics as it interacts with PTH1R are still unknown. This chapter outlines work to develop expression and purification protocols of ^{15}N-PTH(1-34) from *E. coli*, and preliminary 2D NMR experiments to identify changes in the dynamics of ^{15}N - PTH(1-34) under different conditions.

5.2 Experimental Materials and Methods

Expression and purification of recombinant PTH(1-34). PTH(1-34) with an N-terminal thioredoxin (TRX) tag in a pET32a vector was ordered from Genscript (New Jersey) and was transformed into BL21-GOLD cells lines. For expression of unlabeled PTH(1-34), 10 mL of overnight cultures were used to inoculate 1L of growth in LB. For N^{15}-labeled NMR growths, 10 mL of overnight culture were used to inoculate 1L of M9 Minimal media. Cells were grown at 37°C and the OD_{600} was monitored until the cells reached the exponential growth phase. When OD_{600} = ~0.8, the cells were induced with 0.2 mM IPTG and allowed to grow overnight (~16 hours) at room temperature (~27°C). Cells were harvested, lysed by sonication and the clarified lysate applied to Ni^{2+}-NTA beads and eluted with 400 mM imidazole. TRX-PTH(1-34) was concentrated and quantified using the OD_{280}. To remove the TRX tag, 0.25 Units of EK Max (Thermo-Fischer)/mg fusion protein was added to the sample for 1 hr at ~27°C. Cleavage reaction was loaded onto an S75 size exclusion (GE) column in 1 M NaCl, 50 mM Tris-HCl pH 7.4 to separate PTH(1-34) from the TRX tag. PTH(1-34) fractions were pooled, and purified using a reverse-phase HPLC on a C18 column. The peptide was eluted using a 20-60% acetonitrile gradient with 0.1% trifluoroacetic acid over 20 minutes and a flow rate of 5 mL/min. PTH(1-34) identity was monitored throughout using LC/MS.

Expression and purification of PTH1R. PTH1R was expressed and purified as described in chapter 2.

Cell-based cAMP study. Cell based cAMP assays to determine the EC_{50} value of ^{15}N-PTH(1-34) activation of PTH1R was performed as described in chapter 3.

NMR spectroscopy. NMR experiments were performed on Varian 600 MHz, spectrometer at 298 K. ^{1}H-^{15}N TROSY HSQC spectra of ^{15}N - PTH(1-34) were collected with the ^{1}H transmitter and ^{15}N offsets set to the water resonance and 120 ppm, respectively. All spectra were collected with 48 transients (nt), 32 t1 increments (ni), and spectral widths (sw) of 8500 Hz (direct) and (sw1) 3500 Hz (indirect). NMR spectra were processed with NMRPipe[77] and analyzed in nmrFAM-SPARKY[196].

^{15}N R_2 Relaxation rates were measured at 600 MHz using an echo pulse scheme with 5 ms between ^{15}N refocusing pulses for delay times (τ) of: 2 ms (x2), 22 ms, 42 ms, 62 ms, 98ms, 150 ms, 198 ms and 246 ms (x2). Intensities were measured in Sparky and fit to a single exponential in Prism using Eq. 5.1:

$$y = y_0\, e^{-1/R_2 \tau} \tag{5.1}$$

where y is the measure peak intensity, y_0 is the reference intensity.

5.3 Results

5.3.1 PTH(1-34) expression and purification from *E. coli*

I purified unlabeled, recombinant PTH(1-34) from *E. coli* grown in Luria Broth as a proof of concept before moving on to ^{15}N-PTH(1-34) from *E. coli* grown in M9 minimal media supplement with $^{15}NHCl_4$. The ^{15}N-PTH(1-34) is attached to a N-terminal thioredoxin (TRX) tag with an internal 6x-His tag (Figure 5.1A). I purified the fusion protein from the lysate using a Ni-NTA column and cleaved the collected fusion protein with enterokinase. After cleavage, size exclusion chromatography separated the Thioredoxin tag from the ^{15}N-PTH(1-34) (Figure 5.1B). I combined the fractions containing ^{15}N-PTH(1-34) for reverse phase HPLC purification on a C18 column, which separated ^{15}N-PTH(1-34) from impurities (Figure 5.2). I verified the identity of the ^{15}N-PTH(1-34) using LC/MS (Figure 5.2) to confirm the molecular weight. I dried HPLC fractions in a vacuum concentrator to remove the solvent and the remaining solid was re-suspended in the necessary buffer for NMR experiments. The final yield of the purified ^{15}N-PTH(1-34) was 1.9 mg from 1L of growth.

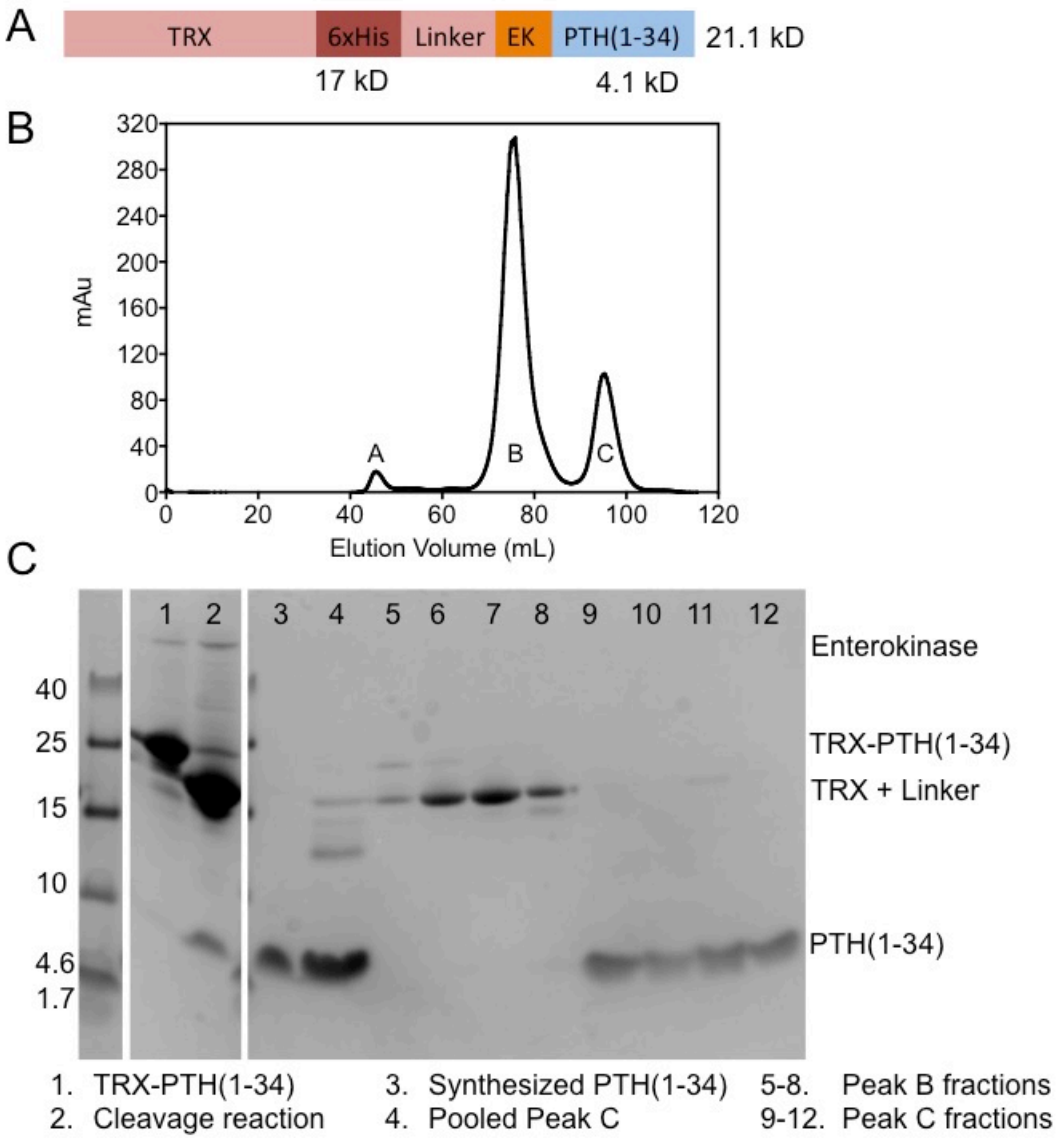

Figure 5.1: Expression and purification of ^{15}N-PTH(1-34). (*A*). Diagram of the TRX-PTH(1-34) fusion construct. (*B*). Size exclusion chromatography of the cleaved fusion protein shows the TRX and PTH(1-34) in Peak B and Peak C, respectively and confirmed by (*C*). 15% Tris-Tricine gel electrophoresis.

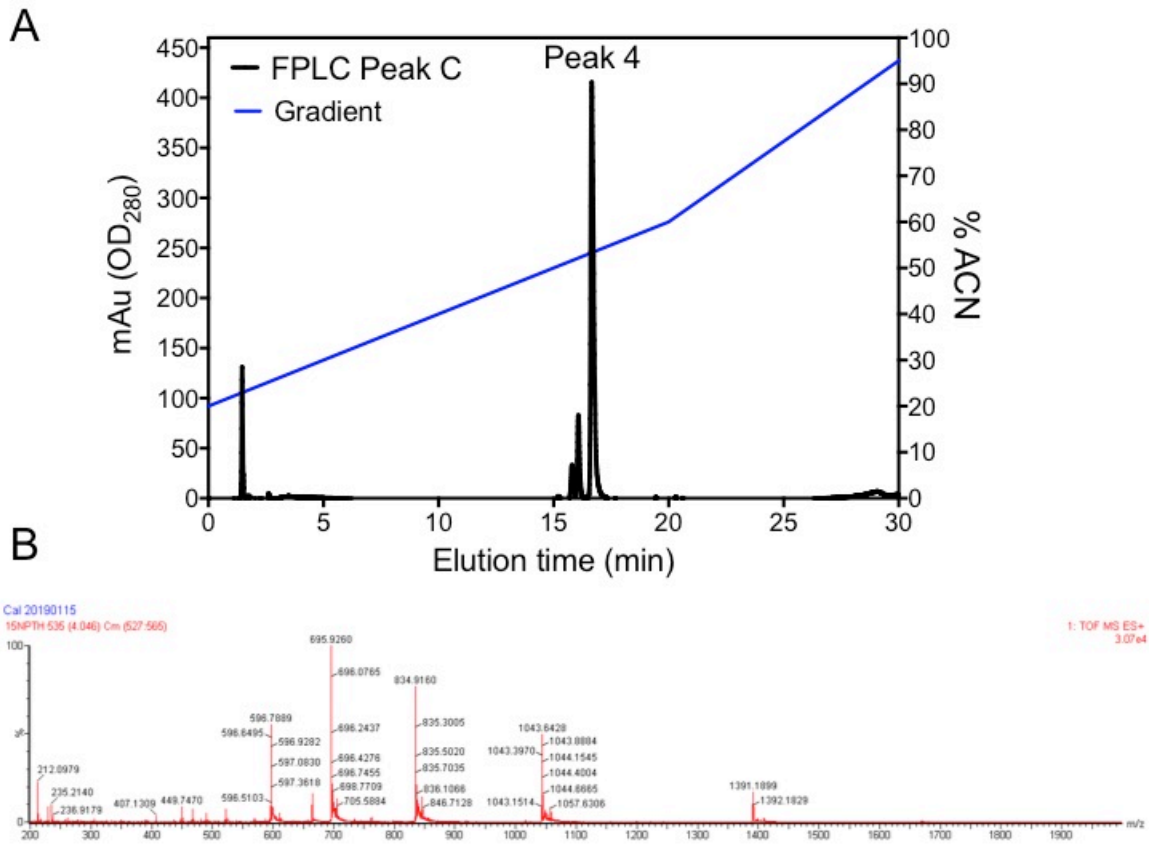

Figure 5.2: Purification and characterization of ^{15}N-PTH(1-34). (*A*). Reverse phase HPLC C18 column shows the purification of ^{15}N-PTH(1-34) (black) and the buffer gradient used (blue). ^{15}N-PTH(1-34) was in peak 4 as confirmed by *(B)*. LC/MS, which shows the m/z spectra for the expected molecular weight of ^{15}N-PTH(1-34).

In order to confirm the recombinant ^{15}N-PTH(1-34) activated PTH1R in cells, I performed cell based cAMP accumulation assays with ^{15}N-PTH(1-34) and synthesized PTH(1-34) as a control to measure changes in the EC_{50} values. ^{15}N-PTH(1-34) showed log(EC_{50}) = -9.49 ± 0.22 M, compared to the PTH(1-34) log(EC_{50}) = -9.47 ± 0.16 M (Figure 5.3). This confirms the purified ^{15}N-PTH(1-34) activates cells with a similar potency.

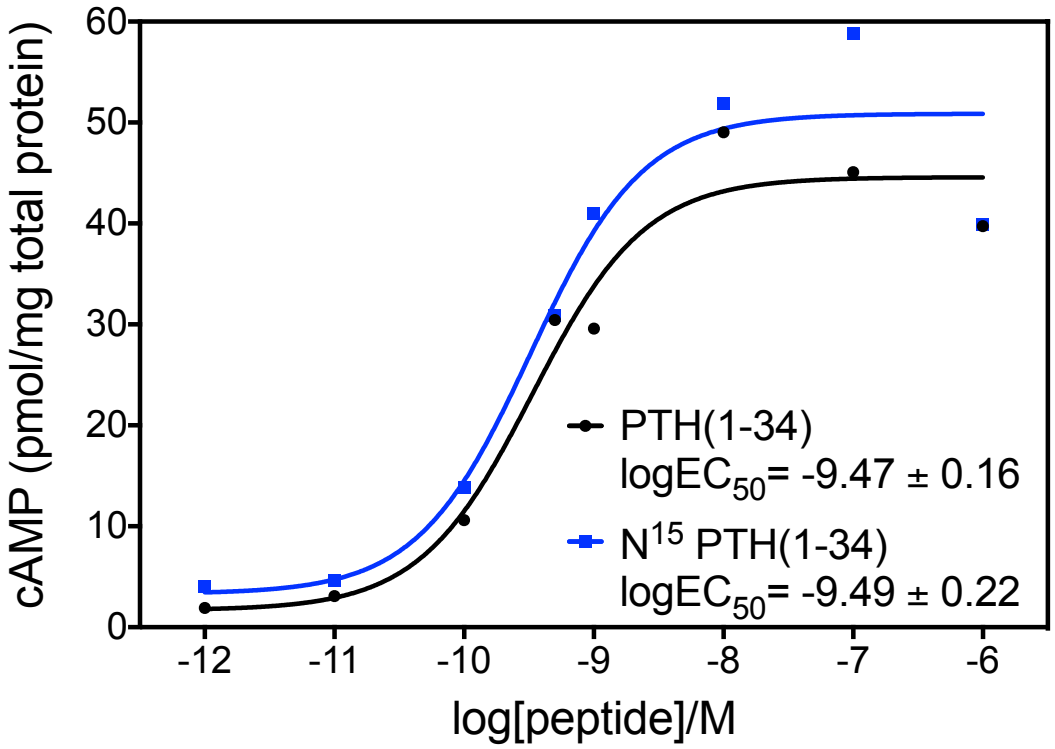

Figure 5.3: Recombinant ^{15}N-PTH(1-34) activates PTH1R. ^{15}N-PTH(1-34) (blue) activates PTH1R with similar potency and efficacy as synthesized PTH(1-34) (black). Data shown represent a single experiment.

5.3.2 2D ^{1}H ^{15}N HSQC of ^{15}N-PTH(1-34)

The 2D HSQC of ^{15}N-PTH(1-34) (260 µM, 20 mM Tris, 100 mM NaCl, 100 µM EDTA, pH6.8) at 25 °C showed 31 peaks (Figure 5.4) The spectra matched previously published spectra of ^{15}N-PTH(1-34) at pH6.8.[193-195] Peak assignments were made based on previously published assignments[195] of ^{15}N-PTH(1-34).

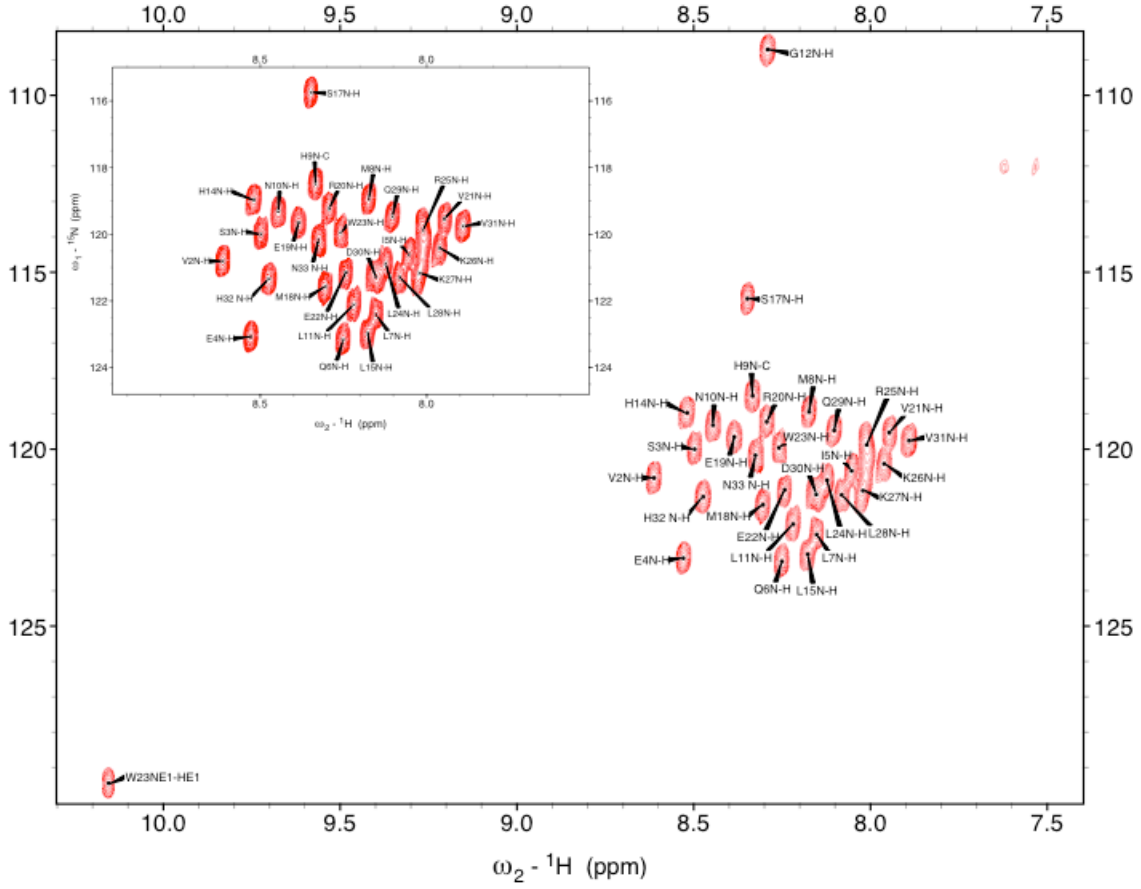

Figure 5.4: 2D spectrum of ^{15}N-PTH(1-34) *(A.)* Assigned peaks for 31 of the 34 residues of PTH(1-34). Spectrum is of 260 µM ^{15}N-PTH(1-34), 20 mM Tris, 100 mM NaCl, 100 µM EDTA, pH6.8 at 25 °C.

5.3.3 R_2 values of each residue of PTH(1-34) indicate rigidity

To determine the transverse relaxation rate of each residue of PTH(1-34), I used a spin-echo pulse sequence.[188] The selected curves of PTH(1-34) in solution show a single exponential decay (Figure 5.5A). By fitting this curve for each residue, I calculated the R_2 value for each reside (Figure 5.5B). The average R_2 value for PTH(1-34) is 2.5 ± 0.7 s^{-1}. However, the N- and C-terminal residues both have lower average R_2 values at the N- and C-terminal residues (average $R_2 = 1.5 \pm 0.3$ s^{-1}), indicating greater conformational flexibility. Furthermore, residues 21-29 of the peptide have a higher average R_2 value of 3.3 ± 0.5 s^{-1}, indicating less conformational flexibility.

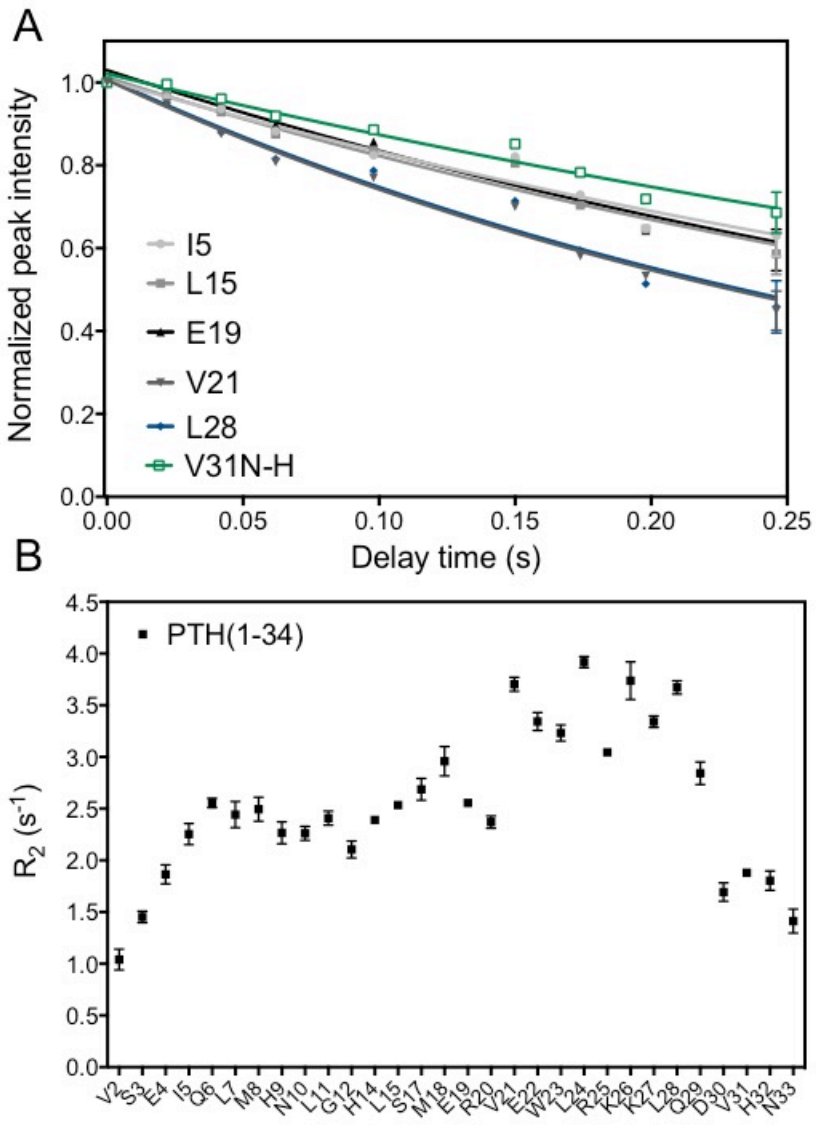

Figure 5.5: R_2 values for each residue of PTH(1-34). *(A)* Normalized peak intensity for six representative residues shows the peak intensity decreases with increasing delay times fitted to a single exponential decay curve with the rate of decay equal to the R_2 value. (*B*) Calculated R_2 values shown for each assigned peak. Data shown from one set of R_2 experiments, with error bars the standard deviation of the fitting to the single exponential decay.

5.3.4 PTH(1-34) R_2 values change in the presence of PTH1R

PTH(1-34) binds to PTH1R with a dissociation constant in the nM-μM range. Thus, by adding PTH1R such that 5-10% of PTH(1-34) is bound to PTH1R at a given time, we should not observe any significant shifts in the peaks for the labeled ^{15}N-PTH(1-34) because we anticipate binding to be a slow exchange process on the NMR timescale. However, the transient interactions between ^{15}N-PTH(1-34) and PTH1R should affect the measured R_2 value for each residue of ^{15}N-PTH(1-34) in the presence of PTH1R. Specifically, residues of ^{15}N-PTH(1-34) that interact with PTH1R should show increased R_2 values because the interaction will increase the rigidity around that particular residue.

Based on the K_D of PTH(1-34) binding to PTH1R measured above, I added in PTH1R purified in nanodiscs to the ^{15}N-PTH(1-34) sample such that 5% of ^{15}N-PTH(1-34) is bound to PTH1R and I repeated the R_2 experiments and observed no change in the peak positions of the ^{15}N-PTH(1-34). For each residue, I fit the peak height intensity at each delayed time to a single exponential decay curve to determine the R_2 value of each residue. Subtracting the values of PTH(1-34) in the presence of PTH1R from the PTH(1-34) alone, I obtained ΔR_2 values (Figure 5.6). The magnitude of the ΔR_2 values varies and the large standard deviations shown make it difficult to analyze how specific residues of PTH(1-34) change upon interacting with the receptors. However, residues Q6, L15 and D30 have ΔR_2 values closest to zero, showing the presence of PTH1R does not affect their conformational flexibility. The residues with the largest ΔR_2 values include I5, G12, S17, E22 and L28. However, due to the large errors in calculating the ΔR_2 values, further experiments are necessary to obtain a more quantitative understanding of the changes in conformational dynamics of PTH(1-34) binding to PTH1R.

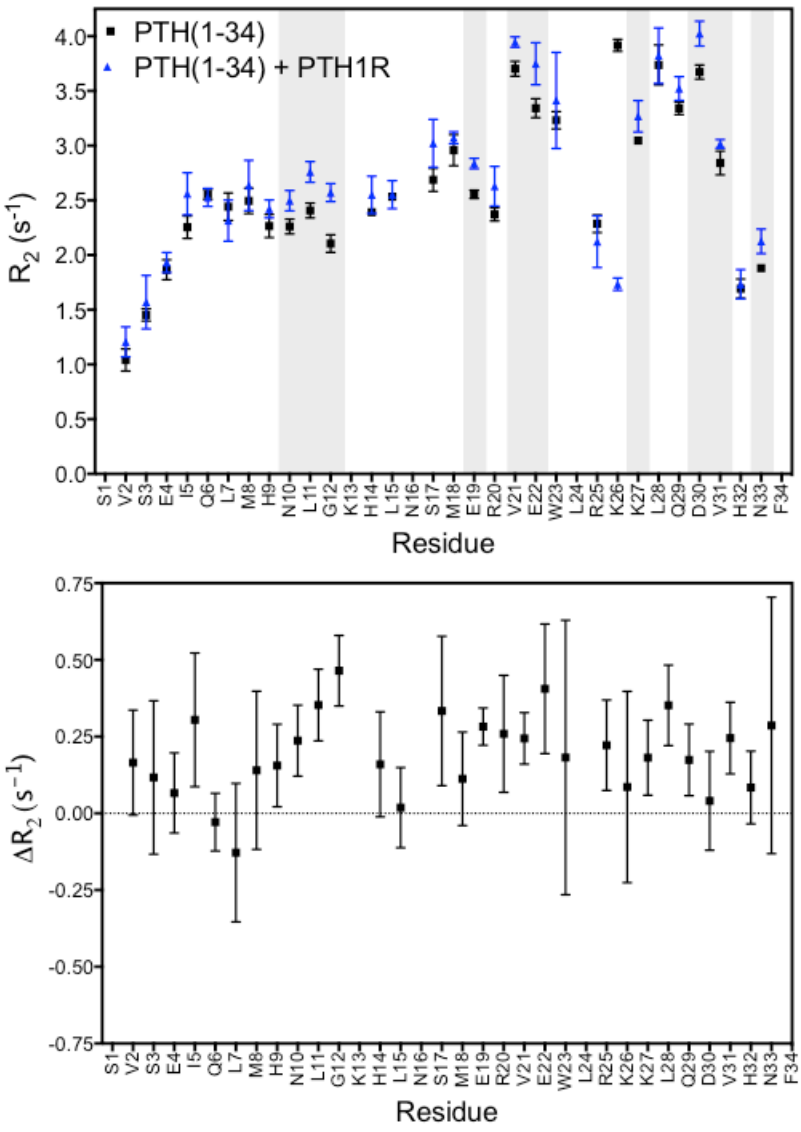

Figure 5.6: Changes in R_2 in the presence of PTH1R. *(A)*. The addition of PTH1R such that 5% PTH(1-34) is bound affects the R_2 values of residues of PTH(1-34) highlighted in gray. *(B)*. ΔR_2 values for each residues of PTH(1-34) (R_2 *PTH1R* + PTH(1-34) - R_2 PTH(1-34)). Each point shows data from a single series of R_2 experiments with error bars showing standard deviation.

5.3.5 15 mM Ca^{2+} does not greatly change the R_2 values of PTH(1-34)

To determine how the presence of millimolar concentrations of Ca^{2+} affects the secondary structure of ^{15}N-PTH(1-34), I recorded HSCQ spectra with increasing concentrations of Ca^{2+} and observed no major shifts in the peaks observed (Figure 5.7). These spectra show that 15 mM Ca^{2+} does not significantly change the structure of the peptide backbone.

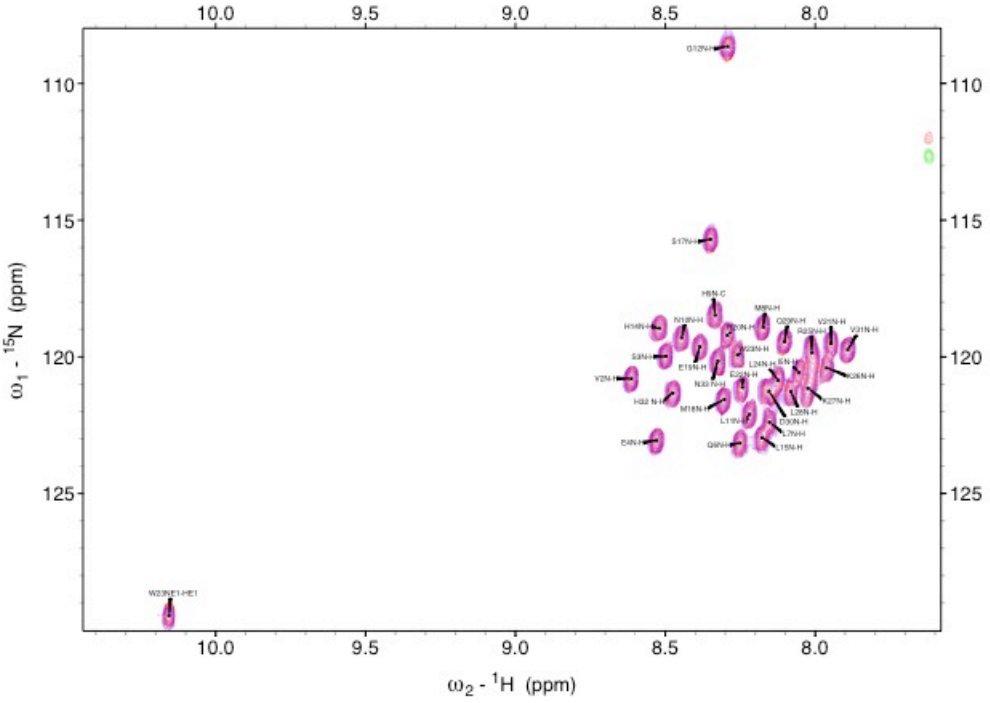

Figure 5.7: 15 mM Ca^{2+} does not affect the backbone structure of PTH(1-34). Spectra of PTH(1-34) alone (red) and PTH(1-34) + 15 mM Ca^{2+} (blue) show no change in peak position.

After demonstrating that 15 mM Ca^{2+} does not change the backbone structure of ^{15}N-PTH(1-34), I performed R_2 experiments of ^{15}N-PTH(1-34) with 15 mM Ca^{2+} present in order to measure changes in the dynamics of residues of ^{15}N-PTH(1-34) (Figure 5.8A). The ΔR_2 of the N-terminal residues (residues 1-11) center around 0, indicating no change in conformational dynamics upon the addition of 15 mM Ca^{2+} (Figure 5.8B). Three residues have positive ΔR_2 values, including G12, S17, and W23, showing 15 mM Ca^{2+} affects the decreases the dynamic motions of these specific residues. Of interest, three residues in the C-terminus of the peptide have negative ΔR_2 values: V21, R25, and D30, indicating increased conformational flexibility. Further studies are necessary to investigate the significance of the changes in ΔR_2 values in the presence of 15 mM Ca^{2+} to better understand the conformational dynamics of PTH(1-34).

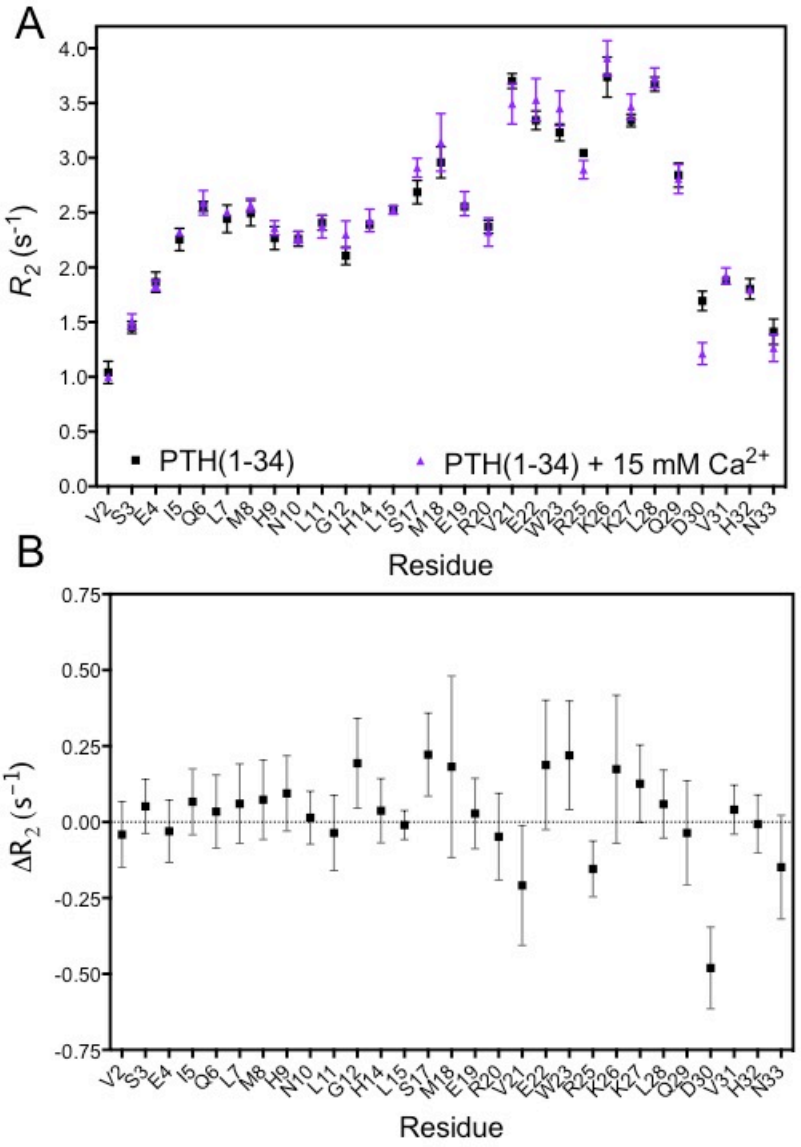

Figure 5.8: Changes in PTH(1-34) R_2 in the presence of 15 mM Ca^{2+} PTH(1-34). *(A)* The calculated R_2 values for each residues of PTH(1-34) with (purple) and without 15 mM Ca^{2+}. *(B)* ΔR_2 values for each residue (R_2 *PTH1R* + PTH(1-34) - R_2 PTH(1-34)). Data shown are fitted values calculated from a single set of R_2 experiments for each condition.

5.4 Discussion and future directions

The dynamics of ligand binding to PTH1R are challenging to study and thus poorly understood. Previous studies of the kinetic rates for the N- and C-terminus of PTH(1-34) upon interaction with PTH1R showed that the N-terminus and C-terminus of PTH(1-34) interact with PTH1R with different rates.[15, 16, 197] Furthermore, the crystal structures of PTH(15-34) bound to the extracellular domain (ECD) of PTH1R and ePTH(1-34) bound to full-length PTH1R show snapshots of the interactions between PTH(1-34) and PTH1R in the ligand binding process.[25, 33] These studies provide an excellent foundation for the interpretation of changes in PTH(1-34) dynamics under different conditions. The preliminary studies presented here lay the foundation for quantifying these dynamic changes.

First, the solution NMR structure of PTH(1-34) under physiological conditions show that the C-terminal residues are helical and the N-terminal residues are disordered (Figure 5.9).[162] The R_2 values presented here are consistent in magnitude for a peptide of this molecular weight and match this structure of PTH(1-34) in solution, with the C-terminal residues showing higher R_2 values and the N-terminal residues lower values (Figure 5.5). The residues in the two helical regions of PTH have distinct R_2 values, with the C-terminal helix showing much greater rigidity. Thus, we have measured R_2 values of PTH(1-34) that support the current structural understanding of PTH(1-34) in solution, highlighting the utility of this novel methods for studying the dynamics of the PTH(1-34).

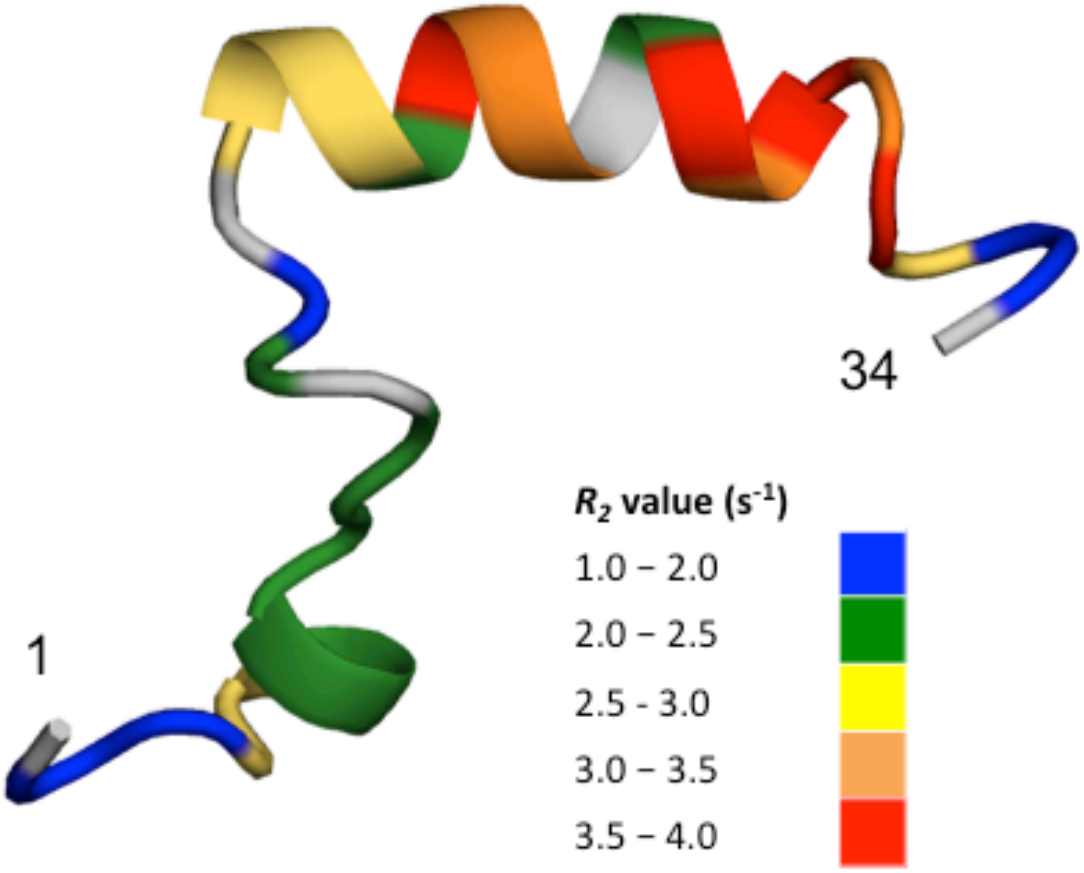

Figure 5.9: Changes in R_2 values show the rigidity of PTH(1-34) in solution. The calculated R_2 values for each residue of PTH(1-34) mapped onto a structure of PTH(1-34) in solution (PDB ID: 1HPH).[162] Residues are colored based on their R_2 values as indicated with the residues with no data shown in gray.

The next step in developing the studies of PTH(1-34) dynamics measured the R_2 values of PTH(1-34) in the presence of PTH1R, which show intriguing preliminary results. With the concentration of PTH1R set such that 5% of PTH(1-34) is bound, there are significant changes in the measured R_2 values compared to PTH(1-34) alone. However, the calculated ΔR_2 values between PTH1R present and PTH(1-34) alone are low in magnitude with large error bars. Thus, the method needs further optimization, such as higher concentrations of PTH1R to observe larger changes in R_2 values. However, even these preliminary results provide novel insights into the interactions of PTH(1-34) with PTH1R.

By mapping the changes in R_2 values of PTH(1-34) onto the crystal structure of PTH1R, I highlighted residues that become more rigid when PTH1R is present (Figure 5.10). I identified residues of PTH(1-34) that show changes in R_2 values in the presence of PTH1R and compared these residues to those shown to interact with PTH1R in the crystal structure.[25] The difference in interactions identified from the R_2 values compared to the crystal structure likely is due to the differences in molecular systems and the need for future experimental optimization. Specifically, the crystal structure shows of ePTH bound to PTH1R, where both ePTH and PTH1R have stabilizing mutations that likely affect how the hormone interacts with the receptor.[25] Furthermore, ECL1 and the flexible loop in the N-terminal extracellular domain of PTH1R are disordered in the crystal structure. These flexible loops may provide crucial interactions that affect the dynamics of specific PTH(1-34) residues. The flexibility of these loops does not affect the identified interactions of the N-terminus of PTH because their interactions occur with residues in the transmembrane domain. In addition, ePTH contains mutations in residues

in the N-terminus of the peptide that constrain the conformation of the peptide and increase ligand-binding affinity, further complicating the comparison between the R_2 values and structural interactions.[25] Regardless, this preliminary data demonstrates the potential power of using solution NMR to study changes in hormone dynamics upon interaction with its receptor. The data collected here and future studies will provide critical commentary on the changes in the dynamics of the native ligand upon binding to the native receptor that is currently unavailable using other structural and biophysical techniques.

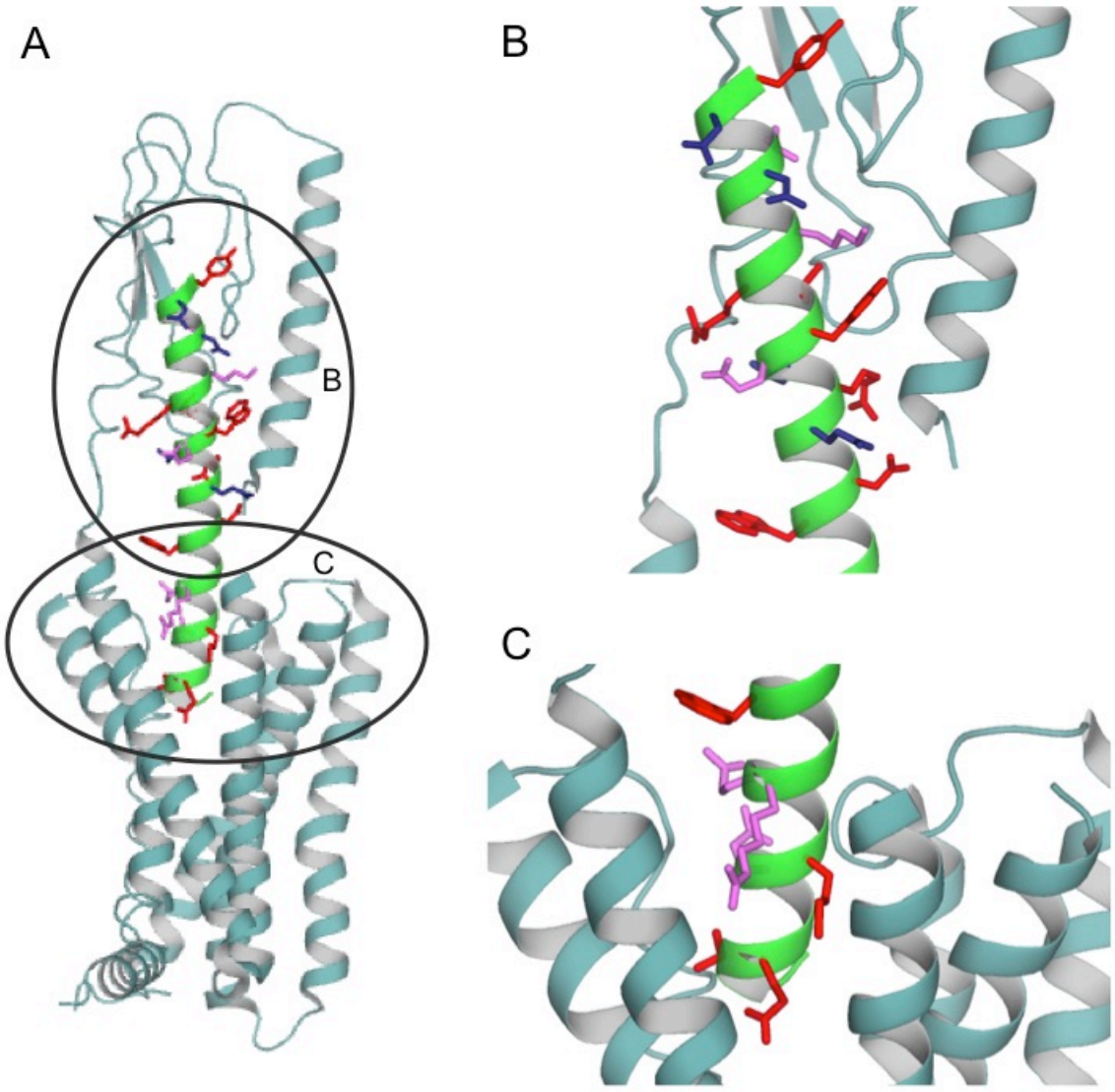

Figure 5.10: Changes in dynamics of residues of PTH(1-34) upon interaction with PTH1R. *(A)*. Crystal structure of ePTH (green) bound to PTH1R (teal) resolved to 2.5 Å (PDB ID: 6FJ3)[25] with *(B)*. interactions of the C-terminus of PTH(1-34) with PTH1R and *(C)*. interactions of the N-terminus of PTH(1-34) with PTH1R. Residues of ePTH that interact with PTH1R in the crystal structure are shown as red sticks. PTH(1-34) residues with changes in R_2 values are shown in blue sticks. PTH(1-34) residues with changes in R_2 that are shown to interact with PTH1R in the crystal structure are shown in pink.

I have established that millimolar concentrations of Ca^{2+} affect PTH(1-34) binding to PTH1R, but do not affect the conformation of PTH(1-34) alone (Figure 5.7). Relaxation experiments showed slight changes in R_2 values of 5 residues of PTH(1-34) in the presence of 15 mM Ca^{2+} (Figure 5.8). Additional experiments are necessary in order to understand if the observed changes in dynamics provide further information about the conformation of PTH(1-34) in solution. However, the observation that Ca^{2+} does not significantly affect the backbone conformation of PTH(1-34) corroborates the hypothesis that Ca^{2+} modulation requires both PTH(1-34) and PTH1R.

The preliminary data presented here illustrate the use of solution NMR as a method to study changes in dynamics of peptide interactions with PTH1R, building the foundation for future studies of PTH(1-34) dynamics upon interaction with PTH1R under different conditions, including the presence of 15 mM Ca^{2+}. Through these experiments, I established that we observe small, but significant changes in R_2 values for residues of PTH(1-34) in the presence of PTH1R, which correlate with current structural studies of the interaction between PTH(1-34) and PTH1R. In addition, I determined the presence of 15 mM Ca^{2+} does not significantly change the backbone conformation of PTH(1-34) but does have small effects on the dynamics of residues in the C-terminus of the peptide. Future studies to combine these two observations will uncover changes in PTH(1-34) as it interacts with PTH1R in the presence of 15 mM Ca^{2+}. Understanding how 15 mM Ca^{2+} changes the dynamics of PTH(1-34) as it binds to PTH1R will provide insight into the mechanism of the Ca^{2+} modulation of ligand binding to PTH1R. In combination with the receptor and peptide mutants described in Chapters 3 and 4, we will be able to determine how specific residues of PTH1R and PTH(1-34) contribute to PTH(1-34) binding to

PTH1R. Identifying changes in conformational dynamics of PTH(1-34) as it binds to PTH1R will lead to a more complete understanding of the mechanisms of PTH1R ligand binding, uncovering novel information about the mechanisms of family B GPCR ligand binding.

Chapter 6: Novel method development to investigate allosteric mechanisms of PTH1R

Thus far, the work presented here has focused on ligand binding interactions of peptide hormones with the extracellular domain of PTH1R. However, allosteric interactions are known to affect both ligand and G protein binding to PTH1R. For example, the data presented in chapter 3 provide evidence that ligand binding to PTH1R is more complex than the two domain binding model, highlighting the importance of allosteric interactions between the N- and C-terminus of the hormone in PTH1R ligand binding. However, it is difficult to study the effect of these allosteric interactions due to the challenge of isolating the N- and C-terminus of the peptide as it interacts with PTH1R. Previous work in the lab established a triblock molecule, which contains three primary components: a lipid anchor, a flexible linker containing a repeating Gly-Ser repeat sequence, and the N-terminus of the peptide of interest. The data presented in this chapter describe preliminary studies using this triblock molecule to separate the N- and C-terminus of the residue to determine how the two portions affect PTH1R. We combined the triblock molecule containing PTH(1-14), PTHrP(1-14), or a mutant PTHrP(1-14), with PTH(15-34) or PTHrP(15-36) for cell based cAMP assays to study how the identity of the C-terminus affects the activation of the N-terminal fragments. Preliminary results show that the identity of the C-terminal fragment affects how each N-terminal fragment activates PTH1R, with position 5 playing an important role. Furthermore, previous studies show that allosteric interactions between extracellular ligand binding and intracellular G protein coupling modulate GPCR function. In order to investigate allosteric interactions of PTH1R, we

developed a surface plasmon resonance (SPR) platform to measure changes in ligand binding and G protein affinity. Preliminary data highlight the feasibility of this new platform. Future studies will investigate how the presence of G protein changes PTH(1-34) and PTHrP(1-36) ligand binding and, conversely, how the presence of PTH(1-34) or PTH(1-36) affects the G protein binding affinity. The new methods developed in this chapter lay a foundation for future studies to identify important allosteric interactions that modulate ligand binding and activation of PTH1R.

The triblock receptor activation studies were done in collaboration with Dr. Yingying Cai. Dr. Cai synthesized and characterized the triblock molecules and performed the preliminary cell based cAMP accumulation assays and I completed the assays. The SPR studies were done in collaboration with Dr. Ewa Folta-Stogneiw and the Biophysics Section of the Discovery Proteomics Core at Yale University.

6.1 Introduction

The work outlined in Chapter 3 determined the components of PTH(1-34) that are important for the Ca^{2+}-dependent binding. Through these studies, I investigated if one or both of the two domains of binding was necessary for Ca^{2+} dependence using chimeric PTH/PTHrP peptides. Of interest, the chimeric peptide PTH(1-14)PTHrP(15-36) bound PTH1R much tighter than either PTH(1-34) or PTHrP(1-36), which suggests an allosteric interaction between the two binding domains, likely through the peptide hormone.[101] We hypothesized the chimeric PTH(1-14)PTHrP(15-36) peptide disrupted these allosteric interactions to cause the tighter binding. Furthermore, the reciprocal chimeric peptide PTHrP(1-14)PTH(15-34) showed no binding to PTH1R, corroborating the idea that there are allosteric interactions between the two domains of binding through the hormone that are necessary for ligand binding interactions.

Previous studies by Gardella et al (1995) also observed that PTHrP(1-14) is incompatible with the fragment PTH(15-34), likely because the combination of the two fragments disrupts important allosteric interactions between the N- and C-terminus of PTH(1-34) through PTH1R.[141] They observed that PTHrP(1-14) is incompatible with the PTH(15-34), but mutating the residue 5 of PTHrP (His) to the PTH residue (Ile) restores binding. To investigate the allosteric interactions between the N- and C-terminus of ligand binding, we designed an assay to isolate the N- and C- terminus of the peptide ligand. Previous work in the lab established a triblock molecule, which contains three primary components: a lipid anchor, a flexible linker containing a repeating Gly-Ser repeat sequence and the N-terminus of the peptide of interest (Figure 6.1).[114] We synthesized triblock constructs for PTH(1-14), PTHrP(1-14) and PTHrP(1-14)H5I, a

mutation that switches the identity of position 5 to the PTHrP residue. Cell-based cAMP accumulation assays tested the activation of the triblock molecules alone, with PTH(15-34) or with PTHrP(15-36) in order to measure how the identity of the C-terminal fragment affects the activation of the N-terminal fragment.

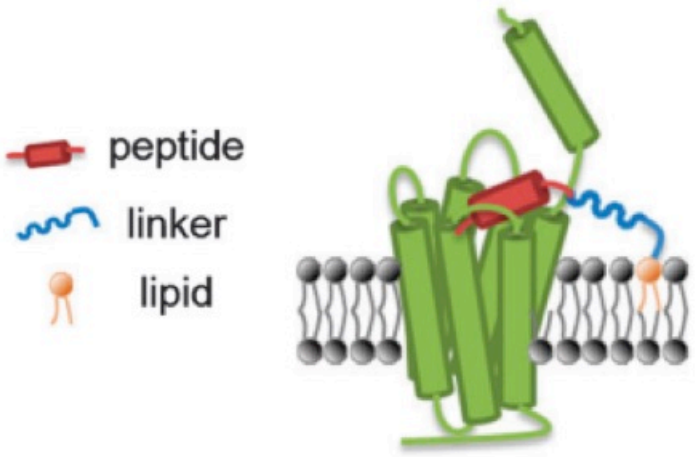

Figure 6.1: Triblock molecules anchor into the lipid bilayer to interact with receptors.[114] Illustration of the three components of the triblock molecule shows the peptide (red), Gly-Ser repeat linker (blue) and the lipid anchor (tan) and its proposed interactions with PTH1R. Figure adapted from [114]

While the majority of the work outlined above focused on ligand binding interactions, many previous studies of GPCRs show important allosteric interactions between G protein binding on the cytoplasmic side of the receptor and ligand binding.[91, 97, 198] In particular, the extended ternary model of GPCR activation proposes the equilibrium between the active and resting state is modulated by the presence of other binding partners.[199] In addition, G protein binding has been shown to affect ligand-binding affinity and ligand binding has also been shown to affect G protein binding and activation.[200, 201] To test how the presence of G protein affects the interactions of ligands with PTH1R, we developed SPR assays in collaboration with Dr. Ewa Folta-Stogneiw.

Combining SPR experiments with the nanodisc purification provides a novel platform to investigate the extended ternary model of GPCR ligand binding and receptor activation. This platform only requires micrograms of purified GPCRs while allowing for the incorporation of many different experimental conditions and binding partners (Figure 6.2).[202, 203] SPR is a label-free method that provides quantitative kinetic and thermodynamic information to elucidate cross-membrane allostery of PTH1R via interactions with its multiple binding partners.

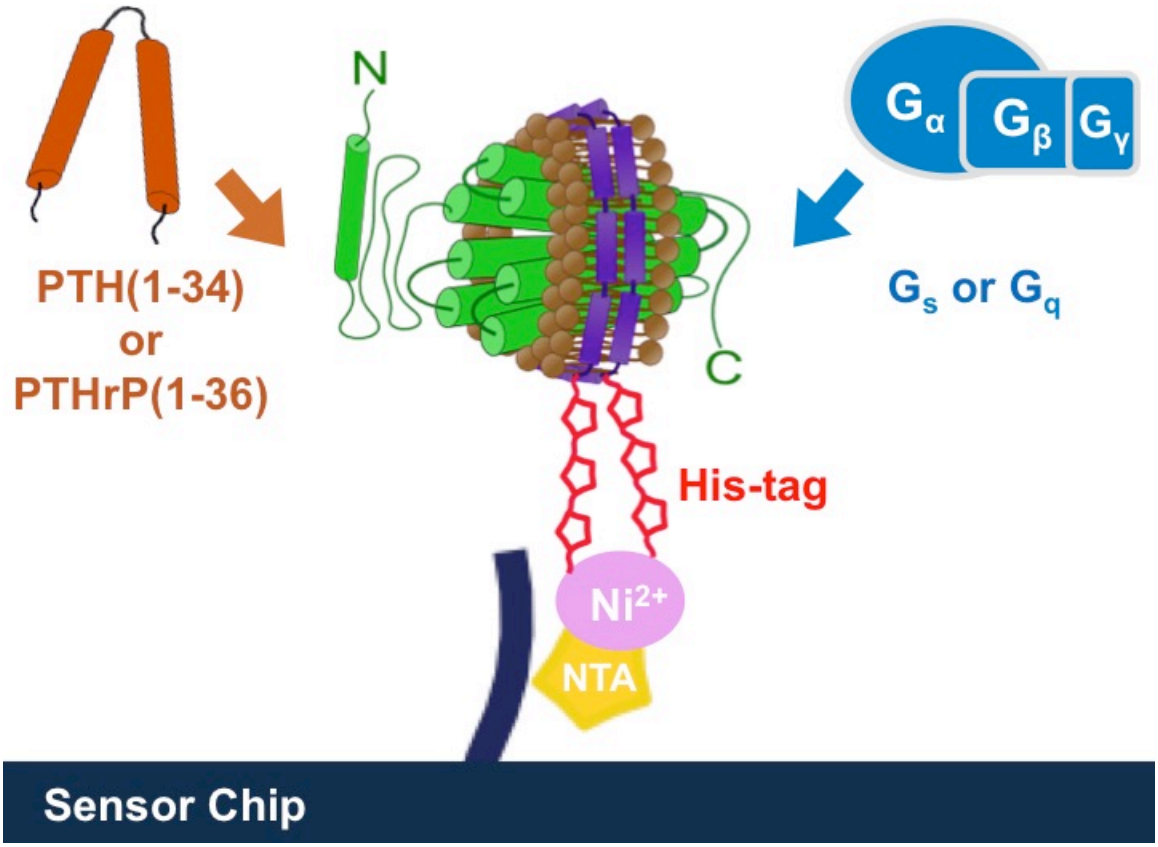

Figure 6.2: SPR platform to study ligand and G protein binding to PTH1R. PTH1R (green) in nanodiscs captured on a Ni^{2+}-NTA on the sensor chip by a 6x-His tag (red) on the membrane scaffold protein (purple) to measure ligand (orange) and G protein (blue) binding.

6.2 Experimental methods

Synthesis of Peptide-Linker-Lipid Triblock Molecules. The triblock molecules were made as described previously.[114] Briefly, PTH(1-14), PTHrP(1-14) and muPTHrP(1-14)H5I (replacing His5 of PTHrP(1-14) with Ile) were purchased with the C-terminal linker and cysteine (peptide-$(GS)_8$-Cys-$CONH_2$, Neobiolab). The lipid with a maleimide-functionalized headgroup (16:0 MPB PE) was obtained from Avanti. For synthesis, the corresponding peptide was dissolved in H_2O with excess TCEP to prevent disulfide bond formation. The lipid was dried under nitrogen then dissolved in 1X PBS/CH_3CN (3:1). The peptide (1 equiv.) and the lipid (3 equiv.) was mixed for 2h at 37°C. The reaction mixture was purified using reverse phase HPLC, and the resulting product was verified using LC-MS.

Cell-Based Activation Assays. Cell-based assays were performed as described in chapter 2 with the following modifications. After ~40 hours induction, cells expressing PTH1R were washed with 200 μL binding buffer (50 mM Tris-HCl, pH 7.4, 100 mM NaCl, 5 mM KCl, 2 mM $CaCl_2$, 0.5% FBS and 5% heat-inactivated FBS) and treated with 120 μL cAMP assay buffer (DMEM containing 200 uM IBMX, 1mg/ml BSA, 35 mM HEPES, pH 7.4) with or without C-terminal portion of the peptides PTH(15-34) or PTHrP(15-36) at 1 μM concentration. Cells were incubated for 20 min, followed by addition of 60 μL binding buffer containing the desired triblock over the concentration range of 1 nM to 1 μM and stimulated for another 20 min. Each point was measured in duplicate in each experiment, and each curve represents an average of two experiments.

Expression and purification of PTH1R. Nanodisc purification of PTH1R was performed as described in Chapter 2 above, except the elution buffer (150 mM NaCl, 50 mM Tris-HCl pH 7.4) was modified to remove EDTA for the SPR studies.

Surface plasmon resonance assays. SPR studies were performed on a BioCore T100 instrument. A solution containing 10 μg/μL of PTH1R was loaded onto a nitrilotriacetic-nickel (NTA-Ni^{2+}) chip with a flow rate of 10 μL/min for 30 minutes in SPR buffer (150 mM NaCl, 50 mM Tris-HCl pH 7.4 1% w/v BSA). The NTA-Ni^{2+} chip capture the nanodiscs through the 6x His tag on the MSP proteins. Serial dilutions of PTH(1-34) from 20 μM were made in SPR buffer. To measure PTH(1-34) binding to the captured PTH1R nanodiscs, the peptide analyte was flown over the cells with a flow rate of 50 μL/min for 2 minute and the resonance recorded. Changes in the response was plotted as a function of PTH(1-34) concentration and fit to determine the binding affinity. Control experiments were performed simultaneously with empty nanodiscs captured on the NTA-Ni^{2+} chip to show PTH(1-34) does not bind to nanodiscs if PTH1R is not present.

6.3 Results

6.3.1 Triblock molecules activate PTH1R

The triblock PTH(1-4) and muPTHrP(1-14)H5I molecules activated PTH1R to produce cAMP (Figure 6.3). However, their EC_{50} values were approximately100-fold worse than full length PTH(1-34) (Figure 3.5). When PTH1R was first incubated with PTH(15-34), the potency of triblock PTH did not change. However, with PTHrP(15-36), the potency of triblock PTH was significantly weaker. In contrast, triblock PTHrP was unable to activate PTH1R in any combination, even when its cognate C-terminus, PTHrP(15-36) was present (Figure 6.3). This shows an important allosteric interaction must be disrupted by separating the N- and C-terminus of PTHrP(1-36). Of note, PTHrP(1-36) activates PTH1R 10 fold weaker than PTH(1-34) in previous cell based assays, with the chimeric ligand PTHrP(1-14)PTH(15-34) also showing weaker activation (Figure 3.5). Thus, in completely separating the two domains of binding for PTHrP, we abolish receptor activation. Most interesting, mutating position 5 of PTHrP from His to Ile makes the muPTHrP triblock activate PTH1R with weaker potency than the triblock PTH (Figure 6.3). However, the ability of the mutant PTHrP triblock restore the activation of PTH1R due to a single point mutation at position 5 highlights the importance of residue 5. When tested with PTH(15-34), the muPThrP triblock shows similar potency to the muPTHrP triblock alone. However, the presence of PTHrP(15-36) increases the potency of the muPTHrP triblock 2-fold. This shows that even with the mutation at PTHrP position 5 to that of the PTH peptide, the presence of the cognate C-terminus has the strongest effect on the potency of the muPTHrP triblock.

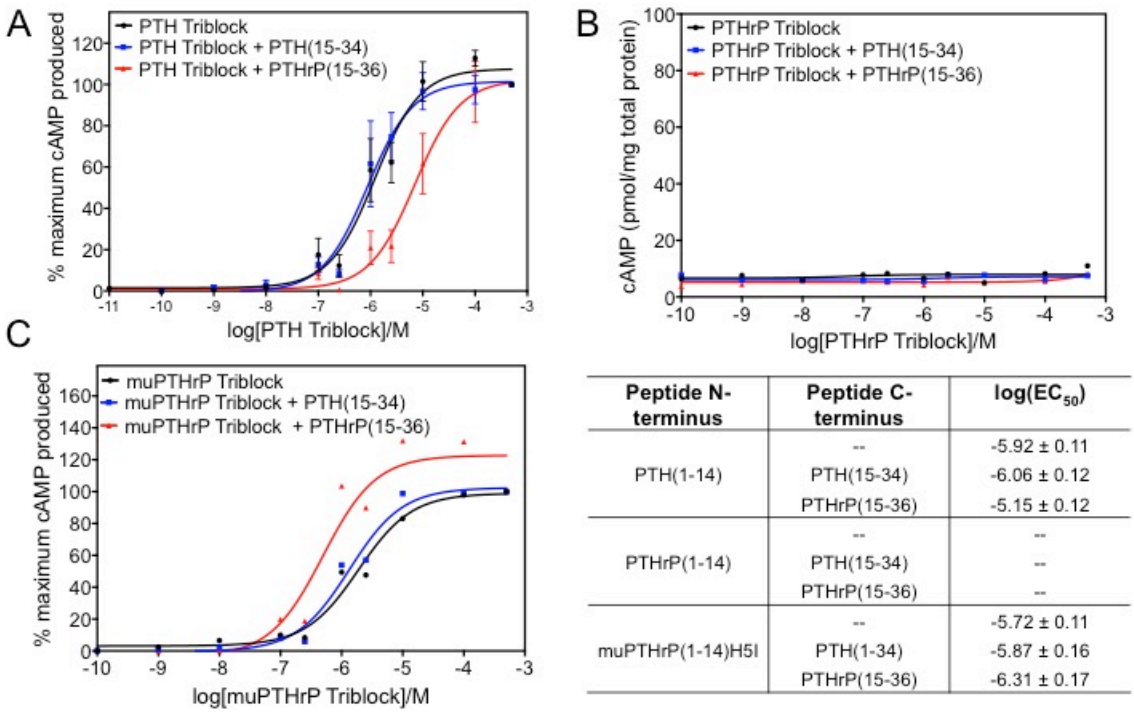

Peptide N-terminus	Peptide C-terminus	log(EC_{50})
PTH(1-14)	--	-5.92 ± 0.11
	PTH(15-34)	-6.06 ± 0.12
	PTHrP(15-36)	-5.15 ± 0.12
PTHrP(1-14)	--	--
	PTH(15-34)	--
	PTHrP(15-36)	--
muPTHrP(1-14)H5I	--	-5.72 ± 0.11
	PTH(1-34)	-5.87 ± 0.16
	PTHrP(15-36)	-6.31 ± 0.17

Figure 6.3: The identity of the peptide N-terminus affects the activation of PTH1R. Cell-based activation of three different triblock molecules (*A)*. PTH(1-14) triblock (n=3), (*B)*. PTHrP(1-14) triblock (n=2) and (*C)*. mutant PTHrP(1-14)H5I (n=2) in the presence of different C-terminal peptide fragments. Data shows the pmols of cAMP produced/mg of total protein for each sample, normalized to the maximum cAMP produced.

6.3.2 Surface plasmon resonance assays show ligand binding to PTH1R

PTH1R purified in nanodiscs containing a 6x-His tag was stably captured by Ni^{2+}-NTA residues on the SPR sensor chips. Flowing increasing concentrations of PTH(1-34) over the sensor chip bound to PTH1R showed increasing resonance units. Fitting the change in response for each PTH(1-34) concentration showed PTH(1-34) binds to PTH1R on the sensor chip with a K_D value of 2.8 ± 1.5 μM. With the addition of 15 mM Ca^{2+} PTH(1-34) binds PTH1R with K_D = 1.9 ± 0.6 μM. Due to the weak binding affinity, the on and off rates were unable to be calculated. These results highlight the feasibility of the SPR platform for studying family B GPCR interactions using PTH1R purified in nanodiscs as a model system.

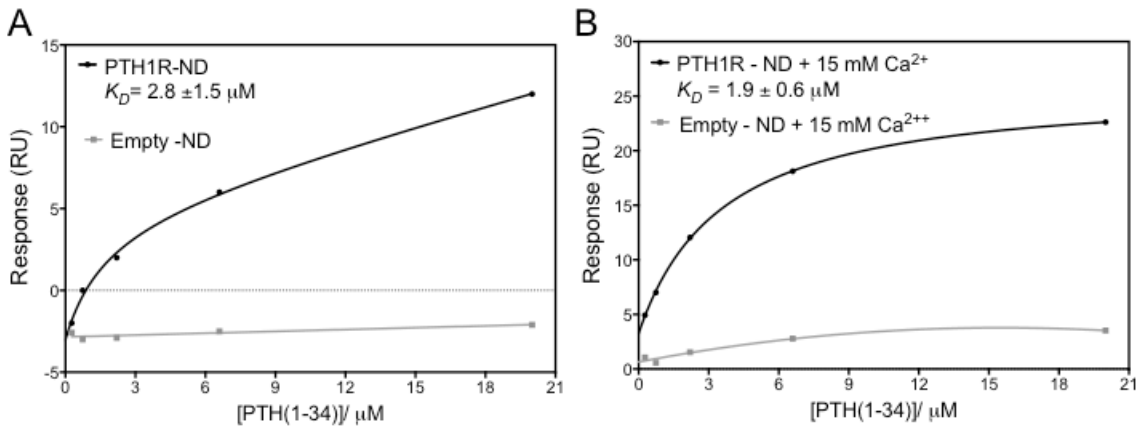

Figure 6.4: SPR analysis of PTH(1-34) binding to PTH1R. PTH(1-34) binds to PTH1R captured on the sensor chip (black), but not empty nanodiscs captured on the nanodisc (gray) with *(A)*. 0 mM Ca^{2+} and *(B)*. 15 mM Ca^{2+}. Data shows a single experiment with the error in K_D value the standard deviation from the fitting.

6.4 Discussion and future directions

The preliminary data presented in this chapter highlight the feasibility of two novel experimental methods to study allosteric interactions of PTH1R. The triblock molecule is an ideal system for separating the N- and C-terminus of the peptide in order to study the allosteric interactions that occur between the two domains of ligand binding. The preliminary results presented here using the triblock PTH, PTHrP and muPTHrP provide additional experimental evidence for the importance of allosteric interactions in modulating ligand binding to PTH1R. We demonstrated that the identity of the C-terminus of the peptide affects the ability of the N-terminus to activate the receptor (Figure 6.3). Future studies to determine if the identity of the N-terminus affects the ligand binding of the C-terminus will help continue to uncover how mechanisms of allosteric interactions within the peptide affect the activation of family B GPCRs.

The development of the SPR platform showed PTH(1-34) bound to PTH1R captured on Ni^{2+}-NTA sensor chips through the 6x-His tag of the MSP (Figure 6.4). This preliminary data is the foundation for additional studies to investigate allosteric interactions between G protein and ligand binding. Future studies will investigate interactions of PTH1R with other binding partners, including PTH, PTHrP, and different G protein isoforms. Identifying changes in the thermodynamics and kinetics of binding interactions of hormones and G proteins will expand our understanding of the activation PTH1R, uncovering the effects of allosteric interactions on GPCR structure and function.

Further development of the two methods described here will lead to a detailed understanding of the complicated allosteric interactions that modulate PTH1R ligand binding and activation. Upon identifying these mechanisms, these studies can be

combined with the novel solution NMR method discussed in chapter 5 to study changes in binding dynamics under many different conditions. For example, we could measure changes in ligand dynamics in the presence of PTH1R bound to G protein. Changes in PTH(1-34) dynamics in the presence of G protein will begin to establish a mechanism for the G protein's effect on ligand binding to PTH1R. This system can be used in many different combinations in order to fully elucidate the dynamics of ligand binding to and G protein interactions with PTH1R.

Chapter 7: Conclusions and future directions

In work presented here, I outline an investigation into the molecular mechanisms of PTH1R ligand binding and receptor activation using biochemical and biophysical assays to study PTH1R purified using a novel nanodisc purification protocol. This project focused primarily on interactions between the peptide hormones and PTH1R, leading to several conclusions that expand upon the existing understanding of ligand binding to family B GPCRs.

Through biochemical assays, I demonstrated that PTH1R purified in nanodiscs binds a truncated version of both PTH(1-34) and PTHrP(1-36). Interestingly, the binding affinity of PTH(1-34) for PTH1R was significantly increased in the presence of 15 mM Ca^{2+}, while the binding affinity of PTHrP(1-36) was unaffected. This Ca^{2+} effect was only observed with the full length PTH1R, and occurred regardless of the presence of the nanodisc. In addition, I confirmed that the ligand-binding enhancement was not promiscuously activated by divalent cations, by showing that ligand binding was unaffected by the presence of Mg^{2+} (Chapter 2). In studying residues of PTH(1-34) that mediate the Ca^{2+}-dependent binding, I identified that the C terminus of PTH(1-34), residues (15-34), was required for the Ca^{2+} effect, likely through residues Glu19 and Glu22 (Chapter 3).

However, the mutations in PTH(1-34) were not sufficient to remove the Ca^{2+}-dependent binding. Therefore, I hypothesized that E19 and E22 of PTH(15-34) interact with negatively charged residues in two non-conserved loops of PTH1R, one in the extracellular domain (ECD) and one in the extracellular loop 1 (ECL1). I mutated the 8

acidic residues in the ECD loop to alanine to create the 8pt PTH1R mutant and 6 acidic residues of ECL1 to create the 6pt PTH1R mutant. I tested ligand binding of PTH(1-34) to each of these mutants and observed a decrease in Ca^{2+}-dependent binding of PTH(1-34) to the 6pt PTH1R. The mutations to PTH1R alone did not abolish the Ca^{2+} effect (Chapter 4). However, combining the mutant 6pt PTH1R with mutant PTH(1-34)E19AE22A eliminated Ca^{2+} dependence. Thus, Ca^{2+} dependence requires residues of both PTH(1-34) and PTH1R in order to affect ligand binding (Chapter 4).

To study the possible mechanisms underlying the Ca^{2+}-dependent binding of PTH(1-34), I used a solution NMR method to observe changes in dynamics of PTH(1-34) upon ligand binding to PTH1R under different conditions (Chapter 5). Preliminary data show changes in the transverse relaxation rates (R_2) for residues of PTH(1-34) in the presence of PTH1R. An increased R_2 value for a given residue indicates an increased rigidity due to interactions with PTH1R. Many of the residues with increased R_2 values in the presence of PTH1R have been previously identified in structural studies to interact with PTH1R. The preliminary data highlights the feasibility of this new method to study changes in ligand dynamics upon interaction with different binding partners and buffer conditions.

Finally, I developed two new platforms to investigate the allosteric interactions involved in ligand binding and activation of PTH1R. Using the novel triblock molecule, our lab observed that identity of the C-terminus of the peptide affects the activation of the N-terminus of the peptide (Chapter 6). In addition, we developed an SPR platform to study allosteric interactions between ligand and G protein binding. The preliminary data

show SPR combined with nanodisc purification of PTH1R is a robust platform for studying interactions between binding partners such as the peptide ligands or G proteins.

The preliminary experiments presented here highlight the development of novel methods to study ligand binding and activation of PTH1R, forming the foundation for many future studies. For example, the triblock molecular system is an effective way to separate the N- and C-terminus of the peptide during ligand binding and receptor activation. Future studies to determine if the identity of the N-terminus of the peptide affects the ligand binding affinity of the C-terminus will provide new information about allosteric interactions of ligand binding to PTH1R. In addition, the novel SPR platform provides a method to investigate the transmembrane allosteric interactions of extracellular and intracellular domains with PTH1R. Using these methods to identify allosteric pathways in PTH1R will inform future protein NMR studies of peptide dynamics under different conditions. For instance, once the effect of the presence of G protein on ligand binding is identified through SPR experiments, solution NMR studies could identify changes in peptide dynamics in the presence of PTH1R with G protein bound. Future studies combining the novel experimental methods developed here will provide the necessary experimental background to develop and test new hypotheses about ligand binding and activation of PTH1R.

The work presented in this thesis builds on the foundation of previous biochemical and structural analysis PTH1R ligand binding and activation. The combination of nanodisc purification with biophysical assays uncovered the importance of allosteric interactions throughout all points of ligand binding and receptor activation. For PTH1R, these interactions are modulated by the presence of millimolar

concentrations of Ca^{2+}. Future investigations into the molecular details of these allosteric interactions will continue to elucidate the complex signaling mechanisms of PTH1R, providing a foundation for interpreting and understanding the structure and function of family B GPCRs. Understanding the molecular mechanisms of PTH1R will elucidate new details about the paradoxical signaling of PTH during the bone remodeling process, potentially leading to novel development of more effective treatments for osteoporosis.

Chapter 8: References

[1] Culhane, K. J., Liu, Y., Cai, Y., and Yan, E. C. Y. (2015) Transmembrane signal transduction by peptide hormones via family B G protein-coupled receptors, *Frontiers in Pharmacology 6*, 246.

[2] Fredriksson, R., Lagerstrom, M. C., Lundin, L. G., and Schioth, H. B. (2003) The G-protein-coupled receptors in the human genome form five main families. Phylogenetic analysis, paralogon groups, and fingerprints, *Molecular Pharmacology 63*, 1256-1272.

[3] Lagerstrom, M. C., and Schioth, H. B. (2008) Structural diversity of G protein-coupled receptors and significance for drug discovery, *Nat Rev Drug Discov 7*, 339-357.

[4] Stevens, R. C., Cherezov, V., Katritch, V., Abagyan, R., Kuhn, P., Rosen, H., and Wuthrich, K. (2013) The GPCR Network: a large-scale collaboration to determine human GPCR structure and function, *Nature Reviews Drug Discovery 12*, 25-34.

[5] Sriram, K., and Insel, P. A. (2018) G Protein-Coupled Receptors as Targets for Approved Drugs: How Many Targets and How Many Drugs?, *Molecular Pharmacology 93*, 251.

[6] Archbold, J. K., Flanagan, J. U., Watkins, H. A., Gingell, J. J., and Hay, D. L. (2011) Structural insights into RAMP modification of secretin family G protein-coupled receptors: implications for drug development, *Trends in pharmacological sciences 32*, 591-600.

[7] Hoare, S. R. (2005) Mechanisms of peptide and nonpeptide ligand binding to Class B G-protein-coupled receptors, *Drug discovery today 10*, 417-427.

[8] Bortolato, A., Doré, A. S., Hollenstein, K., Tehan, B. G., Mason, J. S., and Marshall, F. H. (2014) Structure of Class B GPCRs: new horizons for drug discovery, *British journal of pharmacology 171*, 3132-3145.

[9] Tautermann, C. S. (2014) GPCR structures in drug design, emerging opportunities with new structures, *Bioorganic & Medicinal Chemistry Letters 24*, 4073-4079.

[10] Lau, J. L., and Dunn, M. K. (2018) Therapeutic peptides: Historical perspectives, current development trends, and future directions, *Bioorganic & Medicinal Chemistry 26*, 2700-2707.

[11] Parthier, C., Reedtz-Runge, S., Rudolph, R., and Stubbs, M. T. (2009) Passing the baton in class B GPCRs: peptide hormone activation via helix induction?, *Trends in Biochemical Sciences 34*, 303-310.

[12] Pal, K. M., Karsten: Xu, H Eric. (2012) Structure and mechanism for recognition of peptide hormones by Class B G protein coupled receptors, *Acta Pharmacologica Sinica 33*, 300-311.

[13] Bergwitz, C., Gardella, T. J., Flannery, M. R., Potts, J. T., Kronenberg, H. M., Goldring, S. R., and Jüppner, H. (1996) Full Activation of Chimeric Receptors by Hybrids between Parathyroid Hormone and Calcitonin: EVIDENCE FOR A COMMON PATTERN OF LIGAND-RECEPTOR INTERACTION, *Journal of Biological Chemistry 271*, 26469-26472.

[14] Unson, C. G., Wu, C.-R., Jiang, Y., Yoo, B., Cheung, C., Sakmar, T. P., and Merrifield, R. B. (2002) Roles of Specific Extracellular Domains of the Glucagon Receptor in Ligand Binding and Signaling†, *Biochemistry 41*, 11795-11803.

[15] Vilardaga, J.-P., Romero, G., Friedman, P., and Gardella, T. (2011) Molecular basis of parathyroid hormone receptor signaling and trafficking: a family B GPCR paradigm, *Cell. Mol. Life Sci. 68*, 1-13.
[16] Vilardaga, J. P., Bunemann, M., Krasel, C., Castro, M., and Lohse, M. J. (2003) Measurement of the millisecond activation switch of G protein-coupled receptors in living cells, *Nature Biotechnology 21*, 807-812.
[17] Grace, C. R. R., Perrin, M. H., DiGruccio, M. R., Miller, C. L., Rivier, J. E., Vale, W. W., and Riek, R. (2004) NMR structure and peptide hormone binding site of the first extracellular domain of a type B1 G protein-coupled receptor, *Proceedings of the National Academy of Sciences of the United States of America 101*, 12836-12841.
[18] Koth, C. M., Murray, J. M., Mukund, S., Madjidi, A., Minn, A., Clarke, H. J., Wong, T., Chiang, V., Luis, E., Estevez, A., Rondon, J., Zhang, Y., Hötzel, I., and Allan, B. B. (2012) Molecular basis for negative regulation of the glucagon receptor, *Proceedings of the National Academy of Sciences 109*, 14393-14398.
[19] Parthier, C., Kleinschmidt, M., Neumann, P., Rudolph, R., Manhart, S., Schlenzig, D., Fanghänel, J., Rahfeld, J.-U., Demuth, H.-U., and Stubbs, M. T. (2007) Crystal structure of the incretin-bound extracellular domain of a G protein-coupled receptor, *Proceedings of the National Academy of Sciences 104*, 13942-13947.
[20] Pioszak, A. A., Parker, N. R., Gardella, T. J., and Xu, H. E. (2009) Structural Basis for Parathyroid Hormone-related Protein Binding to the Parathyroid Hormone Receptor and Design of Conformation-selective Peptides, *Journal of Biological Chemistry 284*, 28382-28391.
[21] Pioszak, A. A., Parker, N. R., Suino-Powell, K., and Xu, H. E. (2008) Molecular Recognition of Corticotropin-releasing Factor by Its G-protein-coupled Receptor CRFR1, *Journal of Biological Chemistry 283*, 32900-32912.
[22] Sun, C., Song, D., Davis-Taber, R. A., Barrett, L. W., Scott, V. E., Richardson, P. L., Pereda-Lopez, A., Uchic, M. E., Solomon, L. R., Lake, M. R., Walter, K. A., Hajduk, P. J., and Olejniczak, E. T. (2007) Solution structure and mutational analysis of pituitary adenylate cyclase-activating polypeptide binding to the extracellular domain of PAC1-RS, *Proceedings of the National Academy of Sciences 104*, 7875-7880.
[23] ter Haar, E., Koth, C. M., Abdul-Manan, N., Swenson, L., Coll, J. T., Lippke, J. A., Lepre, C. A., Garcia-Guzman, M., and Moore, J. M. (2010) Crystal Structure of the Ectodomain Complex of the CGRP Receptor, a Class-B GPCR, Reveals the Site of Drug Antagonism, *Structure 18*, 1083-1093.
[24] Underwood, C. R., Garibay, P., Knudsen, L. B., Hastrup, S., Peters, G. H., Rudolph, R., and Reedtz-Runge, S. (2010) Crystal Structure of Glucagon-like Peptide-1 in Complex with the Extracellular Domain of the Glucagon-like Peptide-1 Receptor, *Journal of Biological Chemistry 285*, 723-730.
[25] Ehrenmann, J., Schöppe, J., Klenk, C., Rappas, M., Kummer, L., Doré, A. S., and Plückthun, A. (2018) High-resolution crystal structure of parathyroid hormone 1 receptor in complex with a peptide agonist, *Nature Structural & Molecular Biology 25*, 1086-1092.
[26] Liang, Y.-L., Khoshouei, M., Glukhova, A., Furness, S. G. B., Zhao, P., Clydesdale, L., Koole, C., Truong, T. T., Thal, D. M., Lei, S., Radjainia, M., Danev, R., Baumeister, W., Wang, M.-W., Miller, L. J., Christopoulos, A., Sexton, P. M., and

Wootten, D. (2018) Phase-plate cryo-EM structure of a biased agonist-bound human GLP-1 receptor–Gs complex, *Nature 555*, 121.
[27] Liang, Y.-L., Khoshouei, M., Radjainia, M., Zhang, Y., Glukhova, A., Tarrasch, J., Thal, D. M., Furness, S. G. B., Christopoulos, G., Coudrat, T., Danev, R., Baumeister, W., Miller, L. J., Christopoulos, A., Kobilka, B. K., Wootten, D., Skiniotis, G., and Sexton, P. M. (2017) Phase-plate cryo-EM structure of a class B GPCR–G-protein complex, *Nature 546*, 118.
[28] Song, G., Yang, D., Wang, Y., de Graaf, C., Zhou, Q., Jiang, S., Liu, K., Cai, X., Dai, A., Lin, G., Liu, D., Wu, F., Wu, Y., Zhao, S., Ye, L., Han, G. W., Lau, J., Wu, B., Hanson, M. A., Liu, Z.-J., Wang, M.-W., and Stevens, R. C. (2017) Human GLP-1 receptor transmembrane domain structure in complex with allosteric modulators, *Nature 546*, 312.
[29] Zhang, H., Qiao, A., Yang, D., Yang, L., Dai, A., de Graaf, C., Reedtz-Runge, S., Dharmarajan, V., Zhang, H., Han, G. W., Grant, T. D., Sierra, R. G., Weierstall, U., Nelson, G., Liu, W., Wu, Y., Ma, L., Cai, X., Lin, G., Wu, X., Geng, Z., Dong, Y., Song, G., Griffin, P. R., Lau, J., Cherezov, V., Yang, H., Hanson, M. A., Stevens, R. C., Zhao, Q., Jiang, H., Wang, M.-W., and Wu, B. (2017) Structure of the full-length glucagon class B G-protein-coupled receptor, *Nature 546*, 259.
[30] Zhang, H., Qiao, A., Yang, L., Van Eps, N., Frederiksen, K. S., Yang, D., Dai, A., Cai, X., Zhang, H., Yi, C., Cao, C., He, L., Yang, H., Lau, J., Ernst, O. P., Hanson, M. A., Stevens, R. C., Wang, M.-W., Reedtz-Runge, S., Jiang, H., Zhao, Q., and Wu, B. (2018) Structure of the glucagon receptor in complex with a glucagon analogue, *Nature 553*, 106.
[31] Zhang, Y., Sun, B., Feng, D., Hu, H., Chu, M., Qu, Q., Tarrasch, J. T., Li, S., Sun Kobilka, T., Kobilka, B. K., and Skiniotis, G. (2017) Cryo-EM structure of the activated GLP-1 receptor in complex with a G protein, *Nature 546*, 248.
[32] Hollenstein, K., de Graaf, C., Bortolato, A., Wang, M.-W., Marshall, F. H., and Stevens, R. C. (2014) Insights into the structure of class B GPCRs, *Trends in Pharmacological Sciences 35*, 12-22.
[33] Pioszak, A. A., and Xu, H. E. (2008) Molecular recognition of parathyroid hormone by its G protein-coupled receptor, *Proceedings of the National Academy of Sciences 105*, 5034-5039.
[34] Chen, Q., Pinon, D. I., Miller, L. J., and Dong, M. (2009) Molecular Basis of Glucagon-like Peptide 1 Docking to Its Intact Receptor Studied with Carboxyl-terminal Photolabile Probes, *Journal of Biological Chemistry 284*, 34135-34144.
[35] Dong, M., Lam, P. C.-H., Pinon, D. I., Hosohata, K., Orry, A., Sexton, P. M., Abagyan, R., and Miller, L. J. (2011) Molecular Basis of Secretin Docking to Its Intact Receptor Using Multiple Photolabile Probes Distributed throughout the Pharmacophore, *Journal of Biological Chemistry 286*, 23888-23899.
[36] Miller, L. J., Chen, Q., Lam, P. C.-H., Pinon, D. I., Sexton, P. M., Abagyan, R., and Dong, M. (2011) Refinement of Glucagon-like Peptide 1 Docking to Its Intact Receptor Using Mid-region Photolabile Probes and Molecular Modeling, *Journal of Biological Chemistry 286*, 15895-15907.
[37] Zhou, A. T., Bessalle, R., Bisello, A., Nakamoto, C., Rosenblatt, M., Suva, L. J., and Chorev, M. (1997) Direct mapping of an agonist-binding domain within the parathyroid hormone/parathyroid hormone-related protein receptor by

photoaffinity crosslinking, *Proceedings of the National Academy of Sciences 94*, 3644-3649.
[38] Yang, L., Yang, D., de Graaf, C., Moeller, A., West, G. M., Dharmarajan, V., Wang, C., Siu, F. Y., Song, G., Reedtz-Runge, S., Pascal, B. D., Wu, B., Potter, C. S., Zhou, H., Griffin, P. R., Carragher, B., Yang, H., Wang, M.-W., Stevens, R. C., and Jiang, H. (2015) Conformational states of the full-length glucagon receptor, *Nature Communications 6*, 7859.
[39] Neumann, J.-M., Couvineau, A., Murail, S., Lacapere, J.-J., Jamin, N., and Laburthe, M. (2008) Class-B GPCR activation: is ligand helix-capping the key?, *Trends in biochemical sciences 33*, 314-319.
[40] Yaqub, T., Tikhonova, I. G., Lattig, J., Magnan, R., Laval, M., Escrieut, C., Boulegue, C., Hewage, C., and Fourmy, D. (2010) Identification of determinants of glucose-dependent insulinotropic polypeptide receptor that interact with N-terminal biologically active region of the natural ligand, *Mol Pharmacol 77*, 547-558.
[41] Xiao, Q., Jeng, W., and Wheeler, M. B. (2000) Characterization of glucagon-like peptide-1 receptor-binding determinants, *Journal of molecular endocrinology 25*, 321-335.
[42] Tseng, C. C., and Lin, L. (1997) A point mutation in the glucose-dependent insulinotropic peptide receptor confers constitutive activity, *Biochemical and biophysical research communications 232*, 96-100.
[43] Solano, R. M., Langer, I., Perret, J., Vertongen, P., Juarranz, M. G., Robberecht, P., and Waelbroeck, M. (2001) Two basic residues of the h-VPAC1 receptor second transmembrane helix are essential for ligand binding and signal transduction, *The Journal of biological chemistry 276*, 1084-1088.
[44] Runge, S., Gram, C., Brauner-Osborne, H., Madsen, K., Knudsen, L. B., and Wulff, B. S. (2003) Three distinct epitopes on the extracellular face of the glucagon receptor determine specificity for the glucagon amino terminus, *The Journal of biological chemistry 278*, 28005-28010.
[45] Roberts, D. J., Vertongen, P., and Waelbroeck, M. (2011) Analysis of the glucagon receptor first extracellular loop by the substituted cysteine accessibility method, *Peptides 32*, 1593-1599.
[46] Prevost, M., Vertongen, P., Raussens, V., Roberts, D. J., Cnudde, J., Perret, J., and Waelbroeck, M. (2010) Mutational and cysteine scanning analysis of the glucagon receptor N-terminal domain, *The Journal of biological chemistry 285*, 30951-30958.
[47] Perret, J., Craenenbroeck, M., Langer, I., Vertongen, P., Grégoire, F., Robberecht, P., and Waelbroeck, M. (2002) Mutational analysis of the glucagon receptor: similarities with the vasoactive intestinal peptide (VIP)/pituitary adenylate cyclase-activating peptide (PACAP)/secretin receptors for recognition of the ligand's third residue, *Biochem. J 362*, 389-394.
[48] Mathi, S. K., Chan, Y., Li, X. F., and Wheeler, M. B. (1997) Scanning of the glucagon-like peptide-1 receptor localizes G protein-activating determinants primarily to the N terminus of the third intracellular loop, *Molecular endocrinology 11*, 424-432.
[49] Liaw, C. W., Grigoriadis, D. E., Lovenberg, T. W., De Souza, E. B., and Maki, R. A. (1997) Localization of ligand-binding domains of human corticotropin-releasing factor receptor: a chimeric receptor approach, *Molecular endocrinology 11*, 980-985.

[50] Koole, C., Wootten, D., Simms, J., Miller, L. J., Christopoulos, A., and Sexton, P. M. (2012) Second extracellular loop of human glucagon-like peptide-1 receptor (GLP-1R) has a critical role in GLP-1 peptide binding and receptor activation, *The Journal of biological chemistry 287*, 3642-3658.
[51] Hoare, S. R., Brown, B. T., Santos, M. A., Malany, S., Betz, S. F., and Grigoriadis, D. E. (2006) Single amino acid residue determinants of non-peptide antagonist binding to the corticotropin-releasing factor1 (CRF1) receptor, *Biochemical pharmacology 72*, 244-255.
[52] Gensure, R. C., Shimizu, N., Tsang, J., and Gardella, T. J. (2003) Identification of a contact site for residue 19 of parathyroid hormone (PTH) and PTH-related protein analogs in transmembrane domain two of the type 1 PTH receptor, *Molecular endocrinology 17*, 2647-2658.
[53] Gardella, T. J., and Juppner, H. (2001) Molecular properties of the PTH/PTHrP receptor, *Trends in endocrinology and metabolism: TEM 12*, 210-217.
[54] Donnelly, D. (2012) The structure and function of the glucagon-like peptide-1 receptor and its ligands, *Br J Pharmacol 166*, 27-41.
[55] Dong, M., Pinon, D. I., Cox, R. F., and Miller, L. J. (2004) Importance of the Amino Terminus in Secretin Family G Protein-coupled Receptors: INTRINSIC PHOTOAFFINITY LABELING ESTABLISHES INITIAL DOCKING CONSTRAINTS FOR THE CALCITONIN RECEPTOR, *Journal of Biological Chemistry 279*, 1167-1175.
[56] Di Paolo, E., Petry, H., Moguilevsky, N., Bollen, A., De Neef, P., Waelbroeck, M., and Robberecht, P. (1999) Mutations of aromatic residues in the first transmembrane helix impair signalling by the secretin receptor, *Receptors & channels 6*, 309-315.
[57] Di Paolo, E., De Neef, P., Moguilevsky, N., Petry, H., Bollen, A., Waelbroeck, M., and Robberecht, P. (1998) Contribution of the second transmembrane helix of the secretin receptor to the positioning of secretin, *FEBS letters 424*, 207-210.
[58] Coopman, K., Wallis, R., Robb, G., Brown, A. J., Wilkinson, G. F., Timms, D., and Willars, G. B. (2011) Residues within the transmembrane domain of the glucagon-like peptide-1 receptor involved in ligand binding and receptor activation: modelling the ligand-bound receptor, *Molecular endocrinology 25*, 1804-1818.
[59] Ceraudo, E., Hierso, R., Tan, Y. V., Murail, S., Rouyer-Fessard, C., Nicole, P., Robert, J. C., Jamin, N., Neumann, J. M., Robberecht, P., Laburthe, M., and Couvineau, A. (2012) Spatial proximity between the VPAC1 receptor and the amino terminus of agonist and antagonist peptides reveals distinct sites of interaction, *FASEB journal : official publication of the Federation of American Societies for Experimental Biology 26*, 2060-2071.
[60] Cascieri, M. A., Koch, G. E., Ber, E., Sadowski, S. J., Louizides, D., de Laszlo, S. E., Hacker, C., Hagmann, W. K., MacCoss, M., Chicchi, G. G., and Vicario, P. P. (1999) Characterization of a novel, non-peptidyl antagonist of the human glucagon receptor, *The Journal of biological chemistry 274*, 8694-8697.
[61] Wootten, D., Simms, J., Miller, L. J., Christopoulos, A., and Sexton, P. M. (2013) Polar transmembrane interactions drive formation of ligand-specific and signal pathway-biased family B G protein-coupled receptor conformations, *Proc Natl Acad Sci U S A 110*, 5211-5216.

[62] Hjorth, S. A., Orskov, C., and Schwartz, T. W. (1998) Constitutive activity of glucagon receptor mutants, *Molecular endocrinology 12*, 78-86.
[63] Dong, M., Xu, X., Ball, A. M., Makhoul, J. A., Lam, P. C.-H., Pinon, D. I., Orry, A., Sexton, P. M., Abagyan, R., and Miller, L. J. (2012) Mapping spatial approximations between the amino terminus of secretin and each of the extracellular loops of its receptor using cysteine trapping, *The FASEB Journal 26*, 5092-5105.
[64] Ceraudo, E., Murail, S., Tan, Y.-V., Lacapere, J.-J., Neumann, J.-M., Couvineau, A., and Laburthe, M. (2008) The vasoactive intestinal peptide (VIP) α-Helix up to C terminus interacts with the N-terminal ectodomain of the human VIP/pituitary adenylate cyclase-activating peptide 1 receptor: photoaffinity, molecular modeling, and dynamics, *Molecular Endocrinology 22*, 147-155.
[65] Assil-Kishawi, I., Samra, T. A., Mierke, D. F., and Abou-Samra, A. B. (2008) Residue 17 of sauvagine cross-links to the first transmembrane domain of corticotropin-releasing factor receptor 1 (CRFR1), *The Journal of biological chemistry 283*, 35644-35651.
[66] Ritter, S. L., and Hall, R. A. (2009) Fine-tuning of GPCR activity by receptor-interacting proteins, *Nature Reviews Molecular Cell Biology 10*, 819-830.
[67] Rashid, A. J., O'Dowd, B. F., and George, S. R. (2004) Minireview: diversity and complexity of signaling through peptidergic G protein-coupled receptors, *Endocrinology 145*, 2645-2652.
[68] Bavec, A., Hallbrink, M., Langel, U., and Zorko, M. (2003) Different role of intracellular loops of glucagon-like peptide-1 receptor in G-protein coupling, *Regulatory Peptides 111*, 137-144.
[69] Couvineau, A., and Laburthe, M. (2012) The Family B1 GPCR: Structural Aspects and Interaction with Accessory Proteins, *Current Drug Targets 13*, 103-115.
[70] Christopoulos, A., Christopoulos, G., Morfis, M., Udawela, M., Laburthe, M., Couvineau, A., Kuwasako, K., Tilakaratne, N., and Sexton, P. M. (2003) Novel receptor partners and function of receptor activity-modifying proteins, *Journal of Biological Chemistry 278*, 3293-3297.
[71] Parameswaran, N., and Spielman, W. S. (2006) RAMPs: the past, present and future, *Trends in Biochemical Sciences 31*, 631-638.
[72] Liang, Y.-L., Khoshouei, M., Deganutti, G., Glukhova, A., Koole, C., Peat, T. S., Radjainia, M., Plitzko, J. M., Baumeister, W., Miller, L. J., Hay, D. L., Christopoulos, A., Reynolds, C. A., Wootten, D., and Sexton, P. M. (2018) Cryo-EM structure of the active, Gs-protein complexed, human CGRP receptor, *Nature 561*, 492-497.
[73] McLatchie, L. M., Fraser, N. J., Main, M. J., Wise, A., Brown, J., Thompson, N., Solari, R., Lee, M. G., and Foord, S. M. (1998) RAMPs regulate the transport and ligand specificity of the calcitonin-receptor-like receptor, *Nature 393*, 333-339.
[74] Mannstadt, M., Jüppner, H., and Gardella, T. J. (1999) Receptors for PTH and PTHrP: their biological importance and functional properties, *American Journal of Physiology-Renal Physiology 277*, F665-F675.
[75] Mosekilde, L., Søgaard, C., Danielsen, C., Tørring, O., and Nilsson, M. (1991) The Anabolic Effects of Human Parathyroid Hormone (hPTH) on Rat Vertebral Body Mass Are also Reflected in the Quality of Bone, Assessed by Biomechanical Testing: A Comparison Study between hPTH-(1–34) and hPTH-(1–84)*, *Endocrinology 129*, 421-428.

[76] Silva, B. C., Costa, A. G., Cusano, N. E., Kousteni, S., and Bilezikian, J. P. (2011) Catabolic and anabolic actions of parathyroid hormone on the skeleton, *Journal of endocrinological investigation 34*, 801-810.
[77] Delaglio, F., Grzesiek, S., Vuister, G. W., Zhu, G., Pfeifer, J., and Bax, A. (1995) NMRPipe: A multidimensional spectral processing system based on UNIX pipes, *Journal of Biomolecular NMR 6*, 277-293.
[78] Weilbaecher, K. N., Guise, T. A., and McCauley, L. K. (2011) Cancer to bone: a fatal attraction, *Nature Reviews Cancer 11*, 411.
[79] Manolagas, S. C., and Jilka, R. L. (1995) Mechanisms of disease - bone marrow, cytokines, and bone remodeling - emerging insights into the pathophysiology of osteoporosis, *New England Journal of Medicine 332*, 305-311.
[80] Parfitt, A. M. (2002) Targeted and nontargeted bone remodeling: relationship to basic multicellular unit origination and progression, *Bone 30*, 5-7.
[81] Jilka, R. L. (2007) Molecular and cellular mechanisms of the anabolic effect of intermittent PTH, *Bone 40*, 1434-1446.
[82] Locklin, R. M., Khosla, S., Turner, R. T., and Riggs, B. L. (2003) Mediators of the biphasic responses of bone to intermittent and continuously administered parathyroid hormone, *Journal of cellular biochemistry 89*, 180-190.
[83] Chan, C. K. Y., Mason, A., Cooper, C., and Dennison, E. (2016) Novel advances in the treatment of osteoporosis, *British Medical Bulletin 119*, 129-142.
[84] Chew, C. K., and Clarke, B. L. (2017) Abaloparatide: Recombinant human PTHrP (1–34) anabolic therapy for osteoporosis, *Maturitas 97*, 53-60.
[85] Garcia-Ocana, A., Horwitz, M. J., Tedesco, M. B., Stewart, A. F., and Gundberg, C. (2003) Short-Term, High-Dose Parathyroid Hormone-Related Protein as a Skeletal Anabolic Agent for the Treatment of Postmenopausal Osteoporosis, *The Journal of Clinical Endocrinology & Metabolism 88*, 569-575.
[86] Ohtaki, T., Masuda, Y., Ishibashi, Y., Kitada, C., Arimura, A., and Fujino, M. (1993) Purification and Characterization of the Receptor for Pituitary Adenylate Cyclase-Activating Polypeptide, *Journal of Biological Chemistry 268*, 26650-26657.
[87] Michalke, K., Huyghe, C., Lichiere, J., Graviere, M. E., Siponen, M., Sciara, G., Lepaul, I., Wagner, R., Magg, C., Rudolph, R., Cambillau, C., and Desmyter, A. (2010) Mammalian G protein-coupled receptor expression in Escherichia coli: II. Refolding and biophysical characterization of mouse cannabinoid receptor 1 and human parathyroid hormone receptor 1, *Analytical Biochemistry 401*, 74-80.
[88] Schroder-Tittmann, K., Bosse-Doenecke, E., Reedtz-Runge, S., Ihling, C., Sinz, A., Tittmann, K., and Rudolph, R. (2010) Recombinant Expression, in Vitro Refolding, and Biophysical Characterization of the Human Glucagon-like Peptide-1 Receptor, *Biochemistry 49*, 7956-7965.
[89] Gan, L., Alexander, J. M., Wittelsberger, A., Thomas, B., and Rosenblatt, M. (2006) Large-scale purification and characterization of human parathyroid hormone-1 receptor stably expressed in HEK293S GnTI(-) cells, *Protein Expression and Purification 47*, 296-302.
[90] Mitra, N., Liu, Y. T., Liu, J., Serebryany, E., Mooney, V., DeVree, B. T., Sunahara, R. K., and Yan, E. C. Y. (2013) Calcium-Dependent Ligand Binding and G-protein Signaling of Family B GPCR Parathyroid Hormone 1 Receptor Purified in Nanodiscs, *Acs Chemical Biology 8*, 617-625.

[91] Cai, Y., Liu, Y., Culhane, K. J., DeVree, B. T., Yang, Y., Sunahara, R. K., and Yan, E. C. Y. (2017) Purification of family B G protein-coupled receptors using nanodiscs: Application to human glucagon-like peptide-1 receptor, *PLOS ONE 12*, e0179568.
[92] Unson, C. G. (2008) Expression of glucagon receptors in tetracycline-inducible HEK293S GnT1(-) stable cell lines: An approach toward purification of receptor protein for structural studies, *Biopolymers 90*, 287-296.
[93] Shimada, M., Chen, X., Cvrk, T., Hilfiker, H., Parfenova, M., and Segre, G. V. (2002) Purification and characterization of a receptor for human parathyroid hormone and parathyroid hormone-related peptide, *Journal of Biological Chemistry 277*, 31774-31780.
[94] Ohtaki, T., Ogi, K., Masuda, Y., Mitsuoka, K., Fujiyoshi, Y., Kitada, C., Sawada, H., Onda, H., and Fujino, M. (1998) Expression, Purification, and Reconstitution of Receptor for Pituitary Adenylate Cyclase-activating Polypeptide large - scale purification of a fucntionally active G protein-coupled receptor produced in SF9 insect cells *Journal of Biological Chemistry 273*, 15464-15473.
[95] Klammt, C., Perrin, M. H., Maslennikov, I., Renault, L., Krupa, M., Kwiatkowski, W., Stahlberg, H., Vale, W., and Choe, S. (2011) Polymer-based cell-free expression of ligand-binding family B G-protein coupled receptors without detergents, *Protein Science 20*, 1030-1041.
[96] Serebryany, E., Zhu, G. A., and Yan, E. C. Y. (2012) Artificial membrane-like environments for in vitro studies of purified G-protein coupled receptors, *Biochimica et Biophysica Acta (BBA) - Biomembranes 1818*, 225-233.
[97] Leitz, A. J., Bayburt, T. H., Barnakov, A. N., Springer, B. A., and Sligar, S. G. (2006) Functional reconstitution of beta(2)-adrenergic receptors utilizing self-assembling Nanodisc technology, *Biotechniques 40*, 601-+.
[98] El Moustaine, D., Granier, S., Doumazane, E., Scholler, P., Rahmeh, R., Bron, P., Mouillac, B., Baneres, J. L., Rondard, P., and Pin, J. P. (2012) Distinct roles of metabotropic glutamate receptor dimerization in agonist activation and G-protein coupling, *Proceedings of the National Academy of Sciences of the United States of America 109*, 16342-16347.
[99] Inagaki, S., Ghirlando, R., White, J. F., Gvozdenovic-Jeremic, J., Northup, J. K., and Grisshammer, R. (2012) Modulation of the Interaction between Neurotensin Receptor NTS1 and Gq Protein by Lipid, *Journal of Molecular Biology 417*, 95-111.
[100] Banerjee, S., Huber, T., and Sakmar, T. P. (2008) Rapid incorporation of functional rhodopsin into nanoscale apolipoprotein bound bilayer (NABB) particles, *J Mol Biol 377*, 1067-1081.
[101] Culhane, K. J., Belina, M. E., Sims, J. N., Cai, Y., Liu, Y., Wang, P. S. P., and Yan, E. C. Y. (2018) Parathyroid Hormone Senses Extracellular Calcium To Modulate Endocrine Signaling upon Binding to the Family B GPCR Parathyroid Hormone 1 Receptor, *ACS Chemical Biology 13*, 2347-2358.
[102] Liang, Y. L., Khoshouei, M., Radjainia, M., Zhang, Y., Glukhova, A., Tarrasch, J., Thal, D. M., Furness, S. G. B., Christopoulos, G., Coudrat, T., Danev, R., Baumeister, W., Miller, L. J., Christopoulos, A., Kobilka, B. K., Wootten, D., Skiniotis, G., and Sexton, P. M. (2017) Phase-plate cryo-EM structure of a class B GPCR-G-protein complex, *Nature*.

[103] Gardella, T., and Ju¨ppner, H. (2000) Interaction of PTH and PTHrP with Their Receptors, *Rev Endocr Metab Disord 1*, 317-329.
[104] Wheatley, M., Wootten, D., Conner, M. T., Simms, J., Kendrick, R., Logan, R. T., Poyner, D. R., and Barwell, J. (2012) Lifting the lid on GPCRs: the role of extracellular loops, *British Journal of Pharmacology 165*, 1688-1703.
[105] Castro, M., Nikolaev, V. O., Palm, D., Lohse, M. J., and Vilardaga, J.-P. (2005) Turn-on switch in parathyroid hormone receptor by a two-step parathyroid hormone binding mechanism, *Proceedings of the National Academy of Sciences of the United States of America 102*, 16084-16089.
[106] Thomas, B. E., Woznica, I., Mierke, D. F., Wittelsberger, A., and Rosenblatt, M. (2008) Conformational changes in the parathyroid hormone receptor associated with activation by agonist, *Molecular Endocrinology 22*, 1154-1162.
[107] Cupp, M. E., Nayak, S. K., Adem, A. S., and Thomsen, W. J. (2013) Parathyroid Hormone (PTH) and PTH-Related Peptide Domains Contributing to Activation of Different PTH Receptor–Mediated Signaling Pathways, *Journal of Pharmacology and Experimental Therapeutics 345*, 404-418.
[108] Bisello, A., Chorev, M., Rosenblatt, M., Monticelli, L., Mierke, D. F., and Ferrari, S. L. (2002) Selective ligand-induced stabilization of active and desensitized parathyroid hormone type 1 receptor conformations, *Journal of Biological Chemistry 277*, 38524-38530.
[109] Okazaki, M., Ferrandon, S., Vilardaga, J.-P., Bouxsein, M. L., Potts, J. T., and Gardella, T. J. (2008) Prolonged signaling at the parathyroid hormone receptor by peptide ligands targeted to a specific receptor conformation, *Proceedings of the National Academy of Sciences 105*, 16525-16530.
[110] Shimizu, N., Guo, J., and Gardella, T. J. (2001) Parathyroid Hormone (PTH)-(1–14) and -(1–11) Analogs Conformationally Constrained by α-Aminoisobutyric Acid Mediate Full Agonist Responses via the Juxtamembrane Region of the PTH-1 Receptor, *Journal of Biological Chemistry 276*, 49003-49012.
[111] Takasu, H., Gardella, T. J., Luck, M. D., Potts, J. T., and Bringhurst, F. R. (1999) Amino-terminal modifications of human parathyroid hormone (PTH) selectively alter phospholipase C signaling via the type 1 PTH receptor: implications for design of signal-specific PTH ligands, *Biochemistry 38*, 13453-13460.
[112] Goldman, M. E., McKee, R. L., Caulfield, M. P., Reagan, J. E., Levy, J. J., Gay, C. T., DeHaven, P. A., Rosenblatt, M., and Chorev, M. (1988) A new highly potent parathyroid hormone antagonist: [D-TRPl2, TYR34] bPTH-(7–34) NH2, *Endocrinology 123*, 2597-2599.
[113] Shimizu, N., Dean, T., Tsang, J. C., Khatri, A., Potts, J. T., and Gardella, T. J. (2005) Novel Parathyroid Hormone (PTH) Antagonists That Bind to the Juxtamembrane Portion of the PTH/PTH-related Protein Receptor, *Journal of Biological Chemistry 280*, 1797-1807.
[114] Liu, Y., Cai, Y., Liu, W., Li, X. H., Rhoades, E., and Yan, E. C. (2015) Triblock peptide-linker-lipid molecular design improves potency of peptide ligands targeting family B G protein-coupled receptors, *Chem Commun (Camb) 51*, 6157-6160.
[115] Shimizu, M., Potts, J. T., and Gardella, T. J. (2000) Minimization of Parathyroid Hormone: novel amino-terminal parathyroid hormone fragments with enhanced

potency in activating the type-1 parathyroid hormone receptor, *Journal of Biological Chemistry 275*, 21836-21843.
[116] Shimizu, M., Carter, P. H., Khatri, A., Potts, J. J. T., and Gardella, T. J. (2001) Enhanced Activity in Parathyroid Hormone-(1–14) and -(1–11): Novel Peptides for Probing Ligand-Receptor Interactions*, *Endocrinology 142*, 3068-3074.
[117] Burr, D. B. (2002) Targeted and nontargeted remodeling, *Bone 30*, 2-4.
[118] Silver, I., Murrills, R., and Etherington, D. (1988) Microelectrode studies on the acid microenvironment beneath adherent macrophages and osteoclasts, *Experimental cell research 175*, 266-276.
[119] Aslan, D., Andersen, M. D., Gede, L. B., de Franca, T. K., Jorgensen, S. R., Schwarz, P., and Jorgensen, N. R. (2012) Mechanisms for the bone anabolic effect of parathyroid hormone treatment in humans, *Scandinavian Journal of Clinical & Laboratory Investigation 72*, 14-22.
[120] Yang, D., Singh, R., Diviet, P., Guo, J., Bouxsein, M. L., and Bringhurst, F. R. (2007) Contributions of parathyroid hormone (PTH)/PTH-related peptide receptor signaling pathways to the anabolic effect of PTH on bone, *Bone 40*, 1453-1461.
[121] Mitra, N., Liu, Y., Liu, J., Serebryany, E., Mooney, V., DeVree, B. T., Sunahara, R. K., and Yan, E. C. Y. (2012) Calcium-Dependent Ligand Binding and G-protein Signaling of Family B GPCR Parathyroid Hormone 1 Receptor Purified in Nanodiscs, *ACS Chemical Biology 8*, 617-625.
[122] Schröder-Tittmann, K., Bosse-Doenecke, E., Reedtz-Runge, S., Ihling, C., Sinz, A., Tittmann, K., and Rudolph, R. (2010) Recombinant expression, in vitro refolding, and biophysical characterization of the human glucagon-like peptide-1 receptor, *Biochemistry 49*, 7956-7965.
[123] Unson, C. G. (2008) Expression of glucagon receptors in tetracycline ‐ inducible HEK293S GnT1− stable cell lines: An approach toward purification of receptor protein for structural studies, *Peptide Science 90*, 287-296.
[124] Bayburt, T. H., and Sligar, S. G. (2010) Membrane protein assembly into Nanodiscs, *Febs Letters 584*, 1721-1727.
[125] Civjan, N. R., Bayburt, T. H., Schuler, M. A., and Sligar, S. G. (2003) Direct solubilization of heterologously expressed membrane proteins by incorporation into nanoscale lipid bilayers, *Biotechniques 35*, 556-563.
[126] Reeves, P. J., Kim, J.-M., and Khorana, H. G. (2002) Structure and function in rhodopsin: a tetracycline-inducible system in stable mammalian cell lines for high-level expression of opsin mutants, *Proceedings of the National Academy of Sciences 99*, 13413-13418.
[127] Bayburt, T. H., Grinkova, Y. V., and Sligar, S. G. (2002) Self-assembly of discoidal phospholipid bilayer nanoparticles with membrane scaffold proteins, *Nano Letters 2*, 853-856.
[128] Bajaj, A., Ćelić, A., Ding, F.-X., Naider, F., Becker, J. M., and Dumont, M. E. (2004) A Fluorescent α-Factor Analogue Exhibits Multiple Steps on Binding to Its G Protein Coupled Receptor in Yeast, *Biochemistry 43*, 13564-13578.
[129] Denton, E. V., Craig, C. J., Pongratz, R. L., Appelbaum, J. S., Doerner, A. E., Narayanan, A., Shulman, G. I., Cline, G. W., and Schepartz, A. (2013) A beta-peptide agonist of the GLP-1 receptor, a class B GPCR, *Organic letters 15*, 5318-5321.

[130] Barberis, M., Pagano, M. A., Gioia, L. D., Marin, O., Vanoni, M., Pinna, L. A., and Alberghina, L. (2005) CK2 regulates in vitro the activity of the yeast cyclin-dependent kinase inhibitor Sic1, *Biochemical and Biophysical Research Communications 336*, 1040-1048.
[131] Rossi, A. M., and Taylor, C. W. (2011) Analysis of protein-ligand interactions by fluorescence polarization, *Nature protocols 6*, 365-387.
[132] Nadkarni, P., Chepurny, O. G., and Holz, G. G. (2014) Regulation of glucose homeostasis by GLP-1, In *Progress in molecular biology and translational science*, pp 23-65, Elsevier.
[133] Wang, X., Liu, H., Chen, J., Li, Y., and Qu, S. (2015) Multiple factors related to the secretion of glucagon-like peptide-1, *International journal of endocrinology 2015*.
[134] Han, K.-C., Kim, J. H., Kim, K.-H., Kim, E. E., Seo, J.-H., and Yang, E. G. (2010) Identification of farnesoid X receptor modulators by a fluorescence polarization-based interaction assay, *Analytical biochemistry 398*, 185-190.
[135] Ou, J., Tu, H., Shan, B., Luk, A., DeBose-Boyd, R. A., Bashmakov, Y., Goldstein, J. L., and Brown, M. S. (2001) Unsaturated fatty acids inhibit transcription of the sterol regulatory element-binding protein-1c (SREBP-1c) gene by antagonizing ligand-dependent activation of the LXR, *Proceedings of the National Academy of Sciences 98*, 6027-6032.
[136] Bledsoe, R. K., Montana, V. G., Stanley, T. B., Delves, C. J., Apolito, C. J., McKee, D. D., Consler, T. G., Parks, D. J., Stewart, E. L., and Willson, T. M. (2002) Crystal structure of the glucocorticoid receptor ligand binding domain reveals a novel mode of receptor dimerization and coactivator recognition, *Cell 110*, 93-105.
[137] Larry A. Sklar, Bruce S. Edwards, Steven W. Graves, John P. Nolan, and Prossnitz, E. R. (2002) Flow Cytometric Analysis of Ligand-Receptor Interactions and Molecular Assemblies, *Annual Review of Biophysics and Biomolecular Structure 31*, 97-119.
[138] Sridharan, R., Zuber, J., Connelly, S. M., Mathew, E., and Dumont, M. E. (2014) Fluorescent Approaches for Understanding Interactions of Ligands with G Protein Coupled Receptors, *Biochimica et biophysica acta 1838*, 15-33.
[139] Reeves, P. J., Callewaert, N., Contreras, R., and Khorana, H. G. (2002) Structure and function in rhodopsin: High-level expression of rhodopsin with restricted and homogeneous N-glycosylation by a tetracycline-inducible N-acetylglucosaminyltransferase I-negative HEK293S stable mammalian cell line, *P Natl Acad Sci USA 99*, 13419-13424.
[140] Reeves, P. J., Thurmond, R. L., and Khorana, H. G. (1996) Structure and function in rhodopsin: High level expression of a synthetic bovine opsin gene and its mutants in stable mammalian cell lines, *P Natl Acad Sci USA 93*, 11487-11492.
[141] Gardella, T. J., Luck, M. D., Wilson, A. K., Keutmann, H. T., Nussbaum, S. R., Potts, J. T., and Kronenberg, H. M. (1995) Parathyroid Hormone (PTH)-PTH-related Peptide Hybrid Peptides Reveal Functional Interactions between the 1–14 and 15–34 Domains of the Ligand, *Journal of Biological Chemistry 270*, 6584-6588.
[142] Ye, L., Neale, C., Sljoka, A., Lyda, B., Pichugin, D., Tsuchimura, N., Larda, S. T., Pomès, R., García, A. E., Ernst, O. P., Sunahara, R. K., and Prosser, R. S. (2018) Mechanistic insights into allosteric regulation of the A2A adenosine G protein-coupled receptor by physiological cations, *Nature Communications 9*, 1372.

[143] Brown, E. M., and MacLeod, R. J. (2001) Extracellular Calcium Sensing and Extracellular Calcium Signaling, *Physiological Reviews 81*, 239-297.
[144] Kunishima, N., Shimada, Y., Tsuji, Y., Sato, T., Yamamoto, M., Kumasaka, T., Nakanishi, S., Jingami, H., and Morikawa, K. (2000) Structural basis of glutamate recognition by a dimeric metabotropic glutamate receptor, *Nature 407*, 971-977.
[145] Silve, C., Petrel, C., Leroy, C., Bruel, H., Mallet, E., Rognan, D., and Ruat, M. (2005) Delineating a Ca2+ Binding Pocket within the Venus Flytrap Module of the Human Calcium-sensing Receptor, *Journal of Biological Chemistry 280*, 37917-37923.
[146] Jiang, J. Y., Nagaraju, M., Meyer, R. C., Zhang, L., Hamelberg, D., Hall, R. A., Brown, E. M., Conn, P. J., and Yang, J. J. (2014) Extracellular Calcium Modulates Actions of Orthosteric and Allosteric Ligands on Metabotropic Glutamate Receptor 1α, *Journal of Biological Chemistry 289*, 1649-1661.
[147] Gifford, J. L., Walsh, M. P., and Vogel, H. J. (2007) Structures and metal-ion-binding properties of the Ca2+-binding helix–loop–helix EF-hand motifs, *Biochem J 405*, 199-221.
[148] Ikura, M. (1996) Calcium binding and conformational response in EF-hand proteins, *Trends in Biochemical Sciences 21*, 14-17.
[149] Luck, M. D., Carter, P. H., and Gardella, T. J. (1999) The (1–14) fragment of parathyroid hormone (PTH) activates intact and amino-terminally truncated PTH-1 receptors, *Molecular Endocrinology 13*, 670-680.
[150] Shimizu, M., Shimizu, N., Tsang, J. C., Petroni, B. D., Khatri, A., Potts, J. T., and Gardella, T. J. (2002) Residue 19 of the Parathyroid Hormone (PTH) Modulates Ligand Interaction with the Juxtamembrane Region of the PTH-1 Receptor†, *Biochemistry 41*, 13224-13233.
[151] McPhalen, C. A., Strynadka, N. C. J., and James, M. N. G. (1991) Calcium-Binding Sites in Proteins: A Structural Perspective, In *Advances in Protein Chemistry* (Anfinsen, C. B., Edsall, J. T., Richards, F. M., and Eisenberg, D. S., Eds.), pp 77-144, Academic Press.
[152] Pidcock, E., and Moore, G. R. (2001) Structural characteristics of protein binding sites for calcium and lanthanide ions, *JBIC Journal of Biological Inorganic Chemistry 6*, 479-489.
[153] Kiefer, F., Arnold, K., Kunzli, M., Bordoli, L., and Schwede, T. (2009) The SWISS-MODEL Repository and associated resources, *Nucleic Acids Res 37*, D387-D392.
[154] Guex, N., Peitsch, M. C., and Schwede, T. (2009) Automated comparative protein structure modeling with SWISS-MODEL and Swiss-PdbViewer: A historical perspective, *Electrophoresis 30*, S162-S173.
[155] Bordoli, L., Kiefer, F., Arnold, K., Benkert, P., Battey, J., and Schwede, T. (2009) Protein structure homology modeling using SWISS-MODEL workspace, *Nat Protoc 4*, 1-13.
[156] Biasini, M., Bienert, S., Waterhouse, A., Arnold, K., Studer, G., Schmidt, T., Kiefer, F., Cassarino, T. G., Bertoni, M., Bordoli, L., and Schwede, T. (2014) SWISS-MODEL: modelling protein tertiary and quaternary structure using evolutionary information, *Nucleic Acids Res 42*, W252-W258.

[157] Bienert, S., Waterhouse, A., de Beer, T. A. P., Tauriello, G., Studer, G., Bordoli, L., and Schwede, T. (2017) The SWISS-MODEL Repository-new features and functionality, *Nucleic Acids Res 45*, D313-D319.
[158] Arnold, K., Bordoli, L., Kopp, J., and Schwede, T. (2006) The SWISS-MODEL workspace: a web-based environment for protein structure homology modelling, *Bioinformatics 22*, 195-201.
[159] Siu, F. Y., He, M., de Graaf, C., Han, G. W., Yang, D., Zhang, Z., Zhou, C., Xu, Q., Wacker, D., Joseph, J. S., Liu, W., Lau, J., Cherezov, V., Katritch, V., Wang, M. W., and Stevens, R. C. (2013) Structure of the human glucagon class B G-protein-coupled receptor, *Nature 499*, 444-449.
[160] Greenberg, Z., Bisello, A., Mierke, D. F., Rosenblatt, M., and Chorev, M. (2000) Mapping the bimolecular interface of the parathyroid hormone (PTH)-PTH1 receptor complex: spatial proximity between Lys(27) (of the hormone principal binding domain) and leu(261) (of the first extracellular loop) of the human PTH1 receptor, *Biochemistry 39*, 8142-8152.
[161] Wittelsberger, A., Corich, M., Thomas, B. E., Lee, B. K., Barazza, A., Czodrowski, P., Mierke, D. F., Chorev, M., and Rosenblatt, M. (2006) The mid-region of parathyroid hormone (1-34) serves as a functional docking domain in receptor activation, *Biochemistry 45*, 2027-2034.
[162] Marx, U. C., Austermann, S., Bayer, P., Adermann, K., Ejchart, A., Sticht, H., Walter, S., Schmid, F.-X., Jaenicke, R., Forssmann, W.-G., and Rösch, P. (1995) Structure of Human Parathyroid Hormone 1–37 in Solution, *Journal of Biological Chemistry 270*, 15194-15202.
[163] Maestro. (version 10.2, Schrödinger, LLC, New York, NY 2015.) version 10.2, Schrödinger, LLC, New York, NY, 2015.
[164] Bisello, A., Adams, A. E., Mierke, D. F., Pellegrini, M., Rosenblatt, M., Suva, L. J., and Chorev, M. (1998) Parathyroid hormone-receptor interactions identified directly by photocross-linking and molecular modeling studies, *J Biol Chem 273*, 22498-22505.
[165] Adams, A. E., Bisello, A., Chorev, M., Rosenblatt, M., and Suva, L. J. (1998) Arginine 186 in the extracellular N-terminal region of the human parathyroid hormone 1 receptor is essential for contact with position 13 of the hormone, *Mol Endocrinol 12*, 1673-1683.
[166] Hollenstein, K., Kean, J., Bortolato, A., Cheng, R. K., Dore, A. S., Jazayeri, A., Cooke, R. M., Weir, M., and Marshall, F. H. (2013) Structure of class B GPCR corticotropin-releasing factor receptor 1, *Nature 499*, 438-443.
[167] Lisi, G. P., and Loria, J. P. (2016) Solution NMR Spectroscopy for the Study of Enzyme Allostery, *Chemical Reviews 116*, 6323-6369.
[168] Manley, G., and Loria, J. P. (2012) NMR insights into protein allostery, *Archives of Biochemistry and Biophysics 519*, 223-231.
[169] Palmer, A. G. (2004) NMR Characterization of the Dynamics of Biomacromolecules, *Chemical Reviews 104*, 3623-3640.
[170] Palmer, A. G., Kroenke, C. D., and Patrick Loria, J. (2001) [10] - Nuclear Magnetic Resonance Methods for Quantifying Microsecond-to-Millisecond Motions in Biological Macromolecules, In *Methods in Enzymology* (James, T. L., Dötsch, V., and Schmitz, U., Eds.), pp 204-238, Academic Press.

[171] Levitt, M. H. (2001) Spin dynamics, *Jon Wiley and Sons 196*.
[172] Rosen, N., and Zener, C. (1932) Double Stern-Gerlach Experiment and Related Collision Phenomena, *Physical Review 40*, 502-507.
[173] Ramsey, N., and Purcell, E. (1952) Interactions between nuclear spins in molecules, *Physical Review 85*, 143.
[174] Arnold, J., Dharmatti, S., and Packard, M. (1951) Chemical effects on nuclear induction signals from organic compounds, *The journal of chemical physics 19*, 507-507.
[175] Becker, E. D. (1993) A brief history of nuclear magnetic resonance, *Analytical chemistry 65*, 295A-302A.
[176] Bloch, F. (1946) Nuclear induction, *Physical review 70*, 460.
[177] Hahn, E. L. (1949) An accurate nuclear magnetic resonance method for measuring spin-lattice relaxation times, *Physical Review 76*, 145.
[178] Bloembergen, N., Purcell, E. M., and Pound, R. V. (1948) Relaxation effects in nuclear magnetic resonance absorption, *Physical review 73*, 679.
[179] Cavanagh, J., Fairbrother, W. J., Palmer III, A. G., and Skelton, N. J. (1995) *Protein NMR spectroscopy: principles and practice*, Elsevier.
[180] Keeler, J. (2011) *Understanding NMR spectroscopy*, John Wiley & Sons.
[181] Aue, W., Bartholdi, E., and Ernst, R. R. (1976) Two‐dimensional spectroscopy. Application to nuclear magnetic resonance, *The Journal of Chemical Physics 64*, 2229-2246.
[182] Bax, A., and Lerner, L. (1986) Two-dimensional nuclear magnetic resonance spectroscopy, *Science 232*, 960-967.
[183] Ikura, M., Kay, L. E., and Bax, A. (1990) A novel approach for sequential assignment of 1H, 13C, and 15N spectra of larger proteins: Heteronuclear triple-resonance three-dimensional NMR spectroscopy. Application to calmodulin, *Biochemistry 29*, 4659-4667.
[184] Bodenhausen, G., and Ruben, D. J. (1980) Natural abundance nitrogen-15 NMR by enhanced heteronuclear spectroscopy, *Chemical Physics Letters 69*, 185-189.
[185] Morris, G. A., and Freeman, R. (1979) Enhancement of nuclear magnetic resonance signals by polarization transfer, *Journal of the American Chemical Society 101*, 760-762.
[186] Carr, H. Y., and Purcell, E. M. (1954) Effects of diffusion on free precession in nuclear magnetic resonance experiments, *Physical review 94*, 630.
[187] Meiboom, S., and Gill, D. (1958) Modified spin‐echo method for measuring nuclear relaxation times, *Review of scientific instruments 29*, 688-691.
[188] Loria, J. P., Rance, M., and Palmer, A. G. (1999) A relaxation-compensated Carr–Purcell–Meiboom–Gill sequence for characterizing chemical exchange by NMR spectroscopy, *Journal of the American Chemical Society 121*, 2331-2332.
[189] Barden, J. A., and Cutherbertson, R. M. (1993) Stabilized NMR structure of human parathyroid hormone(1–34), *European Journal of Biochemistry 215*, 315-321.
[190] Barden, J. A., and Kemp, B. E. (1993) NMR solution structure of human parathyroid hormone(1-34), *Biochemistry 32*, 7126-7132.
[191] Klaus, W., Dieckmann, T., Wray, V., Schomburg, D., Wingender, E., and Mayer, H. (1991) Investigation of the solution structure of the human parathyroid hormone

fragment (1-34) by proton NMR spectroscopy, distance geometry, and molecular dynamics calculations, *Biochemistry 30*, 6936-6942.
[192] Audu, C. O., Cochran, J. C., Pellegrini, M., and Mierke, D. F. (2013) Recombinant production of TEV cleaved human parathyroid hormone, *Journal of peptide science : an official publication of the European Peptide Society 19*, 504-510.
[193] Audu, C. O., Plati, J. J., Pellegrini, M., and Mierke, D. F. (2014) Engineering a soluble parathyroid hormone GPCR mimetic, *Proteins: Structure, Function, and Bioinformatics 82*, 1370-1375.
[194] Kumar, A., Baumann, M., and Balbach, J. (2016) Small Molecule Inhibited Parathyroid Hormone Mediated cAMP Response by N–Terminal Peptide Binding, *Scientific Reports 6*, 22533.
[195] Scian, M., Marin, M., Bellanda, M., Tou, L., Alexander, J. M., Rosenblatt, M., Chorev, M., Peggion, E., and Mammi, S. (2006) Backbone dynamics of human parathyroid hormone (1–34): Flexibility of the central region under different environmental conditions, *Peptide Science 84*, 147-160.
[196] Markley, J. L., Tonelli, M., and Lee, W. (2014) NMRFAM-SPARKY: enhanced software for biomolecular NMR spectroscopy, *Bioinformatics 31*, 1325-1327.
[197] Okazaki, M., Ferrandon, S., Vilardaga, J. P., Bouxsein, M. L., Potts, J. T., and Gardella, T. J. (2008) Prolonged signaling at the parathyroid hormone receptor by peptide ligands targeted to a specific receptor conformation (vol 105, pg 16525, 2008), *Proceedings of the National Academy of Sciences of the United States of America 105*, 20559-20559.
[198] Culhane, K. J., Liu, Y., Cai, Y., and Yan, E. C. (2015) Transmembrane signal transduction by peptide hormones via family BG protein-coupled receptors, *Frontiers in pharmacology 6*.
[199] Mahoney, J. P., and Sunahara, R. K. (2016) Mechanistic insights into GPCR-G protein interactions, *Current opinion in structural biology 41*, 247-254.
[200] Malik, R. U., Ritt, M., DeVree, B. T., Neubig, R. R., Sunahara, R. K., and Sivaramakrishnan, S. (2013) Detection of G Protein-selective G Protein-coupled Receptor (GPCR) Conformations in Live Cells, *Journal of Biological Chemistry 288*, 17167-17178.
[201] Yao, X. J., Vélez Ruiz, G., Whorton, M. R., Rasmussen, S. G. F., DeVree, B. T., Deupi, X., Sunahara, R. K., and Kobilka, B. (2009) The effect of ligand efficacy on the formation and stability of a GPCR-G protein complex, *P Natl Acad Sci USA 106*, 9501-9506.
[202] Bocquet, N., Kohler, J., Hug, M. N., Kusznir, E. A., Rufer, A. C., Dawson, R. J., Hennig, M., Ruf, A., Huber, W., and Huber, S. (2015) Real-time monitoring of binding events on a thermostabilized human A2A receptor embedded in a lipid bilayer by surface plasmon resonance, *Biochimica et Biophysica Acta (BBA) - Biomembranes 1848*, 1224-1233.
[203] Patching, S. G. (2014) Surface plasmon resonance spectroscopy for characterisation of membrane protein–ligand interactions and its potential for drug discovery, *Biochimica et Biophysica Acta (BBA) - Biomembranes 1838*, 43-55.